UNIVERSITÀ DEGLI STUDI DI TRENTO

QUEEN MARY
UNIVERSITY OF LONDON

Erasmus Mundus Joint Doctorate School in Science for MAnagement of Rivers and their Tidal System

---

Çağrı Gökdemir

# A three dimension hyporheic model of the River Bure: Understanding the nutrient dynamics and the role of streambed heterogeneity

Erasmus Mundus

October 2014

Doctoral thesis in Science for MAnagement of Rivers and their Tidal System,
**Cycle**: 1
**Primary Institution**:
Department of Civil, Environmental and Mechanical Engineering, University of Trento
**Secondary Institution**:
Department of Physical Geography, Queen Mary: University of London
**Associate partner**:
Department of Ecohydraulics, University of Idaho
**Supervisors**:
Alberto Bellin, University of Trento
Kate Heppell, Queen Mary: University of London
Daniele Tonina, University of Idaho

Academic year 2014/2015

This page is intentionally left blank


# The SMART Joint Doctorate Programme

Research for this thesis was conducted with the support of the Erasmus Mundus Programme [1] , within the framework of the Erasmus Mundus Joint Doctorate (EMJD) SMART (Science for MAnagement of Rivers and their Tidal systems). EMJDs aim to foster cooperation between higher education institutions and academic staff in Europe and third countries with a view to creating centres of excellence and providing a highly skilled 21st century workforce enabled to lead social, cultural and economic developments. All EMJDs involve mandatory mobility between the universities in the consortia and lead to the award of recognised joint, double or multiple degrees. The SMART programme represents a collaboration among the University of Trento, Queen Mary University of London, and Freie Universität Berlin. Each doctoral candidate within the SMART programme has conformed to the following during their 3 years of study:

(i) Supervision by a minimum of two supervisors in two institutions (their primary and secondary institutions).

(ii) Study for a minimum period of 6 months at their secondary institution.

(iii) Successful completion of a minimum of 30 ECTS of taught courses.

(iv) Collaboration with an associate partner to develop a particular component / application of their research that is of mutual interest.

(v) Submission of a thesis within 3 years of commencing the programme.

[1] This project has been funded with support from the European Commission. This publication reflects the views only of the author, and the Commission cannot be held responsible for any use which may be made of the information contained therein.

# Acknowledgements

This thesis and my PhD were founded within the framework of the Erasmus Mundus Joint Doctorate (EMJD) SMART (Science for management of Rivers and their tidal system) program. Completion of this thesis would not have been possible without the support of my main Institution University of Trento, department of Civil, environmental and mechanical engineering, as second institution Queen Mary: University of London, department of physical geography and associated partner University of Idaho, Eco-hydraulics department.

I would like to thank Alberto Bellin as my primary supervisor for making the research possible and for his valuable advice, and Kate Heppell for her support and patience while helping me for the field works, and I am extra thankful for her guidance for the lab works. I would like to mention Daniele Tonina as a third supervisor for coordinating my stay and give me the opportunity to experiencing study at the University of Idaho, and also I am grateful for his practical interventions and guidance in critical situations during this PhD. Without their passion in this field and their help in supporting the project, this work could not have been possible.

I would like to stress that working in all three institutions was an unique opportunity for me. I am thankful all of my colleagues and all members of each department. As a PhD candidate who comes from abroad and experienced different cultures in a short time, I have never felt as a stranger or isolated, and always embraced by all of my colleagues and all valuable lecturers.

# Abstract

The hyporheic zone is often defined as the zone where mixing of surface water and groundwater occurs in shallow sediments beneath and adjacent to rivers. This mixing contributes to create unique biogeochemical conditions that may attenuate contaminants from either upstream surface water or groundwater under gaining and losing conditions. Hyporheic exchange results from differences in the channel near-bed head as it varies in space in response to interactions between surface flow and bed topography, with the interaction with the water table playing an important role too. Reactions of contaminants in groundwater also dependent on mixing between surface and subsurface water, which occurs in this zone. Therefore, representation of the profile of upwelling and downwelling exchange between surface water and groundwater have important consequences for contaminant transport. The present work studies nitrogen fate within a restored reach of the River Bure, Norfolk, United Kingdom. To this end, we confront numerical simulations of the hyporheic flow and tracer transport with field measurements of surface flow properties, nearby groundwater table and nitrogen compound concentration. . We numerically model mixing between hyporheic flow paths induced by sediment, bedform, meanders on riverbed, and flow paths of adjacent upwelling of deeper groundwater. Results of the analysis indicate that despite the coarse topographical data and with limited surface water hydraulic data it is possible to define the spatial extent of hyporheic exchange and potential mixing zones for contaminants as a function of residence time. The proposed work has the potential to depict high residence time zones and biogeochemical reactivity in homogeneous and heterogeneous sediments. Furthermore, fieldwork analysis shows that in this site the hyporheic zone have a little effect on nutrient concentration. In addition, hydraulic modeling results indicate that streambed discharge significantly influences hyporheic exchange. Especially, the residence times under average stream discharge conditions are higher than the ones under the high discharge conditions mostly on the part that has riffle - pool morphology. From hydraulic point of view, heterogeneous domain has higher connectivity than the homogeneous fine sand subsurface set. Such that, subsurface flow has tendency to flow through high hydraulic conductivity zones, which is defined as tunneling effect, therefore, low conductivity zones

have minor effect on hyporheic flow. The predictions based on the $Da_{O_2}$ index proves that heterogeneous sediment formations have more aerobic potential, however, prevailing anaerobic conditions occur mostly vicinity of low hydraulic conductivity zones.

# Contents

# List of Figures

# List of Tables

# Chapter 1

# Introduction

## 1.1 Motivation of the work and approaches

### 1.1.1 Hydraulic context

Over a range of spatial scales, river systems are complex ecosystems characterized by basic chemical, biological and physical phenomenon. As water travels through this network and penetrate into the sediment and interacts with groundwater, particles are being conveyed through those environments within the pathway of the flow. Therefore, different phases of the transformation of the particle can be seen along this pathway, and that leads dynamic connectivity between the networks. Therefore, from this approach, surface and subsurface should be evaluated as physically different domains but as integrated systems . Especially groundwater - surface water interactions are critical in the environments that depends on the groundwater level fluctuations, as groundwater-fed river systems (Hancock et al., 2005). Interaction among groundwater, hyporheic zone and surface water influences many facets of such systems (Brunke and Gonser, 1997; Malard et al., 2002). Hyporheic mechanisms can change the extent of hyporheic exchange thus that may regulate the supply of oxygen and organic carbon into the hyporheic zone (Findlay, 1995; Jones Jr et al., 1995). The direction of flow and hydro connectivity in the hyporheic zone also regulates the nutrient dynamics, thus it is one of the key factor to characterize the dominant biogeochemical processes (Zarnetske et al., 2012; Marzadri et al., 2012; Duff and Triska, 2000). Hyporheic exchange has particular importance in zones that have high connectivity between surface and subsurface water bodies, such as groundwater fed systems. Many chalk and limstone catchments have strong interaction between groundwater and surface water, where aquifers hold importance as public or agricultural water supply (Hiscock et al., 2001; Pretty et al., 2006; Hill et al., 1998), especially in UK. Therefore, understanding the role of hyporheic zones hydraulic processes with complex hydrology and distinctive hydrochemistry should be enhanced for the sake of river manage-

ment of such areas.

Most ecological research on groundwater and rivers treats aquifers and surface waters as separate domains. By this approach the interactions between them have mostly been ignored (Brunke and Gonser, 1997). Main two reason for the differentiation between these two domains have been claimed by (1998) to be: (i) as a consequence of the different disciplinary focus of the researchers and (ii) due to characteristic differences between the two environments. Recent ecological studies focusing on the effect of anthropogenic contamination on surface water mostly use an empirical approach by using field observations (Borisova et al., 2014; Ashckenazi-Polivoda et al., 2014; Moser et al., 2014; Yang et al., 2014; Edwardson et al., 2003). Even empirical works give us strong indications of the general picture of the watersheds and riparian zones by observation; they may not enough for finding out the core reason of the event that is happening and mimicking the actual dynamics of the interested system. Therefore, it would be a suitable approach to subdivide the reach into subsystems that are hydrologically connected to each other through cross-linkages in order to develop a better understanding of the processes that take place within the river system (see Figure 1.1). Definition and depiction of the dynamic system with the help of numerical and analytical approach could provide solid support for such empirical works and help scientists to understand the reasons of the changes in water quality in these particular domains.

From our perspective, a river reach can be treated as an integrated system of subdivided domains. In this work the main focus is the hydraulic and biogeochemical dynamics of a transition zone between groundwater and surface water, which is called the hyporheic zone (HZ) (see Figure 1.1) In the work of Boulton et al. [1998] the hyporheic zone is defined as the saturated volume of sediment surrounding the stream which provides the linkage between the river and the aquifer, while the riparian zone acts as buffer between the hillslopes and rivers. The riparian zone has an important influence on runoff generation and solute transport at the reach scale. Amongst all the processes that occur in each subsystem, we focus our attention on those that take place between the stream and its hyporheic zone. Water movement in the hyporheic zone can be described by Darcy's Law (Darcy, 1856), which represents subsurface flow. According to that processes in HZ depends on hydraulic conductivity of channel bed and pressure heads (Darcy, 1856). Water movements may take long time in subsurface, such that suspended and dissolved materials are stored in it, therefore, the uptake of organic matter and nutrients are propagated by microbiological activities. As water moves through a river network, constant exchange of water between streams and the subsurface occurs, that is called hyporheic exchange (Bencala, 1983; Packman and Bencala, 2000; Salehin et al., 2004). It is critical to understand hyporheic exchange within the stream channel in river systems for modeling purposes. One of the challenges of modeling hyporheic dynamics

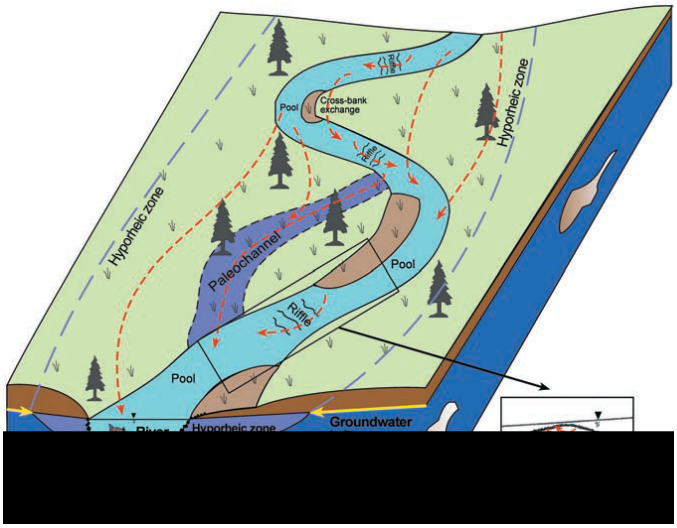


**Figure 1.1:** A schematic representation of the hyporheic zone and exchange dynamics. The hyporheic zone is the region where stream water exchanges with groundwater (delineated with blue dashed lines). Hyporheic exchange operates over many spatial and temporal scales (red dashed lines). Hyporheic exchange is typically induced by variations in the hydraulic head of a stream system. The head gradients are associated with abrupt changes in streambed slope (see inset image of riffle example) or stream meanders and preferential flowpaths. The hyporheic zone at the stream bed and banks represents a unique environment (ecotone) because they are where watershed ground water (yellow arrows) and surface water interact [Figure is taken from the work of Tonina and Buffington 2009]

is to evaluate correctly the effect of hyporheic exchange on the chemistry of the surface and subsurface system. Changes to the chemistry arising from hyporheic exchange can influence biogeochemical processes, and thus downstream water quality (Harvey and Wagner, 2000). For instance, it was proved that nutrient fluxes in HZ is a function of residence time and biological reaction rates, such that redox conditions may operate different in space according to residence times (Pinay et al., 2009).

In the last two decades, increased attention concerning hyporheic processes has led to the development of dynamic models (Packman and Bencala, 2000). Initially the modeling approach, treated the HZ as a storage zone, which idealized mass exchange in terms of a mean exchange rate with a well-mixed hyporheic zone of constant volume (Bencala, 1983). However, evidence from Elliot and Brooks [1997] showed that the hyporheic zone is far from being well mixed and of constant volume (Buffington and Tonina, 2009; Tonina and Buffington, 2009; Wörman et al., 2006) Initial contributions to explain the dynamic behavior of HZ were carried out by Vaux (1968; 1962) then theorized by again Elliot and Brooks (1997). Modeling contributions to these theories have been developed by several studies; as a numerical modeling approach for riffle and pool dynamics (Cardenas and Wilson, 2007b; Janssen et al., 2012; Tonina and Buffington, 2009, e.g.) and additionally as an approach of effect of morphology (meanders, alternate-bars etc.) and groundwater discharge (Wondzell et al., 2009b; Wondzell, 2006; Marzadri et al., 2010) (Figure 1.2). Previously conducted HZ modeling studies influenced by 3-dimensional mechanisms are available through numerical solutions at the reach scale (Trauth et al., 2013; Lautz and Siegel, 2006). The same approach will be followed in this work from a hydraulic point of view. The contribution will be done on the application of hydrodynamic processes in HZ. Numerical representation will be designated on the low-gradient flow stream in order to define redox conditions.

### 1.1.2 Biogeochemical context

Energy and food demand has increased drastically with an increase in human population since the beginning of nineteenth century, therefore the world has faced an acceleration in agricultural and industrial production (Steck et al., 2008). The use of N and C sources has played an important role in meeting the needs of global food and energy production, however, this alteration has also adversely affected the global N and C budget. The biologically available forms of N are typically organic nitrogen, and these bioavailable forms of N are often a limiting nutrient in many terrestrial and aquatic ecosystems. Especially in aquatic systems, nitrogen can be found most commonly in the form of dissolved inorganic nitrogen, which are ammonium $NH_4^+$, nitrate $NO_3^-$, and nitrite $NO_2^-$ ($N_r$ species) (Galloway and Cowling, 2002). As Nr continues to increase so do the frequency and intensity of these detrimental

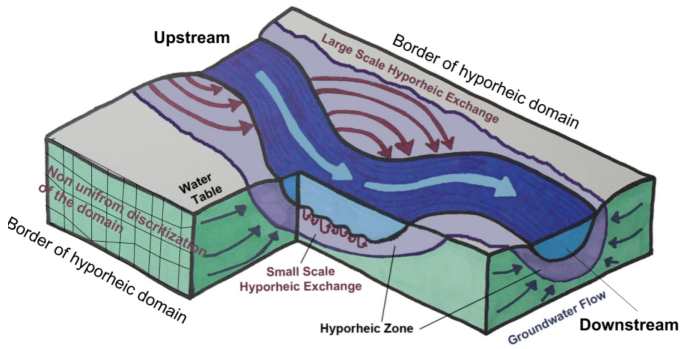


**Figure 1.2:** Typical conceptual diagrams of the hyporheic zone, plan view,lateral cross-section,longitudinal cross-section views that demonstrates the hyproheic fluxes that feeds the hyporheic zone. This figure can be seen as a conceptual diagram for computational domain for discretization. Modified from the work of Stonedahl (Stonedahl et al., 2010)

.

consequences, especially in aquatic ecosystems (Diaz and Rosenberg, 2008). The rate at which humans add Nr to the global budget is also dramatic with rates 5 times greater than that of observed atmospheric $CO_2$ increases over the last 50 years (Davidson and Seitzinger, 2006).

Anthropogenic activities are boosting the rapid accumulation of N and C sources in ecosystems across the planet. The feedbacks between hydrology and biogeochemical cycling of nutrients are of critical importance to global bioavailable nutrient budgets. For instance, human activities are dramatically increasing the amount of Nr in the biosphere, which is causing increasingly frequent and severe impacts on ecosystems (Galloway and Cowling, 2002). These anthropogenic increases in Nr are primarily associated with the increased use of cultivated N-fixing leguminous plants, industrial produced fertilizers, and fossil fuels. Indirectly Nr also alters the global carbon cycle so that C accumulation (Gruber and Galloway, 2008) holds critical importance for climate change. As an integrated part of global ecosystems, streams are important features in the landscape for biogeochemical cycling, because they integrate many sources of terrestrially derived reactive/non-reactive solutes and control export to down-gradient systems via internal source and sink processes. This type of aquatic system is also adversely affected by the detrimental consequences of heavy load of nutrient or contamination. For instance, agricultural pollution and atmospheric deposition with regards to river eutrophication is one important effect that was observed recently especially in England and Wales (Hilton et al., 2006).

River systems have a capacity to reduce the nutrient intrusions, especially via buffering and transformation of $N_r$ species (McClain et al., 2003;

Boano et al., 2010a). Riverine systems also help to rapidly convey excess N, which could not reduced or buffered by the stream or hyporheic zone, from terrestrial environments to groundwater, and coastal marine environments (Tockner et al., 1999). Stream networks have fundamental function as to regulate bioavailable N inputs through biogeochemical processes, therefore, stream systems are important in order to treatment of the excess, or waste nutrients from the environmental system (Hammer and Bastian, 1989). However, it is a challenge to predict and diagnose the variability of the factors controlling biogeochemical dynamics. Nevertheless, it is in our knowledge that the diagnose of the biogeochemical dynamics such as redox conditions, sources and sinks of labile N, is possible once the terrestrial zones were specified and hydraulic dynamics were depicted (Zarnetske et al., 2012; Marzadri et al., 2012; Trauth et al., 2013; Cardenas et al., 2008). HZs are a strategic places in order to initiate depiction of biogeochemical dynamics, because it was proved that a HZ is the most active zone in terms of redox activities inside the river (McClain et al., 2003). The dominant redox activities that are defined in this work is denitrification and nitrification considering $N_r$ species, which in turn leads source and sink conditions (Zarnetske et al., 2012) (See Figure 1.3).

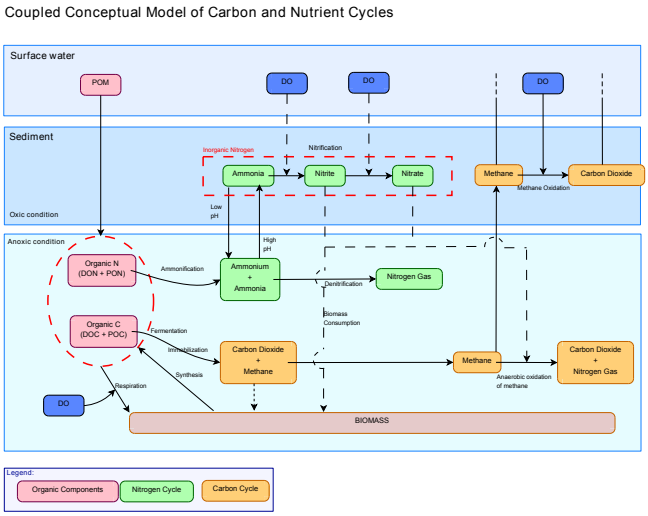


**Figure 1.3:** Conceptual diagram of biogeochemical processes on the hyporheic zone for C and N cycles in the sediment

In this context mixing of solutes such as nutrients or contaminants between sediments and river water is an important concept that involves different disciplines. In the last decades several numerical or statistical models were developed in order to predict spatial and temporal variations of solute concentrations by many different approaches. In this research advec-

tive transport under different discharge conditions is considered as being critical to a biogeochemical approach to depicting redox conditions and aerobic/anaerobic zones. Such a residence time approach, which is different from the transient storage approach that was mentioned in 1.1.1, assumes that the hyporhiec residence time is the concept that links the fate of reactive (bioavailable) solute transport and their biogeochemical transformation with the hydraulic dynamics of the hyporheic zone. Depending on the mechanisms that generate hyporheic exchange, there are different residence time and different mass transfer processes (Elliott and Brooks, 1997; Packman and Brooks, 2001), based on the field and laboratory studies the mass balance is influenced by velocity variations within the river bed (Gomez et al., 2012; Käser et al., 2009). HZ can be characterized by the parameterization of diffusive model and first order mass transfer with neglecting particular source terms (Bencala, 1983), however, in this work the findings of Tonina and Buffington (2007) has been considered as basic mechanisms for our model. In this work, fundamental mechanisms for hyporheic flow dynamics were explained via a numerical model supported by flume experiment in order to investigate 3D pumping process in basic pool-riffle morphology with gravel bed setting.

From biogeochemical perspective, this work is an attempt to describe the relationships between physical and biogeochemical controls and the resulting fate of Nr in a specific reach of River Bure, UK (for details see 2).

The key physical factor investigated is distribution of solutes, which is a function of transport processes - advection and dispersion, and transport conditions – hydraulic conductivity, reaction processes - nitrification and denitrification, and residence time distributions of flow paths.

Different physical conditions such as morphologic, hydraulic and structural result in different characteristic residence times of water and solutes in HZs. The key biogeochemical factors that was modeled and investigated are the dynamics of oxygen ($O_2$), labile dissolved organic carbon (DOC), Nr, typically in the form of ammonium ($NH_4^+$) and nitrate ($NO_3^-$). In this work numerical modeling of coupled transport of the Nr species, ($O_2$) and DOC has been undertaken. To validate the model a suite of pore-water measurements and sediment profiled have been used to identify the key linkages between hydrological and biogeochemical controls on N transformations in a specific HZ.

## 1.2 Motivation and objectives

This work seeks to identify the relationship between the physical advective transport and redox controls within HZs. Currently, there is a gap between known coupling of physical and biological controls on the fate of hyporheic

solutes (Zarnetske et al., 2012). Thus, most investigations of hyporheic biogeochemical controls ignore either the physics or the biology, or are unable to connect the two factors in a robust way (Krause et al., 2009). The limited amount of research that does connect physical and microbiological processes ignores much of the important complexity, such as representing the spatial and temporal coupling of nitrification and denitrification in systems. Furthermore, attempts to incorporate denitrification into stream models do not mechanistically represent the hyporheic zone or incorporate empirical hyporheic field observations (Marzadri et al., 2012; Zarnetske et al., 2012). This work helps to fill this knowledge gap through a combination of field observations and numerical modeling that directly addresses coupled physical transport and redox controls on hyporheic parameters. A multidisciplinary framework was applied to the problem, and methods include fieldwork measurements, mass balance approach, and numerical modeling. The field observations and the numerical experiments of the developed model in this work were completed with the intention to create a new hydro-ecological model, address the role of the HZ on a specific stream system at the reach scale , and to provide a robust data set for future analysis and modeling efforts.

### 1.2.1 Objectives

In practice, the fieldwork component of this work was designed to provide a hydrological conceptualization for the chosen site, and to help develop a 3-D coupled surface-subsurface flow model which enables exploration of hydraulic dynamics and processes in relation to oxic/anoxic zones and redox controls. Specifically the model has been used to explore the spatial distribution of non-reactive particles using the hyporheic residence time concept. A river river reach was created numerically using a process-based framework to predict the changes in residence time of water in the hyporheic zone according to mixed topography and a heterogeneous subsurface system (in terms of stratigraphy and texture). Since biogeochemical processes are directly linked with hyporheic residence time, an increase or decrease in residence times alters the balance of processes occurring in the hyporhiec and thus also the solute concentrations as subsurface flow returns to the river.

The specific objectives and hypothesis of thesis are summarized below:

**Objective 1** A comparison of different discretization of the streambed topography (the boundary between surface and subsurface domains), and an exploration of optimum cell size for interpolation of streambed topography

i An exploration of the effects of differences in detailed topography on water surface elevation for different discharges.

ii Validating whether the 2-D surface-flow model fulfills the cross-validation of water surface elevation and velocity solutions with field measurements.

iii Exploring the effect that the higher resolution discretization has on predicted velocity on bed topography of the reach.

iv Exploring whether detailed topography and morphology has a significant effect on hyporheic residence time.

**Objective 2** Understanding the influence of changes in groundwater on the complex domain;

i Exploring how changes in discharge on surface water influences vertical and lateral hyporheic exchange flows with the effect of regional groundwater flow.

ii An exploration of the extent to which groundwater discharge, resulting from the gradient between the groundwater table and the stream stage, influences surface-subsurface exchange.

iii An exploration of the change in upwelling and downwelling zones under the influence of different surface water and groundwater discharge.

iv Evaluation of the response of the local groundwater to surface water discharge changes

**Objective 3** Creating subsurface heterogeneity by using geostatistical methods for multi-layer and multi-phase models;

i An investigation of the use of core samples (with grain size analysis) for representation of sediment heterogeneity.

ii An exploration of the use of numerical methods for the generation of subsurface heterogeneity (geo-statistical approaches)

**Objective 4** Exploration and analysis of the effect of sediment heterogeneity on hyporheic residence time and the development of aerobic / anaerobic zones

i Exploration of the influence of sediment heterogeneity on hyporheic residence time.

ii Modeling the effect of sediment heterogeneity on aerobic/anaerobic/hypoxic zones to see the changes on transport of particles from the hyporheic residence time perspective.

### 1.2.2 Organizaton of the work

This work addresses the above objectives through a series of five chapters, and each chapter builds on the understanding developed in the preceding text. The thesis starts by presenting a detailed examination of the fieldwork element of the work, with an explanation of the field methods that were followed in order to obtain the hydraulic and biogeochemical observations. The thesis continues with the development and implementation of numerical modeling approaches that are validated by the related field parameter observations. The work was designed in two main parts as follows:

1. Fieldwork practices and methods;

   **Chapter 2** : Field work methods and practices were explained in detail, and a general picture of the reach of interest, in the River Bure (UK) is described. This chapter is designed as three parts; the first section explains the general hydrology of the region and observed hydraulic dynamics at the reach scale, the second aspect focuses on sedimentology and the river bed structure of the reach, the third and the last section describes the hydrochemistry of groundwater and surface water, and provides a biogeochemical explanation of the reach. The chapter seeks to explain the interaction and relationship between these three aspects in order to explain the details of the river and riparian zone.

   **Chapter 3** : The general aim of this chapter is to create the best method that represent river bed topography more accurately by identifying and comparing the most commonly used interpolation methods in the literature. The introduction to this chapter explains the methods and why those methods were chosen. The following sections explain the application of Ordinary Kriging, Inverse Distance Weighting and w/Template methods. In the results section, outputs of the methods were compared using the k-folded cross-validation method. This practice is important because the interpolated bed will be a boundary between the free surface and subsurface model.

2. Hydraulic model and hydraulic analysis of the reach;

   **Chapter 4** : This chapter is the first modeling practice of the thesis. The chapter aims to quantify the effect of complex topography on hyporheic exchange and subsurface flow paths, and the resultant changes in aerobic/anaerobic zones in the subsurface. Model simulations are made under high, mid and low channel discharge conditions in order to predict the changes in effective hyporheic zone by the interaction of measured groundwater boundary conditions. The chapter explains the calibration and validation of the

free surface model via water surface elevation measurements, and the application of bed surface pressure to the subsurface domain which assumes as homogeneous gravel bed. The unitless Unitless Damköhler number (Da) is used with together with chosen reaction rates from the literature in order to depict aerobic/anaerobic zones.

**Chapter 5** : The last methodological chapter of the thesis investigates the effect of heterogeneity on the subsurface model and hyporheic dynamics. This chapter is designed to describe the methodology that was followed in order to create a heterogeneous field using examples from the literature. Heterogeneity is created based on four different textures of materials as gravel, fine sand, silt and clay. The effect of heterogeneity is then evaluated via stochastic hydraulic simulations and compared with the homogeneous case which is considered with fine sand. The change in cumulative residence time distributions was observed in order to explain the effect of heterogeneity. The unitless Damköhler number (Da) is used with the same reaction rates as the previous chapter in order to predict aerobic/anaerobic zones in the heterogeneous case.

# Chapter 2

# Description of Study Reach

## 2.1 Introduction

The hyporheic zone is defined as a region of the riverbed of intensive biogeochemical activities within where surface and groundwaters mix. (Buffington and Tonina, 2009; Boulton et al., 2010). In this zone hyporheic exchange flows through the bed sediment and exchanges dissolved and particulate organic matter,and nutrients (Findlay, 1995). Such exchange maintains the productivity of ecotone of the surrounding reach. (Lansdown et al., 2012). It has been noted that the hyporheic zone is a complex zone which has a functional role on groundwater-surface water interactions (Sophocleous, 2002; Smith et al., 2008), which is significantly diverse in terrestrial boundary, subsurface sediment texture, and effect of watershed hydrology (Triska et al., 1993), and critical with respect to fate of reactive solutes on river environment and groundwater (Storey et al., 2004).

Composition of sediment, groundwater levels and rate of mixing of groundwater into surface water, and river bed topography are the main factors that affect hyporheic exchange on the surrounding riparian zone (Cardenas et al., 2004; Boano et al., 2009; Storey et al., 2003). The changes on topography especially the rapid alteration on sediment along the river bed makes changes on pressure as a result velocities so the exchange flows inside the sediment(Vaux et al., 1962; Vaux, 1968; Elliott and Brooks, 1997). The most dominant formations of a reach can be represented as riffle-pool (Harvey and Bencala, 1993), step-pool (Kasahara and Wondzell, 2003) and meander (Wroblicky et al., 1998) formations over the stream bed which has been defined and modeled by previous works (Tonina and Buffington, 2007; Duff and Triska, 2000; Gooseff, 2010; Cardenas and Wilson, 2007b; Marzadri et al., 2010, e.g.). This formation creates a clear downwelling and upwelling flow over bed topography, where the surface water moves inside the sediment by downwelling zone and turns back to the surface from upwelling zone. Additionally, morphological features of the reach may also play im-

portant role as meanders and bars (Marzadri et al., 2012), such that all formations interactively creates evident downwelling -upwelling zones over river bed.

Hyporheic exchange dynamics are strongly linked with formation of the sediment (surface topography) and groundwater intrusion (McKnight et al., 2004). Early works of Elliott and Brooks (1997) assumes flat boundary at the top of the bed, which is crucial decision for the dynamics of the sediment - water interface, and flow in the vertically semi-infinite domain was driven by sinusoidal pressure distribution along the flat top boundary. Same procedure was followed by Wörman et al. (2006) on three-dimensional domain, however, many field researches show that the models formulated on non-complex of flat bed surface may not be able to accurately represent hyporheic exchange flows (HEFs) (Marion et al., 2002), which in turn may cause mis-prediction of transport of mass in hyporheic zones. The importance of topography of the stream bed as a controlling factor was pointed out by several works (Brunke and Gonser, 1997; Hester and Gooseff, 2010, e.g.). Additional to complex topography, heterogeneous sediments affect HEFs and their dynamics along the subsurface, and which may create oxic - anoxic interfaces as much as delays on median hyporheic residence time (Kessler et al., 2012; Strong and Fillery, 2002; Brandes and Devol, 1995). In order to understand the effect of mixed topography and stream bed heterogeneity on HEF residence time, further modeling efforts were followed in order to evaluate and quantify the effect of heterogeneity on flow, and biogeochemistry of hyporheic zone (Boano et al., 2007; Cardenas et al., 2004; Sawyer and Cardenas, 2009). However, to our knowledge, no study has tested the influence of heterogeneity on complete complex system as highly mixed with meanders and pools scoured out by interaction of flows with woody debris, which has also complex subsurface heterogeneity with different sedimentary components.

This study was carried out within a 300 m reach in an agricultural lowland setting of the River Bure, Norfolk, UK in eastern England chosen because of its complexity on topography as pools created by collapsed woody bodies and, its depositional characteristic in the river bed sediment. The main goal of this chapter to provide information about sampling methods and rationale for studying this reach followed by a presentation and discussion of the hydraulic and biogeochemical observations. The data collected can be divided into four different parts: topographical data for bed topography and interpolation of the reach domain; hydraulic data for checking surface water and global groundwater data for interested reach; and biogeochemical data to diagnose nutrient changes and oxygen status of the reach; and finally, stratigraphy data which is to analyze the texture of the bed sediment in order to classify how heterogeneous the sediment is. Redox conditions of the reach will be diagnosed according to hydraulic observations of channel flow and chemical observations that is analyzed in order to link

the local biogeochemistry, and initial findings of calibrated hydraulic models (see Chapter 4 and Chapter 5).

## 2.2 Methods

### 2.2.1 Study site

Much of the previous research in lowland agricultural catchments has been devoted to resolving the dynamics of nitrate production/consumption and its mechanics within HZs across particular river systems (Duff and Triska, 2000; Fischer et al., 2005; Krause et al., 2009, e.g.). After recognition of the adverse effects of anthropogenic activities, especially an increase in agricultural production, and the consequent drastic increase in nitrate concentrations in surface water and groundwater, the focus of the HZ researches has a tendency to shift to the diminishing function of HZ for removing anthropogenically derived nitrate (Mulholland et al., 2008; Gordon et al., 2013; Lautz and Fanelli, 2008). The study site was known by its rising trend of nitrate level in UK groundwaters (Young et al., 1976; Edmunds and Walton, 1983; Croll and Hayes, 1988). It has been reported that many groundwater boreholes in the UK exceed the current statutory limit on nitrate concentrations in drinking water which applies throughout the European Community (Directive, 1980). Eastern England has been designated as vulnerable area in order to protect ground water from applied nitrogen loads later (Directive et al., 1991). However, the main emphasis of the chosen site is its buffering capacity of biogeochemical parameters in relation with hydraulic dynamics. One important feature of the River Bure catchment is that it is spread over the chalky aquifer system, and groundwater fed chalk streams overlie the catchment, which cause a unique hydrochemistry for the groundwater (Feast et al., 1998), furthermore sand-sized bed sediments overlying chalks and, pronounced meanders and pools make the catchment attractive for further researches on redox complexity interacted with hydrodynamics. Other than quality concerns of the zone, reduction of nitrate has been inferred on several occasions along a low elevations of the catchment and apparent redox control on nitrate distribution, however, there is still no reliable evidence if this reduction results from dominantly in situ denitrification process or simply from an intrusion of different water types in the catchment (Howard, 1985).

#### Catchment and Hydrogeology

The Bure catchment is in the region of East Anglia, where is an area of intense agricultural activity. Most of the land is divided for arable farming that contains a number of main river and wetland habitats. Lower reaches of the River Bure flow through the Broads to the North Sea, this zone can

also be considered as moderately fertile water from bio-ecological aspect (see Figure 2.2). Upper reaches are considered as ecological diverse and an important support for aquatic life therefore some reaches of upper River Bure are designated as Sites of Special Scientific Interest. Interest (Hiscock et al., 2001). Most of the sub-surface geology comprises Cretaceous Chalk, considered as the dominant hydrogeological unit in eastern England, is the major aquifer with a highly basic chemistry (Figure 2.1). Especially in the northern Norfolk area (for location see Figure 2.2), extensive Pleistocene deposits cover the Chalk aquifer and control the distribution of hydrochemical facies which keeps the effective aquifer in the upper layers of the ground (Lin-Hua and Atkinson, 1985; Hiscock, 1993). Aquifer is mostly perceived that the upper $50 - 60$m of the ground formation (Headworth, 1978; Downing et al., 1979).

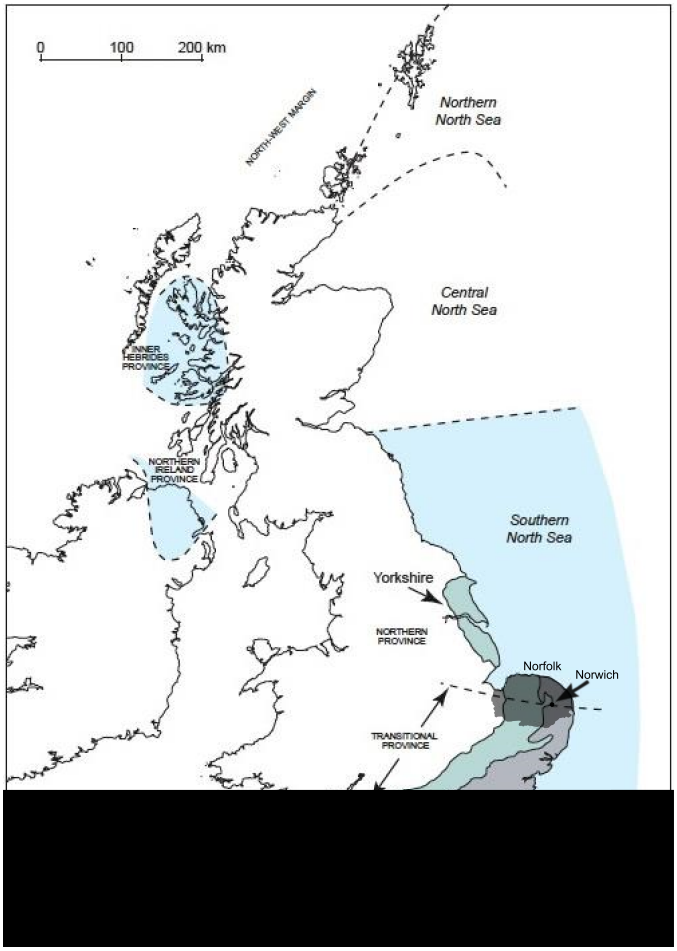


**Figure 2.1:** The Chalk Provinces in the United Kingdom and North Sea, modified from Mortimore et al. (2001)

Riverine areas on unconfined Chalk groundwaters under the river valleys have strictly $Ca-HCO_3$ in character and contain relatively high concentrations of $NO_3$, $SO_4^{2-}$, and $Cl^-$, contributed by mainly agricultural sources according to work of Hiscock (1993). This type of groundwater sourced from an unconfined chalk aquifer accounts for 40% of public water supplies, but can reach as 90% in the rural areas of north Norfolk. In this region, there has already been a dramatic loss of wetlands and the predicted increase in temperature under climate change is expected to have impacts on hydrological regimes, consequently, changes to ground water discharge under baseflow conditions may cause long-term deleterious changes in groundwater hydrochemistry and surface water biogeochemistry in long term (Herrera-Pantoja et al., 2012).

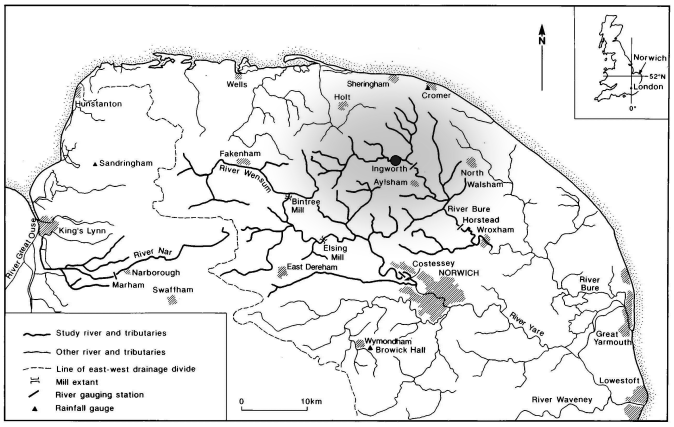


**Figure 2.2:** Location of the catchment and three main rivers that feed sub-catchments; River Bure, Nar and Wensum, and the locations of gauging stations which gives an overall information of groundwater level of the region. Highlighted area is the sub-catchment of River Bure, that flows over Great Yarmouth to North sea, and black dot shows the reach which was investigated. (Modified from Hiscock et al. (2001))

### River reach

The field site comprises a reach 300 m channel of the River Bure within the grounds of Blickling hall, United Kingdom (N 52°49.27′ E 1°12.23′), where surrounding area is predominantly of agricultural land use. The channel can be characterized as sequences of meander parts, and low gradient riffle and pool formations especially on the most forestry and vegetated zones. The sediment structure of the stream bed is composed of mostly very fine sand, silt and deposited organic matter, and partially unconsolidated gravel sands and silts cover the river bed, which stems from the soil erosion from the surrounding arable fields. It was demonstrated that the hydrological and hydrochemical effects of the Chalk aquifer on Bure Catchment and the

main rivers around the catchment in several ways (Hiscock, 1993; Feast et al., 1997; Hiscock et al., 2001; Herrera-Pantoja et al., 2012). The low topographic relief produces a low streambed gradient of $0.2 - 0.5$ m per 100 m. The stream itself lies in a bed of recent alluvium, 1 m deep and at least $7 - 10$ m wide on each side of the stream. At the sampling site the stream is approximately 7 m wide, varying in depth from about 0.15 m to 0.8 m(measurable depth). In summer, base flow discharge is about 0.1 $m^3/s$ (For hydraulic profiles see section 2.3.2).

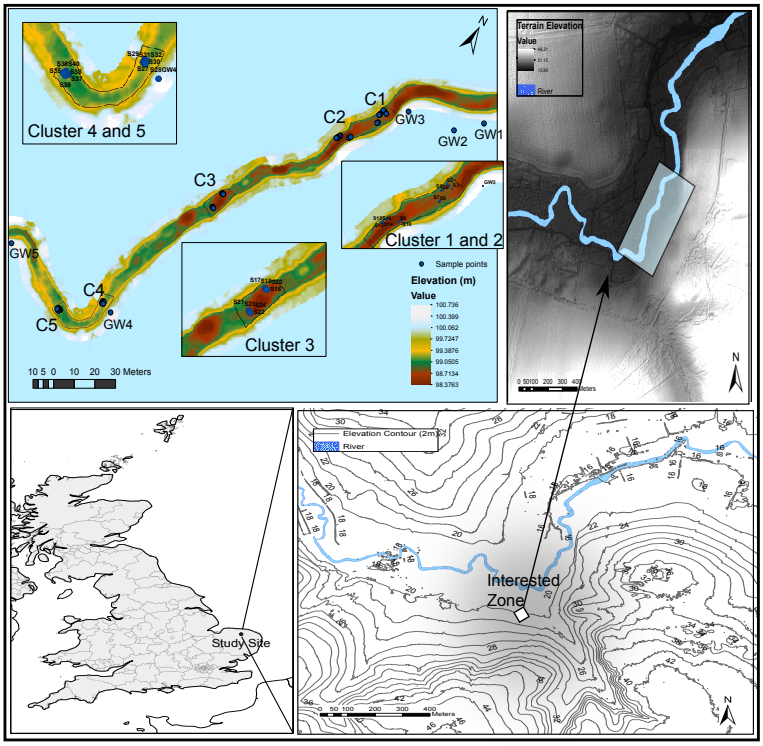


**Figure 2.3:** Map of the reach and its location in east England, Bure Catchment on northern part of River Bure, Blickling hall (bottom). The map to the bottom right shows the location of the region and contour maps of the catchment. On the color map to the upper left, Blue points indicate sampling locations for April 2013 respectively, additional to cluster location from upstream to down stream, points for groundwater measurements have been demonstrated. Color shading on the site map indicates streambed elevation.

### 2.2.2 Field procedures

#### Sampling strategy

Selected reach is important as a feed stock to aquatic life and crucial for riverine ecotone of the zone. The river system on interested catchment ,as

seen in Figure 2.3 (Bottom right), is documented as strongly groundwater fed river, which has The Chalk aquifer underneath (Feast et al., 1998). On top of that the land use in area is mostly based on agriculture, therefore, there is an high expectation of nutrient intrusion to the reach. Another factor should be notified is that the specific reach is highly vegetated therefore, river bed sediment may have big amount of labile organic matter content different than gravel bed rivers. All those factors depicts a picture of a possible hyporheic system which is influenced by complex hydraulic and biogeochemical dynamics.

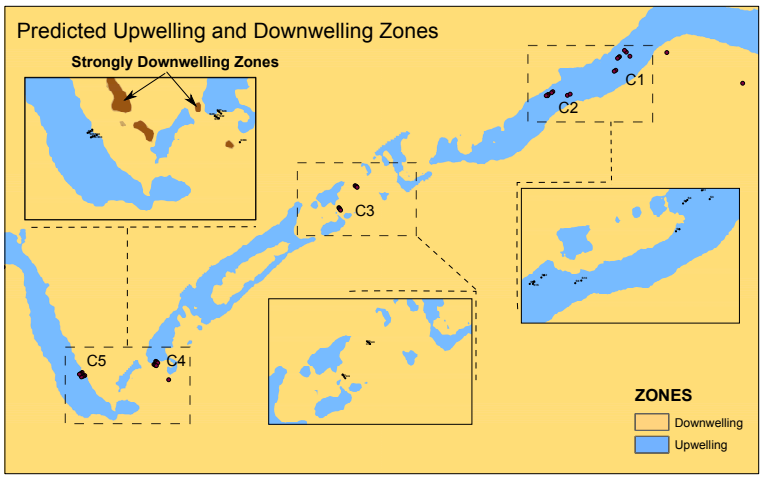


**Figure 2.4:** Demonstration of predicted upwelling and downwelling zones on specified reach. Details are demonstrated according to locations of clusters, red points indicate sampling locations for April 2013. Dark brown areas are notified as high magnitude downwelling zones. Predictions were made by initial numerical model with discharge rate of $0.5\,m^3/s$, and zones are valid for $20\,cm$ depth of the sediment from the bed surface

### *Topographical Data*

The topographical data is needed to depict the banklines and river bed surface of the reach, which is important to create boundary for hydraulic modeling purposes both surface and subsurface domain. Topographical data will be used in the processes of interpolation of the boundary in order to estimate the physical limits of the domain (for details see Chapter 3). The bathymetry data were collected by Total Station equipment which is an electronic theodolite (transit) integrated with an electronic distance meter (EDM) to read slope distances from the instrument to a particular point (Kavanagh, 2010). For each bathymetry point, the measured (x,y) coordinates are the longitude and latitude, and the bed elevation obtained from the readings from Total Station. The bathymetry data for the study reach

comprises a set of 745 points for river reach, which are scattered on the reach as measurements of cross-sections, and 243 points for the banklines. The distance between the points are around 1 to 2 m longitudinally and at 0.30 m intervals across the reach. The average elevation of all points is $99.18 \pm 0.35$ m with maximum elevation of 101.35 m on the upstream bank line, and the minimum elevation is 98.29 m on the central part of the reach which is closer to downstream. The distances among the point elevation data varies and there are zones with scarce measurement as well as more dense point areas because of deep pools and in places marginal vegetation with deep fine sediment bulks which prevent the access (For visual examples of the reach see Figure 2.5).

(a) (b)

**Figure 2.5:** Pictures of central part from the reach. We can see the upper fine sand sediment and unaccessible banks along the reach; (a) right after the meander part; and (b) before the riffle and pool part.

The kernel of sampling strategy in this work relies on the basic theory of riffle and pool (Turnover) dynamics of Elliot and Brooks (1997) as explained in Chapter 1. In which hyperhoic exchange is relies on the pressure difference on the river bed. Therefore, following to this simple assumption, hypothetical upwelling and downwelling zones have been observed in the pilot field work and simulated by numerical model after pilot work. Initial

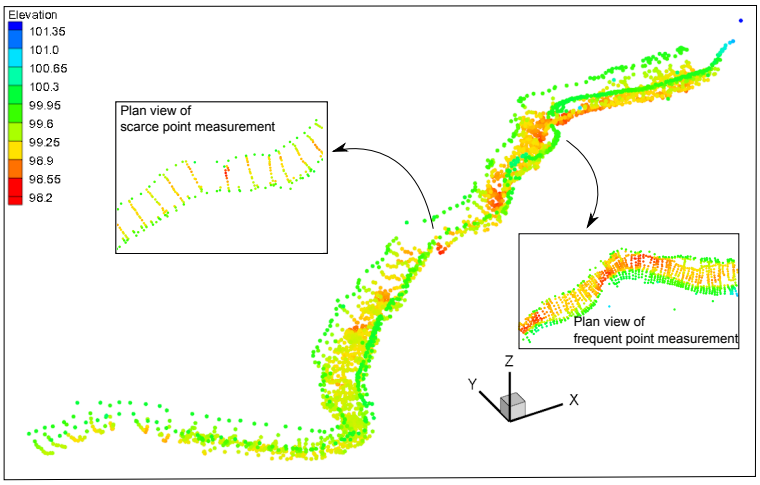


**Figure 2.6:** Demonstration of measures topographical scattered data from the reach. Scattered data over reach has been collected with a varied intervals.

numerical model has been created in order to calculate exchange flows into hypoerheic zone in order to predict downwelling and upwelling zones (See Figure 2.4).

According to strategy, reach has been divided into 5 different zones due to the location of porewater samples, and first allocations of the pore-water samples have been done according to hypothetical representation of upwelling and downwelling zones due to the river bed topography and initial predictions of the model. The estimation of the upwelling and downwelling zones has been made in balance of measurement water surface elevation and in-situ steady state water table levels in vicinity of the river (shown in Figure 2.3).

### *Surface Water and Groundwater Elevation*

Previous research conducted at River Bure catchment and vicinity of the area. Field observations have detailed the geology and hydrology of the selected area. The following section describes the overall stage level and hydraulic characteristics of the study area that are relevant to this work.

Piezometers were constructed from 3 cm(outer) diameter PVC (polyvinyl chloride) pipe with a 50 mm wall thickness in order to withstand high-flow events. Each piezometer has a screen length of 6 cm perforated with 5 mm holes and wrapped with a permeable mesh. A base plug was installed in the piezometer to prevent ingress of sediment during installation and vertical flow within the piezometer, and thus permit more reliable estimates of level with the logging device. Piezometers were installed in September 2013 with a screw auger in the river bank. Four piezometers were installed to determine groundwater levels in upstream, central and downstream sec-

tions of the reach. For each bankside piezometer a target depth of 50 cm below the bed of the center of the adjacent channel was aimed in order to observe hydraulic changes on stage in a consistent manner. It is observed that manual dip of ground water levels are between $24.5 - 75$ cm on site, and initial correction made according to this initial measurements. A Solinst Gold levelogger was inserted into each piezometer, that were barometrically corrected in order to have accurate barometric pressure values. Dataloggers were used recording stage level changes adjacent to the river. Housing the logger instead in a piezometer allows for much more convenient sampling, and provides the logger protection from debris during times of high flow. The datalogger stage data recorded between $5^{th}$ of September 2013 to $16^{th}$ of February 2014. Data were downloaded in order to capture changes in water level arising from storm events as well as investigate relative water levels between rivers and banks under summer base-flow conditions. The groundwater measurement locations were arranged according to observe the direction of the subsurface flow; GW 5 and GW 4 piezometers are to understand the subsurface water level change along the meander part and triangle of piezometers at the upstream location (GW 1-3) are to give the subsurface level and the direction of flow on the bank line.

Field studies, used to support in order to calibrate the boundaries and validate the model results (see Chapter 4 and Chapter 5) , consisted of measuring hydraulic head distributions in three dimensions within the single 280-m-long site. Water surface elevation values have been measured from the thalweg in order to validate the results of the free surface model on September 2013 by using Total station equipment for the rough measurement of water surface. Stream flow velocity profile were collected from 5 cross-sections each has $0.5 - 0.7$ m distance between each other transversally to the bank along the reach that were chosen in order to capture the discharge at different parts of the site and were used to calculate average discharge. The electromagnetic flow meter was also used to capture velocity readings from $10, 30$ and $60$ m depths over each cross-section along the reach. It is observed that there was no measurable change in discharge along the specified reach at the time of measurement that is $7^{th}$ of September, which was estimated as $0.5\,\mathrm{m}^3/\mathrm{s}$.

### *Porewater Collection for Biogeochemical Data*

Porewater sampling involved collection of pore water from 15 cm depth in the river bed using a mini-probe system analysis, which requires water sampling by miniporbe system that involved collection of water samples for standard laboratory analysis. The sampling was followed as two techniques are specifically designated to; measuring in-situ, trace dissolve concentrations of $Cl^-$ and nutrients, providing and integrated measurement of species concentration throughout the monitoring period .

According to work of Trimmer and Sanders (2006), miniprobe system is constructed out in two general parts, Stainless steel tubing (400 mm long by 6 mm ID and 8 mm OD). At the top end, the threaded lure of a 6-inch stainless steel needle screws into a collar insert. The needle runs down the probe, and the tip protrudes through a rubber seal in a collar (PVC) set up from the bottom opening. The miniprobes were inserted individually into the sediment without the use of a collar to ensure wide spatial coverage of sampling ($0.2 - 1$ m between probes within a cluster) (Figure 2.7).

The bottom of the probe is drilled with 2 rings of 4 small holes (2 mm ID). The inside of the 8 holes are covered by a tightly fitting filter (10 by $\times$ 6 mm) trimmed to fit (Slimline Filter Tips, Swan, UK), into which the protruding needle tip is embedded. Probes and fresh filters attached to the probe were flushed with 20 ml deionized water (Purelab Ultra, Elga Lab Water, UK) before insertion into bed sediment to remove and impurities before sampling. The filters serve only to coarsely screen the pore water to prevent needle blockage, and the precise filter properties have not been determined. The probes are inserted observed in order to their decreasing penetration; highly conducted soil tends to be filled faster than the lower one. Since as a pilot project porewater samples were taken in first 20 cm depth in order to quantify the patterns and extent of nitrate concentration changes at small-scale for the top streambed sediment, and each probe pumped individually, the collar was not used. In case of using collar, after insertion of the probe system into the sediment each probe remained can be locked in place by a securing bolt.

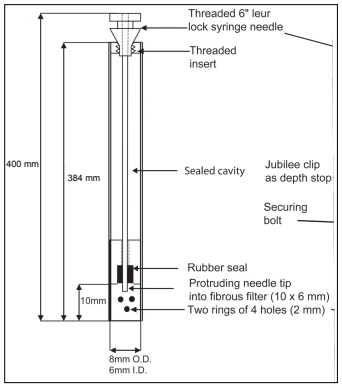


**Figure 2.7:** Detailed diagram of a single probe (modified from (2006))

### *Treatment of samples for Biogeochemical data*

10 ml of porewater were collected from each location for chemical analysis of DIN species (nitrate and ammonium), dissolved organic carbon (DOC), chloride, sulphate and dissolved oxygen (DO). DIN species, DO and DOC were chosen in order to observe if there is complete denitrification/nitrification processes prevailing according to redox conditions in the top streambed sediment, chloride, sulphate were chosen in order to observe the groundwater intrusion to the hyporheic zone. DIN species were measured from the same porewater samples. General treatment in the field trial is same for all DIN species. After collecting porewater samples by typical medical syringe for 10 ml , all water samples (with the exception of those collected for DO) were filtered at 0.2 µm into different vials depending on the solute of inter-

est. After filtration samples were taken into coolbox to keep the samples in an optimum temperature. Additionally, samples were filtered through a 0.45 µm Jim filter following extraction and then split. Samples for DIN and anion analysis ($SO_4^{2-}$, and $Cl^-$) were frozen in the field until analysis on a Dionex ICS-2000 or Skalar San++, pH of the pore water was measured in the field using a WTW 340i multi-parameter probe. The detection limit and precision of $Cl^-$ and $SO_4^{2-}$ was 2 µmol/l ± 1%, 5 µmol/l ± 1% respectively by measuring Dionex. $NO_3$−N, $NH_3$−N and $NO_2$−N were measured via auto analyzer (Skalar San++) and standard colorimetric techniques, with detection limit and precision of in turn 3 µmol/l ± 3%, 0.3 µmol/l ± 5%, 0.1 µmol/l ± 1%.

Exetainers for collection of DOC samples were pre-heated to 500 °C to remove any impurities and the caps of the exetainers are covered with sterilized aluminium foil. After sampling process, %18 hydrochloric acid (HCL) added into exetainers to acidify samples.

Dissolved oxygen (DO) samples also measured from the same locations of DIN parameters of the specified reach. Since DO parameter is crucial for the evidence of redox conditions and locations of aerobic/anaerobic zones extra care was taken and in-situ method was used instead of laboratory intensive methods. The Winkler method Montgomery et al. (1964) was followed in order to keep and analyze dissolved oxygen concentrations in the sediment in-situ. Prior to fieldwork, Winkler A (*Manganese (II) chloride*) and Winkler B (*Alkaline iodide*) solutions were prepared. 0.1 ml of Winkler A and 0.1 ml of Winkler B were added to 12 ml of sample. Solutions were drawn slightly more than the required volume in to 1 mL syringes. A precipitate forms in the container and samples were turned over to ensure complete reaction of the reagents with the water sample. The samples were stored upside down to ensure no oxygen reached the sample in a coolbox.

### *Sediment Core Sampling*

The use of sediment samples was necessitated by the need to designate accurate, in-situ, sediment types and their texture, and observe the layers in order to understand the river bed sediment content and texture. In this work the purpose of sediment core sampling was done in order to explain calculating average grain size for the homogeneous subsurface modeling condition along with permeability and hydraulic conductivity estimates. The analyses were followed due to sorting quality of the sediment and the patterns in sediment texture in order to describe realistic heterogeneous subsurface conditions. We used 22 independent sediment cores recovered from different parts of reach which corresponds to the pore-water sampling points. 50 cm long and 4 cm diameter (inner) cylinder tubes were used to collect sediment cores (Figure 2.8). Stratigraphy of sediment cores was described in the field. Cores were sub-divided according to observed stratigraphy and the layers

were individually bagged for analysis. In order to treat sediment samples for particle size analysis, gravels were removed from the samples by passing wet sediment through a 2-mm sieve by gentle shaking. The removal of gravels was necessary to allow homogenous subsamples of , 3 g of wet sediment to be transferred into gas-tight vials (12 ml Exetainer, Labco) in order to determine absolute particle size of $< 2$ mm fraction. In order to define sediment structure and texture along the reach accurately gravel layer measurements and depths have been noted and sorted out.

The absolute particle-size distribution of the sieved samples was determined by laser diffraction (LS 13 320 Beckman Coulter Counter) after digestion with 30% hydrogen peroxide to remove organic matter. Particles $> 2$ mm were sorted by sieving air-dried material and weighing the separated fractions. The organic carbon content of reduced sediments was treated using elemental analysis (Thermo Finnigan Flash elemental analyzer) after treatment of 1 mol/lHCl to remove carbonates as defined in the work of Hedges and Stern (1984).

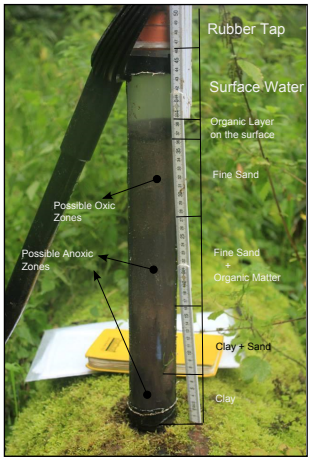


**Figure 2.8:** Example of a core sample from sediment. Thickness of all layers and textures were noted for each sediment cores.

### *Sediment Core Analysis*

Particle size is a fundamental property for sediment formations where most of biochemical activities occur, hyporheic fluxes diversifies strongly according to changes in particle size and sediment texture. Particle size affects sediment entrainment, transport and deposition, and therefore provides important clues to the sediment provenance, transport history and depositional conditions (Friedman, 1979; Sheridan et al., 1987). The core samples were observed and divided into layers, and documented according to different textures in-situ in order to prepare the sediment specimens for lab analysis.

Statistical summary parameters generated, which mathematically describe the particle size distribution, including mean, median, mode, standard deviation, variance, skewness (degree of symmetry), kurtosis (degree of peakedness), and cumulative percentile values (the particle size at which a specified percentage of the particles are finer). The implication is that several sub-samples of each core samples and averages of the all main parameters were taken in order to adopt general statistics. Statistics were calculated based on the method of moments (either normal and log-normal distribution). Size distribution data from laser granulametry. Statistical

parameters have been calculated by using the GRADSTAT statistical package (Blott and Pye, 2001). The value of secondary and tertiary modes were calculated and particle size statistics using alternative Folk and Ward (Folk and Ward, 1957) equations were determined. With this method the relative proportions of sand, silt and clay in the sample were estimated.

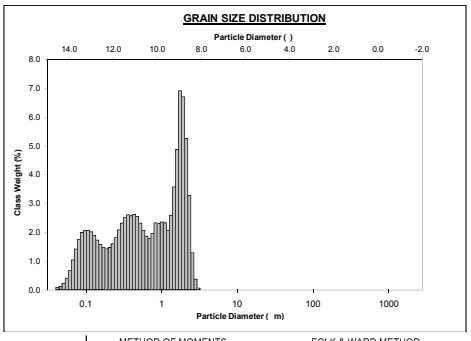


| | METHOD OF MOMENTS | | | FOLK & WARD METHOD | | |
|---|---|---|---|---|---|---|
| | Arithmetic | Geometric | Logarithmic | Geometric | Logarithmic | Description |
| | µm | µm | ϕ | µm | ϕ | |
| MEAN ($\overline{x}$): | 0.919 | 0.563 | 10.80 | 0.550 | 10.83 | Clay |
| SORTING ($\sigma$): | 0.754 | 3.042 | 1.605 | 3.161 | 1.660 | Poorly Sorted |
| SKEWNESS ($Sk$): | 0.530 | -0.408 | 0.408 | -0.230 | 0.230 | Fine Skewed |
| KURTOSIS ($K$): | 1.892 | 1.897 | 1.897 | 0.701 | 0.701 | Platykurtic |

(a)

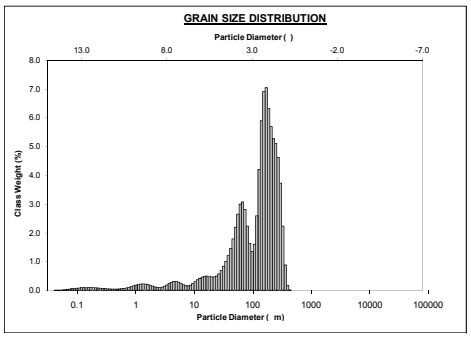


| | METHOD OF MOMENTS | | | FOLK & WARD METHOD | | |
|---|---|---|---|---|---|---|
| | Arithmetic | Geometric | Logarithmic | Geometric | Logarithmic | Description |
| | µm | µm | ϕ | µm | ϕ | |
| MEAN ($\overline{x}$): | 139.6 | 87.69 | 3.511 | 110.8 | 3.174 | Very Fine Sand |
| SORTING ($\sigma$): | 90.29 | 4.010 | 2.004 | 2.956 | 1.563 | Poorly Sorted |
| SKEWNESS ($Sk$): | 0.272 | -2.379 | 2.379 | -0.536 | 0.536 | Very Fine Skewed |
| KURTOSIS ($K$): | 2.223 | 9.665 | 9.665 | 1.424 | 1.424 | Leptokurtic |

(b)

**Figure 2.9:** Grain size distributions was documented according to percentage of class Weight over particle diameters in logaritmic scale; (a) Clay sediment with calculated ststistics; and (b) poorly sorted very fine sand distribution.

Samples were compared, selection of the most appropriate statistical measures is partly a matter of user preference and partly determined by sample type (e.g., whether the sample is unimodal, multi-modal, or log-normally distributed or not). The most robust (i.e., least subject to random variation) measures for discriminating between samples have been found to be the modal particle size, the median size ($D_{50}$ value) and the measure of

distribution spread defined by the difference between the $90^{th}$ and $10^{th}$ percentile values ($D_{90} - D_{10}$). When comparing samples, a number of statistical measures need to be used, including the percentages of sand (63–2000 µm), silt (2–63 µm) and clay (< 2 µm), mean, median, primary mode, secondary and tertiary modes , standard deviation and $D_{90} - D_{10}$ (measure of sorting). In addition, the shape of the particle size distribution curve, plotted using a logarithmic size scale. Great care is needed when interpreting open-ended (i.e., truncated) distributions, or where the sediment is not unimodal, since many of the statistical parameters, including the mean, skewness and kurtosis can become unreliable. In such instances, the sediment is best described by the position of the modal size values, defined percentile values, and inflection and turning points on the particle size curve (see Figure 2.9).

## 2.3 Results

### 2.3.1 Observations of Sediment

Variation in results due to core sampling is determined by analyzing multiple sub-samples taken from the same parent sample. As illustrated on Table 2.1 presents particle size summary data obtained by running 22 different core samples of three contrasting sample types. Sediment characteristics were refined according to repetition of the same sediment types along the different parts of the reach. According to analysis from all core samples three contrasting sample types defined as (a)Modaretaly sorted polymodal fine sand (b)poorly sorted polymodal silt and, (c) poorly sorted polymodal muddy clay sediments. In this analysis particles more than 2mm have not taken account, depths and locations of gravel were noted by the time of sediment core sampling.

Find sand is predominantly composed of medium sized, fine and very fine sand, and has polymodel asymmetrical poorly sorted size distribution (see Figure 2.9(b)). In most of the core samples the very coarse silty fine sand was observed which has the average grain size of 114.1 µm, and corresponds to classification of fine sand, also some samples show transactional characteristic from very fine sediment to silt or vice versa which are also classified as very poorly sorted polymodal sample. The mud exhibits also poorly sorted, compilation of bimodal to polymodal distributions in some locations of the reach, predominantly composed of mostly clay and proportionally small amount of silt, however, no sand component was observed.

Sample heterogeneity was found to be the dominant factor influencing the reproducibility of the sediment type, moderately sorted fine sand and poorly sorted silt were found to be the most reproducible with the coefficient of variation for the mean size as of 0.82% and 0.55% respectively. On the other hand Clay have a higher coefficient of variation of 3.47% for the mean particle size. In general evaluation, according to core sample analy-

**Table 2.1:** Average particle size distribution data for 22 separate core samples of three contrasting sediment types

| scale | Fine sand | | | Silt | | | Clay | | |
|---|---|---|---|---|---|---|---|---|---|
| | Average (µm) | SD. (µm) | CV (µm) | Average (µm) | SD. (µm) | CV (µm) | Average (µm) | SD. (µm) | CV (µm) |
| Mean (µm) | 114.1 | 3.6 | 0.8 | 22.8 | 1.8 | 0.6 | 0.6 | 2.1 | 3.5 |
| Median (µm) | 181.1 | 1.6 | 0.5 | 36.4 | 2.0 | 0.6 | 0.5 | 1.8 | 0.6 |
| Primary mode (µm) | 232.1 | 1.4 | 0.3 | 76.9 | 3.4 | 0.7 | 1.2 | 2.8 | 0.5 |
| Secondary mode (µm) | 127.0 | 2.1 | 1.1 | 60.0 | 1.8 | 0.7 | 0.3 | 2.9 | 1.7 |
| $D_{90} - D_{10}$(µm) | 199.0 | 2.9 | 0.5 | 114.9 | 1.9 | 0.5 | 1.9 | 1.2 | 0.3 |
| Std. Dev | 1.8 | 0.2 | 0.1 | 1.8 | 1.1 | 0.1 | 3.1 | 1.2 | 0.2 |
| Sand (%) | 77.8 | 12.5 | 0.2 | 34.2 | 18.3 | 0.5 | 0.0 | 0.0 | 0.0 |
| Silt (%) | 18.6 | 10.5 | 0.6 | 54.4 | 16.0 | 0.3 | 9 | 4.4 | 0.5 |
| Clay (%) | 3.6 | 2.2 | 0.6 | 11.4 | 3.5 | 0.3 | 91 | 4.4 | 0.1 |

Standard deviation (S.D.) and coefficient of variation (CV) are given to illustrate the reproducibility in the various parameters. Median value represents $D_{50}$. All parameters were adopted by averaging several statistics calculated from core sub-samples. Averaging of particle size related parameters were calculated as geometric and percentages were calculated as arithmetic mean.

sis and resulting texture/sediment type assuming a hydraulic conductivity of 0.00254 m/min appropriate for these sediments (median particle size between 1 and 2 mm, $D_{10}$ 0.1 mm, (Domenico and Schwartz, 1998; Fetter and Fetter, 2001)).

### 2.3.2 Hydrological observations

Horizontal stream water velocity was relatively high in the channel thalweg sites ($0.1 - 0.4$ m/s) with relatively coarse sediment (Average $D_{50}$ is 200 µm and the $D_{10}$'s averaging on 50 µm that were likely to have lesser grain surface and greater hydraulic conductivity if we omit relatively small area of gravel on the riverbed. Side cavities,in contrast, had slower stream water velocities ($< 0.01 - 0.1$ ms) that created lesser driving force for hyporheic flow through the finer than average sediments (Average $D_{50}$ is $1 - 10$ µm and the $D_{10}$'s averaging on $< 0.1 - 1$ µm such as clay and silt textures. Small size sediment types were likely to have greater surface area per volume, however, lower hydraulic conductivity (see Table 5.1). However, the average grain sizes of the core samples on thalweg and the ones on the vicinity of bank does not show any significant difference (ANOVA $p = 0.36$)(see Figure 2.10). The cause in difference of velocity can be expected from shear stress of open channel flow dynamics and vegetation closer to the banks.

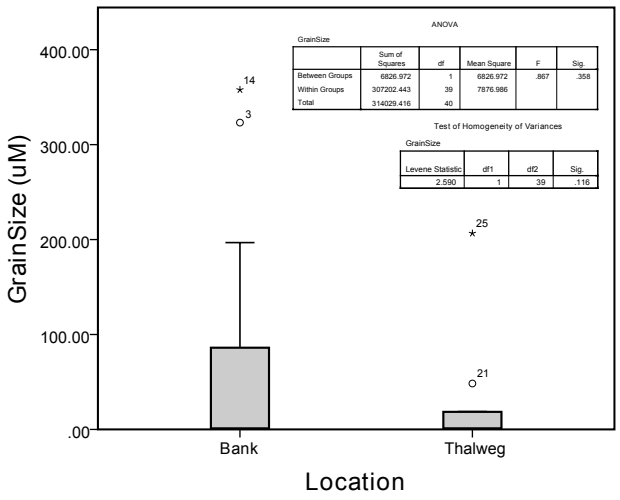


**Figure 2.10:** Box-plot of average grain sizes of the core samples from Thalweg and from the vicinity of the bank. Statistics of ANOVA is also showed

The height of the subsurface water table in meandering part of the river changed at least 20 cm along the river during the logging time (Figure 2.11), indicating movements of large quantities of water in and out of the bar over fairly short periods of time (possible rainfall event). For instance, the water

table dropped 7 cm in 5 d between September 10 to 15 and recovered in 3 days higher level than previous one after a probable heavy rainstorm ( $10^{th}$ and $15^{th}$ of November in Figure 2.11). The slope of the water table ranged from a maximum of 0.001 % to a non-detectable difference in height from the upstream to downstream end of the well transect (Figure 2.11) which shows a slight change inside the level of water towards the river channel. When there was a measurable slope to the water table, the implied direction of water movement was always from the upstream to the downstream ends of the transect. Water velocities on the order of $0.03 - 0.05$ cm in a day were estimated from the water-table slope of the groundwater level measurements.

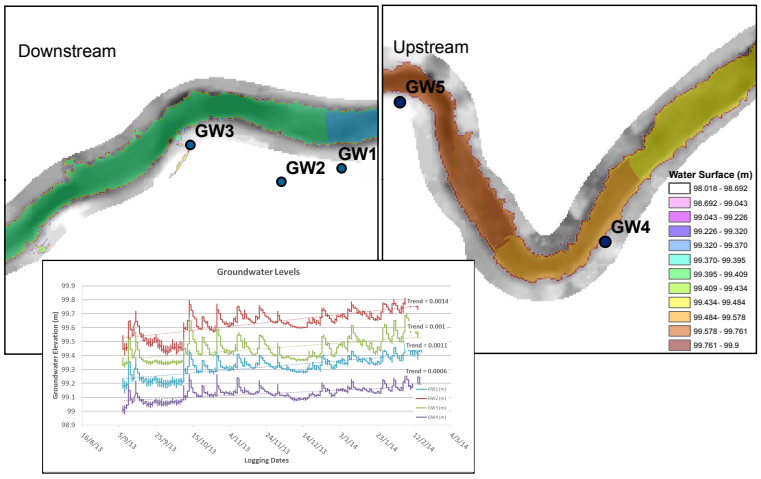


**Figure 2.11:** Color map of spatially distributed water surface elevations and ground water level observations on the vicinity of the reach during the time of measurement. The locations of data loggers have been demonstrated on reach scale with spatially distributed water surface elevation values. The graph shows (one on the bottom) the groundwater level readings of four piezometers from 5th of September to 16th of February.

### 2.3.3 Biogeochemical Observations

The river reach was in average-flow conditions as $0.5\,m^3/s$ and average groundwater level was not exceeding water surface elevations (see previous section) by the time that data collection was being done. Data collected from surface and groundwater indicates some differences in between, in surface water average values show that since there are relatively high amount of $NO_3{-}N$ as 5.05 mg/l and higher value $SO_4^{2-}$ and $Cl^-$ as 27.36 and 18.31 mg/l respectively. The other parameters as $NO_2^{2-}$-N , $NH_3^+$-N and DOC remains lower as $0.031, 0.00$ and 3.7 mg/l respectively. $NO_3{-}N$ values of surface water indicates that the river holds the characteristic of agricultural area and this amount may show organic intrusion from sur-

rounding area (Harvey et al., 2013), fortunately there is no transformation of organic matter into $NH_3^+$-N, which may ecologically harmful. On the other hand, average groundwater $NH_3^+$-N is around $0.47 \pm 0.12$ mg/l in the upper levels of groundwater, where also DOC values are significantly higher as $9.28 \pm 5.6$ mg/l. $SO_4^{2-}$ and $Cl^-$ measurements show similar range with respect to surface water as $24.9 \pm 4.9$ and $16 \pm 10.3$ mg/l respectively. Since the measured sample sizes are 5 and from different locations (piezometers) the range of the values are varies, however, it is suffice to compare the average values.

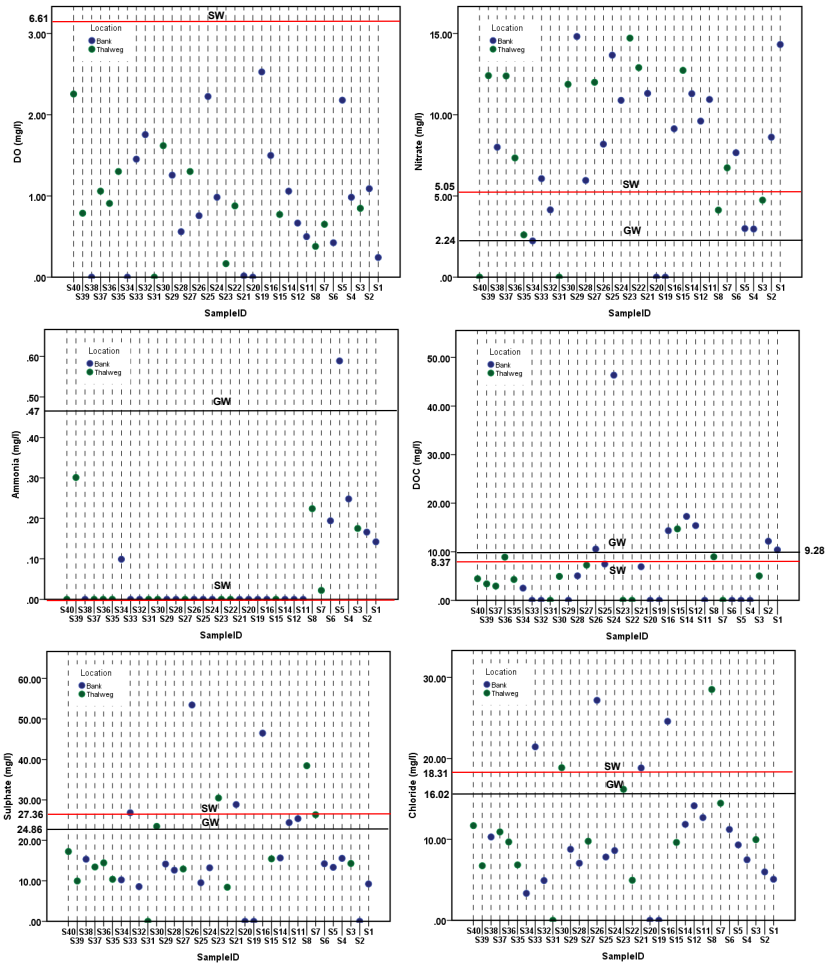


**Figure 2.12:** Point graphs of biogeochemical parameteres along the reach from upstream to downstream (starting from S40). Blue dots represent the sample points close to the bank, green points represent the measurement on or close to thalweg. Red and black lines show in turn the average surfacewater and groundwater values of the measured parameters.

Channel thalweg sediments had pore water chemistry nearly similar to

the stream and groundwater values. Conversely, especially ammonia concentrations in porewater were generally below detection limits (Figure 2.12) with the exception of C1 (S1-8,see Figure 2.3), where ammonium concentrations were about half that found in the groundwater (0.47 mg/l). Ammonia concentrations again are significantly different from the other porewater clusters ( multiple comparison post hoc $p < 0.05$, and according to ANOVA analysis, see Tukey's homogeneous subset analysis in Appendix A). Comparing with groundwater samples, however, according to ANOVA analysis, pore water samples of C1 is also not significantly related with groundwater neither ( $p = 0.001$). Therefore, most probably groundwater intrusion is higher in downstream part than the rest of the reach, where also groundwater and surface water levels are in agreement with each other ( 99.3 m (see Figure 2.11)).

Sediment grain size (according to $D_{50}$), dissolved nitrogen species, dissolved oxygen, microbial activities, Sulphate and Chloride values are compared for representative channel thalweg and side cavities. According to analysis in spite of the slight difference among, Nitrate,DO and DOC parameters which are lower on the thalweg and relatively higher on the sides, no significant difference is observed between the sides and thalweg concentrations (See ANOVA analysis, Appendix A). Even the microbial activity is slightly lower on the sides, there is not particular difference on particle sizes. Particulate organic carbon (POC) is the highest in surface layer of very fine sediments. The analysis show that the POC values are ranging between 1 and 3% by weight, which is in agreement with surface water POC percentage. In this set of materials measurements indicates that the hydraulic changes on surface water, as velocity changes on margins and thalweg of the channel does not have direct effect on biogeochemistry in 15 cm deep sediment from the surface.

At all sites $NO_3{-}N$ in pore water ranged between 0 to 15 mg/l, and average porewater $NO_3{-}N$ concentrations are higher than surface and groundwater (in turn 5.05 mg/l and 2.24 mg/l). Measurements along the clusters starting from upstream to downstream do not show any significant pattern, nevertheless, difference between porewater measurements with the ones of groundwater is significant ( ANOVA and Tukey's comparison $p = 0.023 < 0.05$ ). Concentrations of porewater are closer to average surface water values of $NO_3{-}N$. DO measurements in porewater ranged between 0 to 2.5 (without extreme values) that are significantly lower than average surface water values (ANOVA $p < 0.01$), and show hypoxic conditions in porewater in 15 cm depth.

Variogram analysis have been applied along the downstream to upstream in order to diagnose and analyze the trend and change along the river reach. Correlations and variogram trends among the physical and chemical variables measured in the hyporheic zone do not show any favorable trend and

denitrification conditions in hyporheic flow (Figure 2.13). Since trend in DO is not clear, the oxygen level is in the band of $0.2 - 1.2\,\mathrm{mg/l}$ in the range of 180 m distance on linear transect of the reach, which can be considered as hypoxic conditions. Nitrate and ammonia compounds show oscillatory behavior in the range of $10 - 35\,\mathrm{mg/l}$ concentration, however, for this set of data it is not possible to capture a significant trend along the reach. Instead of reducing nitrate value, reach behaves as a source of nitrate. DOC transect shows a reduction on 80 m distance, which is central part and shows a significant increase on downstream part of the reach ($140 - 160\,\mathrm{m}$), where we can see significant increase on $NH_3{-}N$ and decomposition activity, on top of that, percentage difference of carbon and nitrogen compound is significantly increasing on the same part.

## 2.4 Discussion and Conclusions

In this section discussion is followed alike as the design of this chapter. Interpretations of hyporheic zone in this particular reach are divided into three aspects that are; 1) Hydraulic 2) Biogeochemical and 3)sedimentological aspects, and the summary of the results have been evaluated according to interaction and observations of these three aspects. Biogeochemical parameters of the reach evaluated according to porewater samples that are compared with groundwater and surface water observations considering location of the samples under 15 cm depth.

Hyporheic flow has critical influence on denitrification and nitrification processes in hyporheic zone, it was proved that hyporheic flow paths and associated residence time causes often favoriable conditions for denitrification (Zarnetske et al., 2012; Marzadri et al., 2012; Holmes et al., 1996; Böhlke et al., 2009; Hubbard et al., 2010). Most of the works claim that the higher residence time zones prone to have more denitrification processes (Galloway and Cowling, 2002; Green et al., 2009). As a general assumption smaller streams are expected as more active in sense of denitrification due to higher concentration of nitrate and due to the larger contact times within hyporheic sediments (Alexander et al., 2000). Recent hyporheic zone researches and models have more tendency to consider local residence time (Marzadri et al., 2010; Cardenas et al., 2004,?; Gooseff, 2010) rather than storage time or storage zone (Mulholland et al., 2008; Webster et al., 2003). Our approach was more focusing on hyporheic paths in terms of residence time ,and concentrations of biochemical parameters that are related with denitrification/nitrification processes. Nevertheless, comparison of the concentrations was made according to global concentration values as well as spatial measurements.

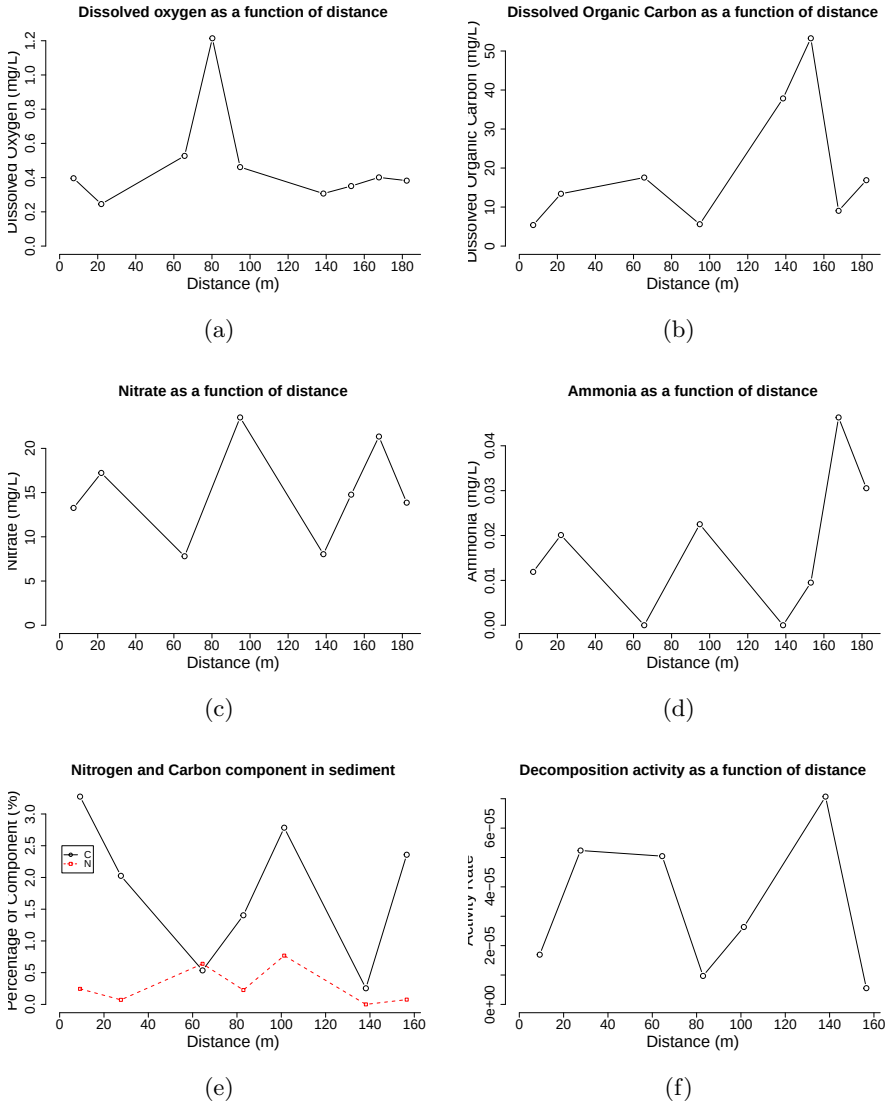


**Figure 2.13:** Semi-variogram graphs as a function of distance starting from upstream to downstream demonstrated as; (a) Dissolved Oxygen values as mg/l; (b) Dissolved Organic Carbon as mg/l; (c) $NO_3$ values as mg/l; and (d) $NH_3$ values were given as mg/l; and (e) percentage ratio of Nitrogen and Carbon values according to sediment sample (%); and (f) Organic matter consumption rates or Activity rates, $\mu mol\, g^{-1}\, min^{-1}$.

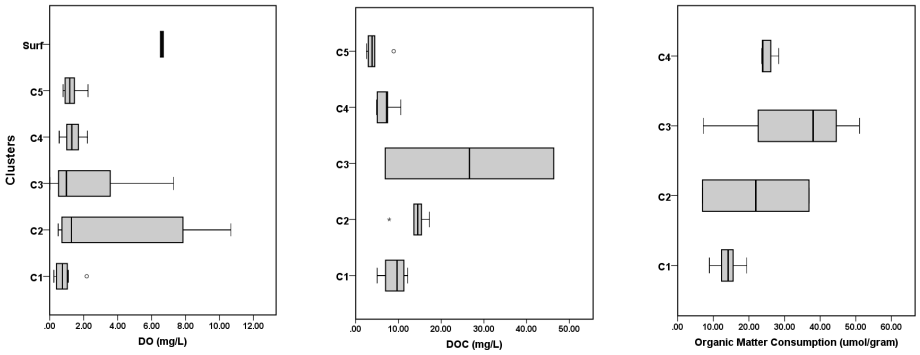


(a) (b) (c)

**Figure 2.14:** Box-Whisker plots of DO and DOC values with organic matter consumption rates per according to clusters; (a) DO values are also demonstrated with surface water values mg/l; (b) DOC values according to different clusters were given as mg/l; and (c) Organic matter consumption rates have been calculated with the multiplication of residence times for specified sample depth and location as $\mu\text{mol}\,\text{g}^{-1}\,\text{min}^{-1}$.

### 2.4.1 Hydrology of the reach

From our perspective, spatial water surface elevation and groundwater levels were showing varied levels in different zones. Data from water surface elevation and that on upstream of the reach show difference between groundwater levels. Measured water surface elevation values give information about steady state conditions, however, we can get transient information of groundwater data. Averaging discharge conditions from cross-sections demonstrates $0.5\,\text{m}^3/\text{s}$ discharge by the time of measurement. Measured head values and in situ groundwater levels demonstrate that there is discrepancy between groundwater and surface water where water table is lower than water surface elevation on upstream part (also meander part), conversely, opposite conditions can be seen on downstream part. Another observation also indicates that the subsurface water level is getting higher once moved away from the reach towards outside on upstream part. This indicates that the gradient of water surface level (and river bed elevation) is lower than the gradient of subsurface water level. Since transient data of groundwater shows periodic changes, as increasing and decreasing patterns, (see Figure 2.11) which may stem from local floods and precipitation, it is not possible to observe the respond of water surface elevation on these changes with this set of hydrological measurements. However, we can presume that slight increase of subsurface water levels (with the trend range from 0.0006 to 0.0014), that is around 1 m, may not cause a big difference on water surface elevation and average discharge values.

### 2.4.2 Heterogeneity of Sediment

22 different core samples formed by 50 subsamples were individually identified and classified according to certain statistics. 4 main type of sediment was defined. Three of them were classified by sediment analysis, and small size gravel has been considered as the fourth one ($> 2\,\text{mm}$). In some parts of the reach small size gravel were observed inside the medium size sand layers, however, the bigger size of gravel was observed in meander part in 30cm depth of sediment. Some cases were taken for analysis, since collection was done according to observation and selection of significant type of sediments. Repeated sediment types were not taken second time for the analysis. Therefore, it was not possible to summarize whole core profiles, nevertheless, all types of sediments and average grain sizes of the reach were statistically defined. Nearly all cores have this four defined sediment materials regarding to some exceptions, however, the mixture layers and their frequencies, and volumetric proportions are changing depending on the location. This arbitrariness could influence the development of residence time distributions and hence the one of anoxic/oxic zones.

Analysis indicates that all the sediment types are poorly sorted. We can find mixed types of sediments that shows the intersection points of the sediments. Such that, sediments are not sorted clearly, this characteristic shows itself as polymodal distributions of each sediment sample. In our case, up to second mode was calculated (see Figure 2.1), and compared. The relation of the organic matter content of the sediment, sediment types and labile carbon were observed.In addition, organic consumption rates were demonstrated (see Figure 2.15). According to set of data, mean organic matter consumption rates for each cases are ranging between 0.0055 to 0.022, however, the change of the rate is independent from gravel size or sediment type even in some cases rate is higher than others.

### 2.4.3 Biogeochemical evidences and redox conditions

Our results depicts the dynamics and prevailing biogeochemical processes around 15 cm depth from the surface, such that, instead of a spatial process it shows a state of location on a particular time (steady-state) from hydrological and biogeochemical point of view. In this work it was used as how particle size analysis with the combination of chemical and mineralogical analysis can be used to narrow down the search of a relatively large area,and determine the provenance of sediment sample. Analysis were applied along the knowledge of the underlying sediment formation withing few meters or less. More specifically, site location normally requires additional information, including the identification of inorganic or organic sediment constituents. It was generally seen that there are sediment layers that are fully organic and trapped between low permeable layers as very fine sand

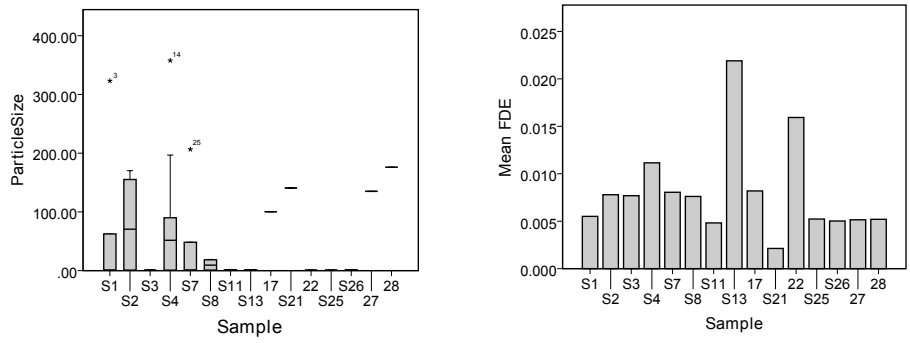


(a) (b)

**Figure 2.15:** Particle sizes with mean consumption values; (a) Box-plots demonstrates different sediment layer properties of each case; and (b) mean consumption values of each sediment

and silt. It is clear that the stock of organic matter within the sediments is an important predictor of bacterial abundance in sediments (Schallenberg and Kalff, 1993). As well as the type of DOC in the sediment, similarly, there must be relatively good water exchange between the stream channel and hyporheic sediments to maximize the extent of hyporheic metabolism of surface water DOC (Knorr, 2013). Therefore, fluctuations in subsurface flow and river discharge holds importance on the concentration of DOC in hyporheic zone (Vervier and Naiman, 1992). Conversely, in the reach it seems like DOC level of groundwater and surface water are in the same level of average DOC in porewater (see Figure 2.12), therefore, we can conclude that river discharge and weak hyporheic exchange conditions do not cause any change on DOC between 15 cm sediment depth and transaction of DOC is smooth between groundwater and surface. It is possible that the source of DOC is layers that have organic content trapped between small grain size sediment.

Greater denitrification potential should be expected under high magnitude flux conditions and, consequently, faster hyporheic exchange, in other words existence of shorter residence times in hyporheic zone (Cook et al., 2006; O'Connor and Hondzo, 2007). In case of low hyporheic flux the resupply of substrates limits the denitrification, conversely, in case of increase size of hyporheic zone and denitrification rate proportionally increase (Cook et al., 2006). It has been observed that the hyporheic feeding of $O_2$ into the system initiates organic matter composition, so the nitrification as a following process (Holmes et al., 1996; Koch et al., 2010). Once hyporheic zone turns into anoxic conditions denitrification prevails. There are evidences that denitrification does not occur above oxygen concentration of 0.2 mg/l

(Skerman and MacRae, 1957).

The denitrification rate is correlated positively with the concentrations of DOC and $NO_3$ which are substrates for the reaction denitrification rate was also negatively correlated with residence time, indicating the importance of shorter residence times in transporting substrate from surface water to reaction sites in the sediment (Harvey et al., 2013). However, evident pattern of denitrification could not be found according to our set of data, even there are oscillations along the reach they are not statistically significant (see Appendix A). Therefore, considering with low grain size and low conductive material texture in the sediment, the hyporheic dynamic of the reach is not the dominant factor in order to control redox conditions along the reach. This shows that the reach has the feature of low magnitude hyporheic flux and long hyporheic residence time river conditions (Stelzer et al., 2011; Lansdown et al., 2012).

With respect to $NO_3$−N the data set suggest that porewater nitrate is slightly higher than surface water average nitrate content, however, the difference does not provide statistical significance (ANOVA $p = 0.421$), conversely, the difference is significant comparing with groundwater level (ANOVA $p = 0.023$). On the other hand, the most significant difference can be seen with respect to $NH_3$−N parameter both as a highest concentration on groundwater that is 1.5 m depth from the bank site (ANOVA $p < 0.001$ ) and significantly higher on downstream part (Figure 2.13(d)). Even the difference in nitrate is statistically insignificant, higher concentrations in porewater might show that there is slight nitrification. It is possible that among the channel water advected laterally supplied dissolved oxygen, and groundwater supplied ammonium to support hyporheic nitrification, ammonium amendment to sediment slurries only slightly enhanced nitrate production indicating that sorption competed with biota for available substrate (Triska et al., 1990). However, significantly higher $NH_3$−N on downstream part of the reach proves that this process may not prevailing in the zone, considering that shallow groundwater level (on the bank) is matching with surface water elevation measurement. Therefore, it can be expected that the effect of groundwater may increase on downstream zone, where nitrification could be inhibited by chloride, which is slightly higher both in groundwater and surface water than average porewater concentrations (see Table 2.2) (Westerman and Tucker, 1974; Tubbing and Admiraal, 1991).

Considering the agricultural influence over the reach, interactions between the stream hydrology, morphology and biology such as we observed nitrate concentration depends on more dynamics than it was reported, However, the magnitude of the resulting nutrient flux will depend on factors which determine the depth and lateral extension of suitable hyporheic habitat. Conversely, observations provide that hyporheic zone is a transactional area that connects groundwater and surface water, instead of a controlling

media for redox condition. such that the lack of major differentiation between high flows may show that the runoff infiltrates shallow storage and mixes with groundwater there, displacing the mixed water into the river and maintaining a high level of hydrochemical and biogeochemical homogeneity from high flows to low flows (Wexler et al., 2012).

**Table 2.2:** Geochemistry results for stream water, groundwater and streambed porewater along the reach

| | $NO_3^-$-N mg/l | $NO_2^{2-}$-N mg/l | $NH_3^+$-N mg/l | DO mg/l | DOC mg/l | $SO_4^{2-}$ mg/l | $Cl^-$ mg/l |
|---|---|---|---|---|---|---|---|
| Surface Water | 5.05 | 0.031 | 0.00 | 6.61 | 3.70 | 27.36 | 18.31 |
| | (1.170) | (0.008) | (0.000) | (0.083) | (0.996) | (6.349) | (4.760) |
| Groundwater Water | 2.24 | 0.24 | 0.47 | - | 9.28 | 24.86 | 16.02 |
| | (1.580) | (0.068) | (0.115) | - | (5.580) | (4.90) | (10.32) |
| Porewater | 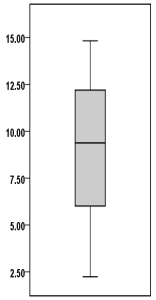 | 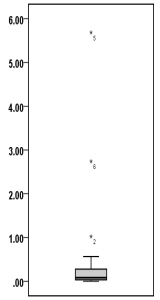 | 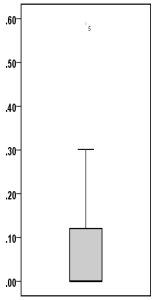 | 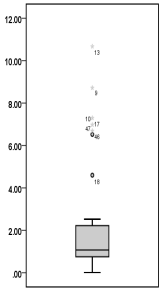 | 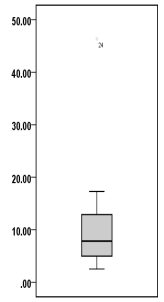 | 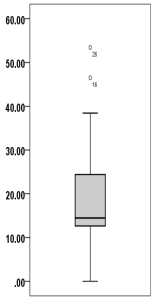 | 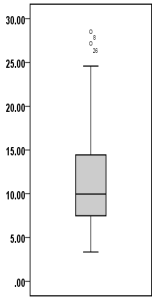 |

For stream water and groundwater samples, means and stabdard deviations (in parentheses) are for each parameter. Box plots are shown which demonstrates quartiles, median and average. Concentrations not detected in the chemical analysis are considered to be null. Box plots through the stream bed showing 95th and 5th percentile, 90th and 10th percentile (error bars), 75th and 25th percentile (box), arithmetic mean (solid line).

# Chapter 3

# Spatial Interpolation for River Topography and The Comparison of The Spatial Interpolation Methods

## 3.1 Representation of data to study site

Topography is of fundamental importance in controlling interactions between groundwater and surface water. The gradient of slope in land surface create numerous localized shallow groundwater paths that are isolated from the regional groundwater flow Toth (1963) which may also strongly feed hyporheic exchange flows which are generated dominantly by convective flow of stream water around macroforms and microforms into bed sediments Thibodeaux and Boyle (1987). Patterns of downwelling water at the upstream face and upwelling water at the downstream face of these roughness elements have been identified by modelling streamflow over small bed forms and by dye tracing experiments in flumes Thibodeaux and Boyle (1987); Savant et al. (1987). Hyporheic exchanges across the bed also can be produced by large scale roughness elements that are steeper channel units, such as riffles, and step-pool formations. The first researchers used temperature and chemistry profiles beneath a riffle-pool in order to indicate vertical convective exchange, in other words hyporheic exchange triggered by changes in bed surface White et al. (1987); Hendricks and White (1991). Hydraulic head and tracer experiments have also demonstrated horizontal exchanges in which stream water recharges to stream-side sediments above a steeper channel unit and follows an arc-shaped subsurface flow path that returns to the stream at the downstream end of the unit Harvey and Bencala (1993)

Detailed numerical modeling of flow dynamics in river channels requires the spatial interpolation of scattered measurements of bathymetry eleva-

tion on reach scale, in order to draw the details of the river bed surface. In this work surface model was followed as the traditional approach with complex geometry involves fitting a mesh to available topographica data and parameterizing smaller scale aspects of topography using roughness parameter Hodskinson and Ferguson (1998); Lane et al. (1999) (see Chapter 4). Therefore, choosing an appropriate interpolation scheme is a critical step in producing an accurate bed surface for river channels from scattered bathymetry points. The creation of spatial domain holds major role on accuracy of model simulation results and predictions of the model Crowder and Diplas (2000); French and Clifford (2000); Merwade et al. (2008). The creation of an accurate spatial domain is critical for successful model simulation and prediction. Topographical variations are significant especially at smaller scales such on reach scale. The effects of subgrid-scale topography as grain surface morphology, formations less than the grid size, are represented as frictional retardation of the flow at the bed Lane et al. (2004), and creation from banks through the thalweg with capturing bigger formations as meander and riffle-pool is the first approach in order to have valid representation of subgrid-scale. Therefore, different approaches to interpolating river topography may cause big differences in the spatial domain especially where the bed slope varies Carter and Shankar (1997); Franke and Nielson (1991); Goff and Nordfjord (2004).

The main focus of this chapter is to define a spatial topography for both the computational fluid dynamics model representing surface water, and, the upper boundary of 3D groundwater model which predicts hyporheic exchange flows through the hyporheic zone for the chosen reach (see Chapter 2). The chapter also addresses the sufficiency of resolution of the spatial data, by evaluating the optimum distance between sample points during the interpolation process. In general this chapter aims to estimate the best interpolation approach concerning channel bathymetry and mapping.

- Comparing output from six selected models commonly used for data interpolation.
- Assessing the data quality from each method and applicability to point elevation data (to see the structure of point topographical data; Chapter 2, Figure 2.6).

## 3.2 Methods

This section describes the methods that are commonly used for interpolating scattered point data so as to create streambed topography. In the works of Carter and Shankar (1997) ordinary kriging has been used as a spatial interpolation scheme, in the same work of Merwade et al.(2005) also Inverse Distance Weighting (IDW) method has been utilized. As an alternative to

conventional stochastic interpolation methods, there are several researchers approaching analyzing the data in a channel-fitted coordinate system in order to interpolate channel topography Merwade and Maidment (2005); Goff and Nordfjord (2004); Merwade et al. (2008).W/Template method relies on such a channel-fitted coordinate system approach. Following the literature specified, six models have been used for this study. These are; Ordinary Kriging, IDW, and four w/Template interpolation model. w/Template method is an integrated method with the nearest neighbor search method. All these models are implemented on a computational grid system, whereas for Kriging and IDW Cartesian, and for w/Template method, curvilinear mesh type used. Such that gird spacing holds importance for the sake of bathymetry interpolations. Lane and Richards (1998) suggest in their work that the grid spacing must be of the same order as the resolution of the topographic representation. In the same work, it has been suggested that for 50cm point spacing at least 10cm mesh spacing should be used. From that point considering the resolution of our data, which is also irregular, for comparison of interpolation methods, a $50 \times 50$cm grid size was chosen. In order to keep integrity and reduce the error of subsurface flow model grid spacing that was chosen for interpolation of surface water model adjusted also for the upper boundary of the subsurface domain (see Chapters 4 and 5 ).

### 3.2.1 Kriging

The principles of geostatistics and interpolation by Kriging are mentioned and criticized by a large amount of literature Journel and Huijbregts (1978); Isaaks and Srivastava (1989); Hengl et al. (2009); Deutsch and Journel (1992); Goovaerts (1997); Cressie (1992). Therefore, the notions that are associated with the general aim of this chapter are outlined here. In this section, we applied Ordinary kriging method to compare the quality of topographical representation and to evaluate the success of the method. Kriging process will be followed by creating a variogram based on the spatial data, and finding the best fit onto the variogram and demonstration of a kriged surface.

#### Principle of Ordinary Kriging

One of the most well know spatial interpolation techniques is kriging. Ordinary kriging assigns weights according to a (moderately) data-driven weighting function, rather than an arbitrary function, but it is still just an interpolation algorithm and will give very similar results to others in many cases Isaaks and Srivastava (1989). In general like all spatial interpolation methods ordinary kriging estimates variables at an unmeasured location from observed values at surrounding locations over a grid of locations Oliver and

Webster (1990). Rather than assuming that the mean is constant over the entire domain, it is assumed as constant in the local neighborhood of each estimation point for ordinary kriging, with this method kriging can capture local changes on the spatial data Goovaerts (1997).

Summar of Ordinary Kriging is a stochastic technique that uses a linear combination of weights at known points to estimate the value at an unknown point. the weights are assigned based on the spatial correlation between the points. The spatial correlation is characterized through the use of a semi-variogram model, which provides a measure of variance of differences as a function of distance between the observation points Cressie (1992). This technique is also similar to the IDW method except kriging calculates elevation values according to a function, conversely IDW only calculates average values inside a moving specified domain or according to specified number of data.

The parameters of these functions are optimized to yield the best fit for the empirical semi-variograms . The fitting procedure continues to compute until minimum variance and unbiasedness conditions has been satisfied, as shown in following equation,

$$\sigma^2 = E\left[(z^* - \hat{z})\right] \tag{3.1}$$

where $z^*$ is the prediction value at $\hat{z}^*$, $\lambda_i$ is the weight associated with the $i$th observation, $E\,[]$ is the expectation operator. Following the equation 3.1;

$$\hat{z}^* = \sum_{i=1}^{n} \lambda_i z_i \tag{3.2}$$

Solution of $\lambda_i$ can be calculated by solving equations 3.1 and 3.2 as a set of linear equations. Once weights for each observation value are determined, $\hat{z}^*$ can be calculated.

### Application of Ordinary Kriging and cross-validation

The steps of the application of Ordinary Kriging are as follows; 1)calculation of experimental semi-variogram and fitting variogram models, 2)spatial interpolation of best fitted variogram models, 3)cross-validation between krigged maps. At the beginning, 16 variogram model fits were applied on an omnidirectional variogram. Following to that, the goodness of fit of the variogram models compared with fit sum of square errors (SSE) statistic. SSE is based on the objective function of the fitting process;

$$SSE = \sum_{i=1}^{k} \left[\gamma_z^*(h_i) - \gamma_z(h_i;\theta)\right]^2 \tag{3.3}$$

Where $\gamma_z^*(h_i)$ can be either the classical robust semi-variance estimate of theoretical semi-variance $\gamma_z(h_i;\theta)$ at the $i$th lag and the weights $\lambda_i^2$ are taken at lags $i = 1, ..., k$ fittings that have high SSE value were excluded. According to this analysis 8 variogram model have been chosen regarding to their SSE values Goovaerts (1997).

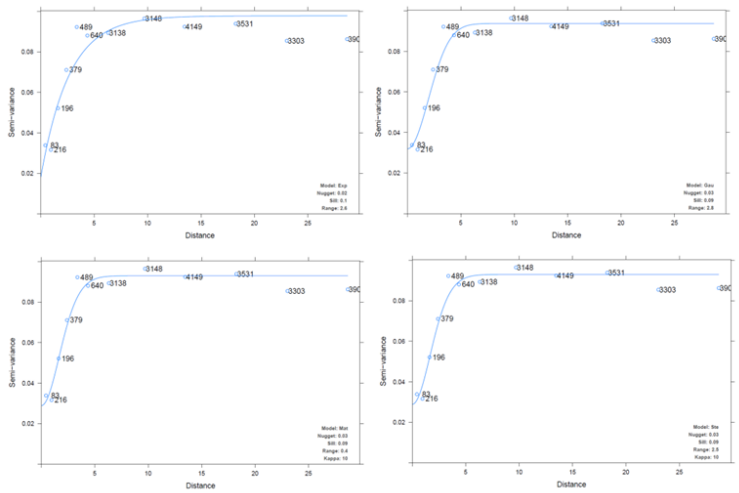


**Figure 3.1:** Best fitted variogram models of Ordinary Kriging by the comparison of SSE parameter.

According to semi-varogram functions as shown in Figure 3.1, SSE values have been calculated for each variogram-model. According to SSE statistics (see Figure 3.2) the worst fitted function is the one created by exponential fitting but the best representation (with the lowest SSE) are Gaussian, Stern's and Mattern fitting models.

The cross-validation technique proposed by (1976) is used here to allow us to compare the impact of different models on interpolation results. In particular, interpolated and actual values are compared, and the model that yields the most accurate predictions is retained. The procedure used for this purpose is named 'leaving-one-out cross-validation' (LOOCV) method in which one sample point is excluded from the data set and the value at the location is estimated by kriging with the selected variogram model and the remaining data Guarascio et al. (1976); Knudsen and Kim (1978); Cooper and Istok (1988). This procedure repeats for each data from whole data set.

According to works that focus on cross-validation procedure Zhang et al. (1992); Prudhomme and Reed (1999); Tomczak (1998); Merwade and Maidment (2005), root mean square error (RMSE) and correlation measures were chosen to compare the accuracy of different krigged maps. Estimates can

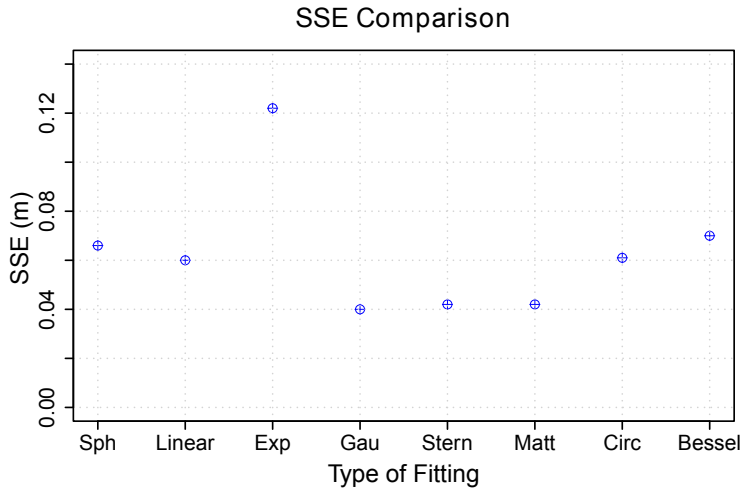


**Figure 3.2:** Comparison of variogram models by sum of square error (SSE) values. 8 models that has close error values have been compared

be considered accurate if RMSE is close to zero;

$$RMSE = \frac{1}{n}\sum_{i=1}^{n}\sqrt{[z_i - \hat{z}_i]^2} \tag{3.4}$$

Where $n$ is the number of data points in the data set, and $z_i$, and $\hat{z}_i$ are the corresponding values estimated by different kriging. A correlation coefficient was used to observe how well the kriging models represents the observed data.;

$$R^2 \equiv 1 - \frac{VSSE}{SST} \tag{3.5}$$

Where $VSSE$ stands for sum of square for validation process to not to mixed with $SSE$ for fitting process, $SST$ represents total sum of square,

$$VSSE = \sum_{i=1}^{k}[z_i - \hat{z}_i]^2 \tag{3.6}$$

$$SST = \sum_{i=1}^{k}[z_i - \bar{\hat{z}}_i]^2 \tag{3.7}$$

where $R^2$ value of more than 0.7 can be considered as a successful representation.

Figure 3.3 demonstrates that the Exponential variogram model gives the best accuracy and representation with an RMSE equal to 0.205 and correlation equal to 0.743. Furthermore, It should be stressed that Exponential

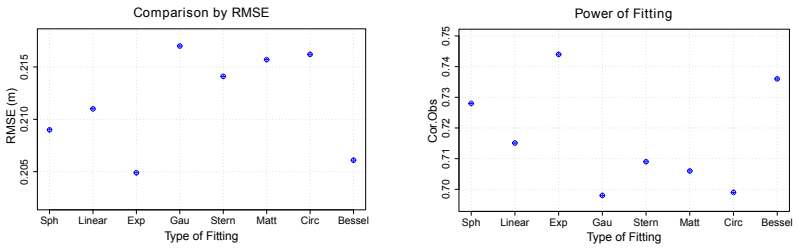


(a) (b)

**Figure 3.3:** Comparison of kriging model by leave-one-out cross-validation; (a) comparison of the models by RMSE; and (b) evaluation of the models according to the correlation of observed values.

fitting is more prone to error in comparison to other methods according to SSE values (Figure 3.2), however cross-validation procedure proved that even the variogram model does not fit best on experimental semi-variogram, it can be better on estimating krigged values.

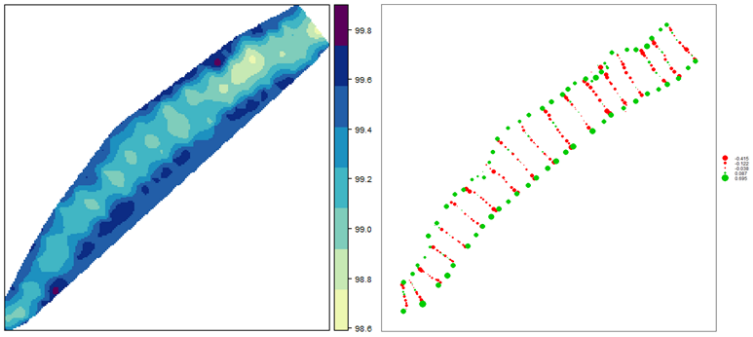

**Figure 3.4:** Krigged map of central part of the reach interpolated by exponential semi-variogram model (on the left) and point values that is used for validation process with error values for exponential model (on the right)

### 3.2.2 Inverse Distance Weighting (IDW)

Inverse distance weighted (IDW) interpolation is based on an assumption that the value at a non-sampled point can be approximated by a weighted average of observed values within a circular or Cartesian mesh search neighborhood, whose radius defined by the range of a fixed number of closest points (see Figure 3.5) Watson and Philip (1987). The simplest and most commonly used form of inverse distance weighted interpolation was proposed

by Shepard (1968). The equation used as follows; 3.8;

$$z^* = \sum_{i=1}^{N} \lambda_i z_i \tag{3.8}$$

Where $z_i (i = 1...N)$ are the observed elevations at N points, and the weights $\lambda_i$ can be calculated as

$$\lambda_i = \frac{\frac{1}{d_i^p}}{\sum_{i=1}^{N} \frac{1}{d_i^p}} \tag{3.9}$$

in this equation $d_i$ is the distance between $i$th sampled point ($z_i$) and the non-sampled point ($z^*$), and $p$, which controls the contribution of the measurement points to calculate non-sampled point, is the power variable.

Several options are available for inverse distance weighted interpolation. This method can be used alone for interpolation or coupled with other methods. Inverse distance weighting (IDW) is a deterministic estimation interpolator by which unknown values are computed by a linear combination of values at known points Collins (1995). Unlike kriging, IDW does not require selecting a semi-variogram model to create an interpolated surface. This lowers the level of subjectivity of this interpolator and also provides faster calculating speeds Tomczak (1998).

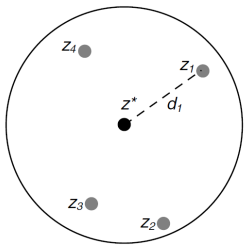


**Figure 3.5:** Distance and aerial weighted interpolation methods. $z^*$ is non-sampled point, and $z_i$ represents sampled points

Weighting is assigned to data through the use of a weighting power that controls how the weighting factors drop off as distance from a grid node increases. Weights are usually inversely proportional to a power of distance PIZOR (1987); Watson et al. (1992). As the power increases, the grid node value approaches the value of the nearest point. For a smaller power, the weights are more evenly distributed among the neighboring data points. The smoothing parameter is a mechanism for buffering this behavior Yilmaz (2007). In this work, the Smooth Interpolation option creates an outer ellipse and an inner ellipse at a distance equal to the Major Semi-axis multiplied by the Smoothing factor. The points that fall outside the smaller ellipse but inside the largest ellipse are weighted using a sigmoidal function with a value between zero and one.

For Smoothing and Weighting power, it has been suggested that weighting power typically gives the best result when a value of $p = 2$ is chosen and smoothing should be avoided Watson et al. (1992). Values of more than 2

cause over weight on measured values as seen from the last two topography maps of Figure 3.7.

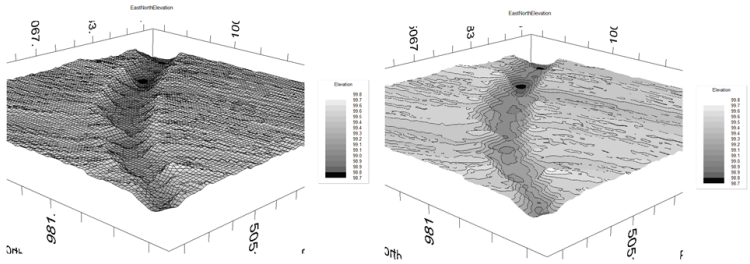

**Figure 3.6:** Demonstration of IDW mapping with wired frame (on the left) and contour lines (on the right)

Interpolation result of IDW using $p = 2$ without smoothing factor is shown in Figure 3.7, which was created along the suggested parameters on a Cartesian grid system. Comparison of the best IDW interpolation representation is tested and chosen in Performance Evaluation section in which cross-validation procedure is applied for comparison of different interpolations.

### 3.2.3 Delaunay Triangulation and mapping with w/Template

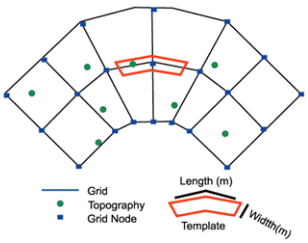


**Figure 3.8:** An illustration of the w/Template method

This section discusses the w/Template method for mapping ancillary data such as topography or grain size to the computational grid. Previous methods were applied on a Cartesian grid system, conversely w/Template uses a curvilinear grid system to interpolate river bathymetry. The key novelty of interpolation of river bathymetry on a curvilinear grid is to fit data onto a channel fitted (s,n) coordinate system (for an example see Figure 3.9). The main advantages of using (s,n) coordinate system for analyzing data can be stressed as; the evaluation of anisotropy in the river channel bathymetry such that data can be treated differently along and across the flow; it can interpolate morphological complexities such as channel meanders or point bars Merwade et al. (2008). The idea of this approach is to try to use the fact that the riverine topography tends to vary more in the cross-stream direction than it does in the streamwise direction.

w/Template is a method combined with modified version of a nearest neighbor search method Knuth (1973); Yianilos (1993); Beis and Lowe (1997), which is similar to IDW in that it calculates unsampled location by

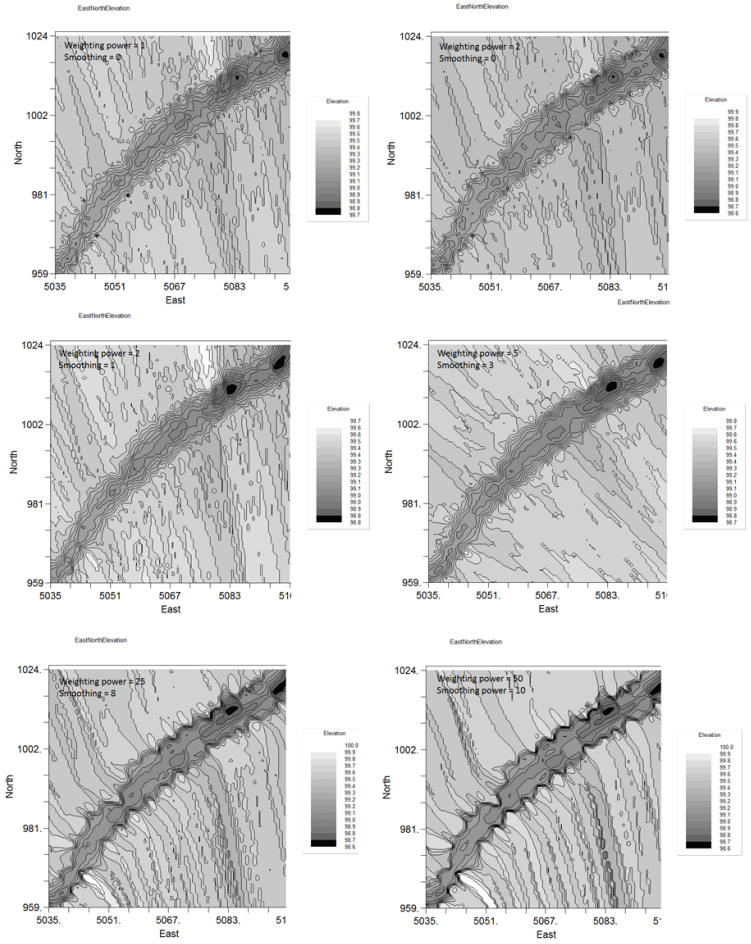


**Figure 3.7:** Demonstration of different reach maps using different weighting power and smoothing values with IDW method

weights. Unlike the IDW, however, the weights are computed based on the areas, rather than distances. Conversely, in w/Template, the search uses a template or bin with a specified width and length over the sample points and grid nodes. The length follows the local stream-wise curvature of the grid. The value of the mapped variable is computed by linear interpolation between the three nodes of the triangular cell. The template algorithm follows the same general algorithm, but uses a search bin with a specified width and length instead of a simple radius around the node (Figure 3.8). The estimate of unsampled point is computed using equation 3.8.

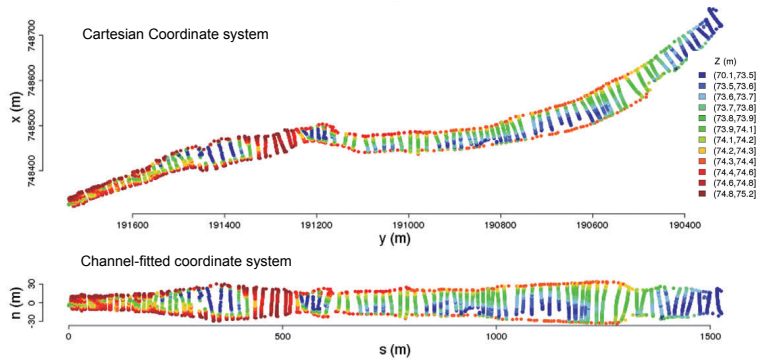


**Figure 3.9:** Different approaches by the coordinate systems and transformation of cross-sectional data points. Upper graph shows Cartesian $(x, y)$ and the graph on the bottom demonstrates channel-centered $(s, n)$ coordinates ( Modified from Bailly et al. (2010))

In order to apply the process above steps for application of w/Template method followed by;

1. Define the channel centerline to use as a reference for coordinate and curvilinear mesh,

2. Assign a curvilinear grid on to measurements to fit coordinate system, s coordinate is the distance along the channel centerline, and n coordinate is the distance across the channel from the centerline,

3. Assign specific length and width to the template and interpolate data points that fall on the template using nodal points.

This method is unique as the bin follows the local curvature. In other words, the length or streamwise orientation of the bin maps to the local streamwise curvature of the grid. The critical factors for w/Template method are the chosen mesh, length and width of template, and weighting power for interpolation. Appropriate weighting power that was chosen for IDW method ( Section 3.2.2) is also applicable for w/Template method.

Node spacing (grid size) has been chosen as $50 \times 50$cm as discussed in methods section. Anisotropy can be taken into account by assigning different length and width to computational template. Different length/width ratios used from low to high isotropic representation, also weight power was reduced in order to increase the anisotropy (see Figure 3.10).

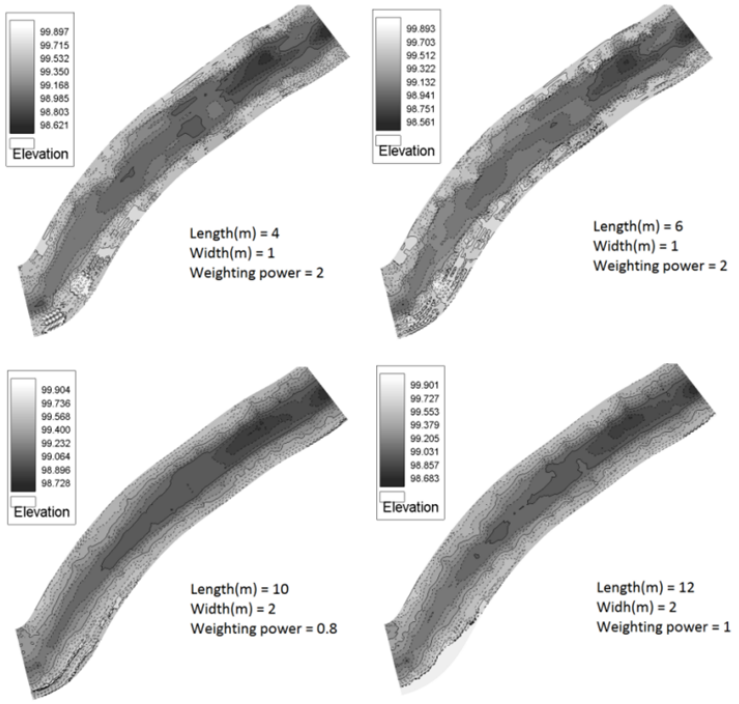


**Figure 3.10:** Demonstration of mapping with w/Template method by using different weighting power and Length/width ratio

### 3.2.4 Performance evaluation

The methods proposed in this paper can be applied to different types of rivers. However, the success of these techniques in creating river terrain models depends on the quality of interpolation predictions in areas with no measurements. A rigorous evaluation or testing of proposed techniques will involve running a free surface flow and hyporheic exchange model simulations, but such hydraulic models would also require additional data, eg. flow measurement, bed pressure measurements, which is discussed mostly in Chapter 2. Therefore, a simple cross-validation approach is taken to test the accuracy of the proposed interpolation methods.

Generally k-fold is an alternative to other validation methods which involves withholding a fraction of the data using a sub-group of the original

observations Fielding and Bell (1997). Where $k$ represents the number of the original samples ranging from 2 to $N-1$, and where $N$ is the number of observation points. This method works particularly well for studies having a single intensive period of data across only one region Nielsen et al. (2002) instead of spread or averaged readings of a parameter (e.g. concentration, soil or sediment of hydraulic conductivity, local reaction rates).

Application of the K-fold cross-validation technique to this study involves excluding particular data from cross-sections and interpolating to generate an estimate at the location of the removed values. Basically, the predicted values were compared with the measured values. In our case $k$ number is chosen as 5, which means up to 5 predictions removed from the cross-sections by turn and compared with the observation data after interpolation. Same locations of observed data were used for the readings of interpolated variables, therefore, comparison has been performed not only on excluded points but also between observed points.

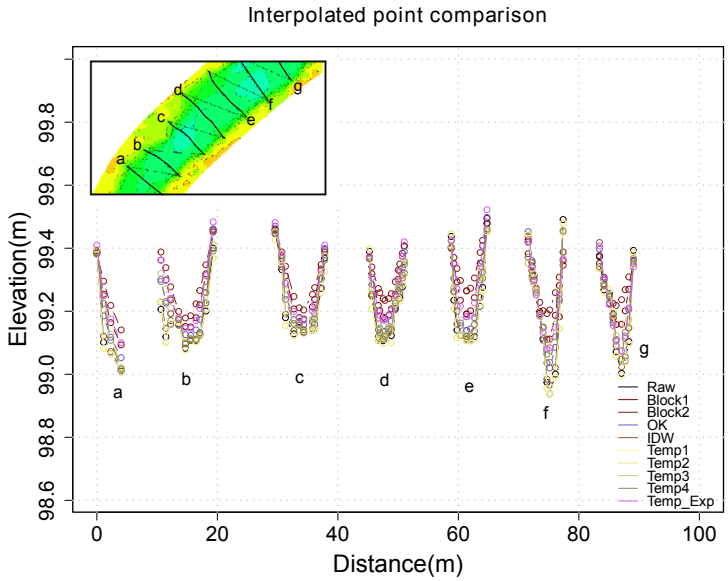


**Figure 3.11:** Demonstration of excluded data set for cross-validation process. Each bunch shows a series of excluded data of cross-sections and predicted to compare raw (observed) data. The distance depends on the line that crosses over the cross-section points (see plan view), the lines between points and crosswise lines were not taken into account in cross-validation.

In Figure 3.11, comparison of the points for each method can be seen as transect along the specified part of the reach. In this test, seven interpolated bathymetries were compared. The models are named as OK generated by ordinary kriging, IDW stands for inverse distance weighted method and Temp $1-4$ maps are generated by w/template method by dif-

ferent anisotropies(length/width), and Temp-Exp is combined interpolations of exponential kriging and w/template method.

This method is applied for finding the interpolations which has the best performance between methods and within the methods except Ordinary Kriging. It was proved that in section 3.2.1 , Exponential model has the best representation for kriging, However, it should be noted that, LOOCV and k-fold cross-validation methods should not be confused, different than LOOCV, k-fold cross-validation excludes up to 5 data points from the cross sections and follows by in turn, on the other hand, bank elevation points were not taken into account in k-fold cross-validation method. Conversely, the LOOCV method excludes chosen data points one by one, and interpolations have been repeated according to different semi-variogram models. Same as the LOOCV method, random mean square error (RMSE) and correlation to observations (Cor. Obs.) were used for comparison in k-fold cross-validation (see Figure 3.12 ).

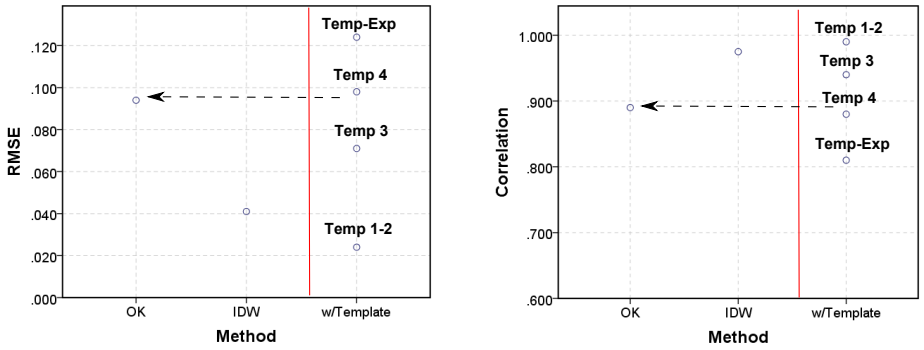


(a) (b)

**Figure 3.12:** Comparison of the interpolation methods by k-fold cross-validation. The interpolations of the left side of the vertical red line was made based on the assumption of isotropic bed, conversely, the ones on the right side interpolated according to different anisotropic conditions. OK, IDW and Temp stand for respectively Ordinary Kriging, Inverse Distance Weighted, and w/Template methods; (a) comparison of the models by RMSE; and (b) evaluation of the models according to the correlation of observed values.

In Figure 3.12, the interpolations which have lowest errors within methods are shown. Here OK stands for exponential fit for ordinary kriging, IDW is the one generated by $p = 3$ and smoothing factor 1, for Template $1, 2, 3$ and 4 length/width ratios are in turn $4, 6, 5$ and 6, and $p$ values are $2, 2, 0.8$ and1. Temp-Exp is the exponential kriging output that was fitted onto curvilinear mesh and interpolated with template method with length/width ration 1 and $p = 1$.

According to cross-validation results w/Template method shows better performance with respect to OK and IDW, which also shows that representation of anisotropic methods are superior to isotropic ones for this case. It can be seen from Figure 3.12, Template 1 and 2 interpolations have the highest performance with anisotropy. However, comparison between Template methods shows that increasing anisotropy and decreasing $p$ values aggravates the representation power of the river bathymetry.

### 3.2.5 Summary and conclusion

Choosing an appropriate interpolation scheme is a critical step in producing an accurate surface for river channels from cross-sectional points of bathymetry. This step holds critical importance for free surface flow model of river channel where hydraulic parameters such as shear stress, and directly Reynold stresses are dependent on streambed and morphological properties Lane et al. (2004). Good representation of topography is significant so as to represent hyporheic exchange flows through streambed by hyporheic flow models Elliott and Brooks (1997); Cardenas et al. (2004); Tonina and Buffington (2009). It is also crucial to accurately compute the profile of pressure gradient over the streambed so as to define upwelling and downwelling zones on a river reach.

Several interpolation techniques were applied to the topographical data so as to create a continuous bed topography. In spatial points perspective, interpolation followed as fitting a function (linear, polynomial, cubic etc..) between at least two points, and finding predicted values on specified distances over the domain Bergh and Löfström (1976).

Three different interpolation methods and six different models were applied in order to create a streambed bathymetry. An Ordinary Kriging method was used on the cross-sectional data, on a Cartesian grid Carter and Shankar (1997); Merwade and Maidment (2005); Merwade et al. (2008); Bailly et al. (2010), which assigns weights according to a (moderately) data-driven weighting function by semi-varogram model in order to predict non-sampled locations. Additional to Kriging, Inverse distance weighted methods are based on the assumption that the interpolating surface should be influenced most by the nearby points and less by the more distant points. The interpolating surface is a weighted average of the scatter points and the weight assigned to each scatter point diminishes as the distance from the interpolation point to the scatter point increases Shepard (1968). W/Template method uses Delaunay triangulation of irregularly spaced data on curvilinear grid by the nearest neighbor search algorithm. In detail template operator has been proposed, which can be considered as the domain which replaced by the circular domain of the nearest-neighbor search method. For w/template method different interpolations were tested according to their length/width ratios and weighting power (exponent).

**Conclusions**

K-fold cross-validation technique has been applied to each interpolation method to compare the predicted values with the bathymetry data by excluding some points from the measured points of cross-sections.

Interpolation in order to create a river channel bathymetry was applied with a cross-validation procedure. Cross-validation results prove that the best representation is interpolated by w/Template method producing the lowest RMSE value of 0.023m. The analysis shows that the anisotropy of the river reach can be evaluated with a length/width ratio, which was estimated between 4–6. Also, it was experienced that decreasing or increasing the weighting power significantly influences the predicted values, and an optimum value is $p = 2$.

Results from kriging interpolation show slight disagreement with observed cross-sectional data, on the other hand, IDW method shows better performance than OK. A better representation of the river bed topography might be achieved by incorporating anisotropy into ordinary kriging method and modifying it as a curvilinear grid system, as suggested by Legleiter and Kyriakidis (2008). According to these findings, anisotropic models give rise to more accurate representations of river bed topography, and this has also been noted by Merwade et al. (2005).

w/Template and IDW methods demonstrates the advantage of combining of curvilinear grid and associated (s,n) coordinate system with neighbor search methods. As proposed by Merwade et al. (2005) an algorithm using Elliptical inverse distance weighting (EIDW) merged with (s,n) coordinate system on curvilinear grid may represent the riverbed topography better than w/Template and IDW methods.

Interpolations have been done, to represent riffle and pool formations, along the study reach, which can be classified as macro-forms ( ¿ 1 m length). The broad interpretation of our work also includes microforms (such as grain surface and patches with a length of 0.01 - 1 m), which are embedded into the macro-forms. Considering that hyporheic exchange flows microforms over the streambed are considered as $0.01-1$ m and macroforms are over 1 m ( eg. bars, pools, riffles) Käser et al. (2013). Observations and comparison tests of the elevation points show that the data available can capture particular size of microforms, nevertheless, macroforms can be fully represented. The mesh sizes have been chosen as $50 \times 50$ cm to compare the performances of the interpolations. Computational mesh sizes can be smaller than the ones chosen for river bed in order to simulate CFD parameters over interpolated bed topography, which is at the same time bottom boundary for surface water model.

# Chapter 4

# Delineating Aerobic and Anaerobic Zones:A coupled Subsurface Model

## 4.1 Introduction

The exchange of water between streams and streambed systems, known as hyporheic exchange, is chiefly the result of hydraulic head gradients in and around streams (Bencala, 1983; Dudley Williams and Hynes, 1974; Baxter et al., 2003; Buffington and Tonina, 2009).Strong hyporheic exchange can be observed at transitional streambed features such as near riffle crests. The subsurface environment,which constitutes the hyporheic zone, HZ, may present highly heterogeneous sediment structures, through which surface water flows before upwelling into the stream. Sediment properties, groundwater water table, and river bed topography are the main factors that affect hyporheic exchange (Cardenas et al., 2004; Boano et al., 2009, 2010a). Those properties also set the lateral and horizontal boundaries of the hyporheic zone (Haggerty et al., 2002; Tonina and Buffington, 2007; Hester et al., 2013).The lateral exchange through the riparian zone might be large enough that all surface water of a small stream can recirculate as pore water within kilometers (Choi et al., 2000).

Hyporheic exchange induced by flow-streambed interaction is an essential information to quantify stream water residence time and its pathways through the streambed sediment. Hyporheic exchange originates from the uneven distribution of near-bed pressure caused primarily by the interaction between stream flow and river morphology (Elliott and Brooks, 1997; Thibodeaux and Boyle, 1987; Vaux, 1968). Near-bed pressure gradients over the stream boundary originate from the interaction between stream flow and topographic features, which include meanders, point- bars and riffle-pool sequences. The near-bed pressure changes drive stream water to enter the

sediments in high pressure zones and to exit the sediment in low pressure zones generating the so call pumping mechanism (Buffington and Tonina, 2009; Elliott and Brooks, 1997; Marion et al., 2002; Tonina and Buffington, 2009; Wörman et al., 2006).

This basic physical dynamic that generates hyporheic exchange, affect the water quality in the riparian system. Hyporheic exchange thus potentially affects the fate of the in-stream solutes with implication for water quality and habitat quality of aquatic and semiterrestrial organisms. Hyporheic exchange induces phisical and chemical gradients, which support a reach ecotone. Nutrients and dissolved gas transported into the streambed sediment are necessary for the suitability of habitat (Triska et al., 1989). The transport and distributions of a wide array of solutes and particles, either reactive or non-reactive, are also controlled by this processes (Jones and Mulholland, 1999; Winter, 1999; Wörman et al., 2002).

Transport of reactive solutes such as dissolved inorganic reactive nitrogen (Galloway and Cowling, 2002) in the hyporheic zone is controlled by the combination of hyporheic exchange, sorption processes, and biogechemical dynamics (Kim et al., 1992; Runkel and Bencala, 1995; Wood and Baptista, 1993). Residence time distribution is a key information to quantify the concentration of reactive solutes within the hyporheic zone (Bencala, 1983; Runkel and Bencala, 1995; Wörman et al., 2002). Residence time distribution should be identified well in order to quantify the concentration of the reactive solutes within the hyporheic zone (Bencala, 1983; Cardenas et al., 2004; Elliott and Brooks, 1997; Haggerty et al., 2002; Stonedahl et al., 2010). The particle travel time within the hyporheic zone identify the hyporheic residence time of stream water within the streambed sediment (Gooseff, 2010). It has been observed as an important information in explaining biogeochemical processes such as nitrification and denitrification within the streambed (Duff and Triska, 2000; Mulholland and DeAngelis, 2000; Naiman and Bilby, 1998; Thomas et al., 2003).

Because hyporheic flows are a function of the interaction between stream flow and streambed topography, it is expected that also biogeochemical reactions, which depends on residence time distributions, are in turn dependent on streambed morphology. Studies on hyporheic flows induced by large-scale three-dimensional bedforms, such as those considered in the present work, were examined through field measurements and numerical models (Gooseff et al., 2003; Kasahara and Wondzell, 2003; Storey et al., 2003; Saenger et al., 2005; Wondzell, 2006). One set of laboratory experiments (Tonina and Buffington, 2007) and an analytical solution applied at a large watershed scale (Wörman et al., 2002), and the work of Marzadri et al. (2010) provided analytical relationship between bed form morphology and hyporheic flow. Also groundwater modeling approach has been used in several studies (Harvey and Bencala, 1993; Wondzell and Swanson, 1996; Wroblicky et al., 1998; Woessner, 2000; Wondzell et al., 2009a; Ward et al., 2013) to examine factors

controlling hyporheic zone size and flow paths dominated by groundwater level.

These models have helped to develop our understanding of the factors that control the hyporheic exchange. Some of the models in regional scale represented the stream as a single cell wide, which neglect lateral hyporheic flows. Some models were two-dimensional models, such that, none have attempted to compare the behavior of vertical versus lateral flow paths under varying hydrological conditions. Some of the models in regional scale represented the stream as a single cell wide, which neglect lateral hyporheic flows. Some models were two-dimensional models, such that none have attempted to compare the behavior of vertical versus lateral flow paths under varying hydrological conditions. Three dimensional semi-analytical models as the one of Marzadri et al. (2012) and Stonedahl et al. (2010) are appropriate for increasing our understanding of hyporheic biogeochemical processes, however, in hydraulic point of view model boundary conditions need to include the groundwater flow field surrounding the stream of interest under the complex channel geometry. Fully 3D numerical models in which groundwater effect was evaluated well with the work of Lautz et al. (Lautz and Siegel, 2006) for bigger reach scale as a part of regional scale perspective, or in the work of Trauth et al. (Trauth et al., 2013) by including different surface water discharge levels on a single riffle and pool sequence in order to see the differences of gaining-losing conditions. Nevertheless, additional effort on characterizing channel geometry and flow variability, hydraulic conductivity and interactions with groundwater surrounding the stream can lead us likely to be more improved model for valid quantitative predictions of surface-subsurface solute transport and effects on related biogeochemical processes.

Specifically, it was determined that the conditions governing the fate of N in the hyporheic zone are both the physical transport, which control the residence time, and reaction kinetics, which control aerobic and anaerobic conditions. An important scaling relationship, called Damkohler number for the dissolved oxygen, $Da_{O_2}$, has been proposed for scaling different streams hyporheic zones and their role on the fate of stream N. This dimensionless number relates a characteristic timescale of the hyporheic residence time and that of DO consumption. This index can be use to investigate the control of stream morphology, flow and temperature regime on prevailing aerobic and anaerobic. It has also been shown that it could help in identify when the hyporheic zone could be potentially a source or sink (Zarnetske et al., 2012; Marzadri et al., 2012) of N.

The aims of this present work are (1) to describe and explain differences in vertical versus lateral exchange flows and changes on flow paths that are occurring in different parts of the streambed; (2) to explore the role of groundwater discharge induced by head gradients between groundwater table and stream stage on local hyporheic flows; (3) to describe the change

in upwelling and downwelling zones under the influence of different surface water and groundwater discharge; (4) to quantify the hyporheic residence time distributions at the reach and bedform scales; (5) to demonstrate potential aerobic/anaerobic zones that the subsurface model predicts by using Damkohler number for dissolved oxygen ($Da_{O_2}$).

## 4.2 Methods

The reach bathymetry was created by interpolation from a topographical survey of the River Bure (see Chapter2). We assumed that surface and subsurface water hydraulics can be studied separately, because of small water and momentum exchanges between the two flows. Thus we developed a two dimensional hydraulic model to quantify water surface elevation and depth with the assumption of non-erodible banks. We treated the hyporheic fow as a Darcy's flow in homogeneous media. Additionally, The two systems are connected via the near-bed pressure distribution. In the following sections, each model was described in detail.

### 4.2.1 Free surface-flow model description

#### Bed topography

For the interpolation of riverbed w/Template method has been used which a method combined with modified version of nearest neighbor search method on curvilinear grid. (Knuth, 1973; Yianilos, 1993; Beis and Lowe, 1997). In this method, the search uses a template or bin with a specified width and length specified by grid prepared, aimed locations have been computed by linear interpolation between three nodes that corresponds to measured ancillary data. Created bathymetry has the functionality as a mediator between free-surface flow model and subsurface model. Longitudinal profile of the topography was imported as the upper boundary into subsurface model (see Chapter 3 for details),water surface elevation in our case, which is expressed in meter and defined as the total head normal to the bed surface plus the bed surface height above the datum.

As a further step, computational nodes between the measured cross sections were added, such that the nodes have a spacing of 0.3m in the flow direction. Then the longitudinal profile of topography has been interpolated between measured cross-sections as necessary to provide values at all nodes.

#### Mathematical basis

The Multi-Dimensional Surface-Water Modeling System (MD-SWMS) which has been developed by U.S. Geological Survey (USGS) was used to perform numerical solutions of computational models of surface-water hydraulics

(McDonald et al., 2001, 2005). The model chosen is two-dimensional flow model in a single reach a shallow stream. The model solves the depth-averaged form of the Navier-Stokes equations for open channel flow on a curvilinear coordinate system grid, incorporating a two-equation turbulence closure, which is assumed to be isotropic (Nezu et al., 1993), with an analytical correction for the effects of secondary circulation. The model requires channel bed topography, measured water surface (Stage) and inflow discharge and, bed roughness as input. It predicts the spatial distribution of depth-averaged velocity and water surface elevation. Flow properties for different discharge and boundary conditions were estimated.

Model requires values for boundary roughness over streambed which is typically quantifies by the equivalent height from the bed surface, $z_0$, where the bottom velocity is zero. The roughness coefficient is calibrated so that the surface water elevations measured match the simulated surface water elevations (see Figure 4.1).

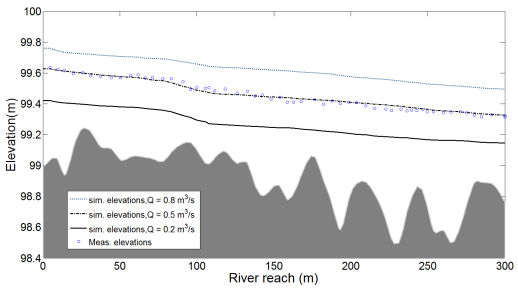


**Figure 4.1:** Simulated steady-state surface water elevation values for different flow conditions and the observations from fieldwork for the calibration for free-surface flow model

### 4.2.2 Subsurface-flow model description

#### Steady-State flow equation

A subsurface model is utilized to calculate the three dimensional flow in the porous medium, the riverbed, as influenced by topography, surface water flow. Hyporheic flow was treated as groundwater flow through the homogeneous porous media using Darcy's law. The Darcy equation is typically written in terms of laminar pore flow (Small Reynolds number, $Re \approx 1$) (Hassanizadeh and Gray, 1987) and locally uniform velocities. It was assumed that the laminar Darcy flow through a homogeneous and isotropic sediment for modeling purposes and our analysis.

$$\mathbf{u} = -k\frac{\partial h}{\partial \mathbf{x}} \tag{4.1}$$

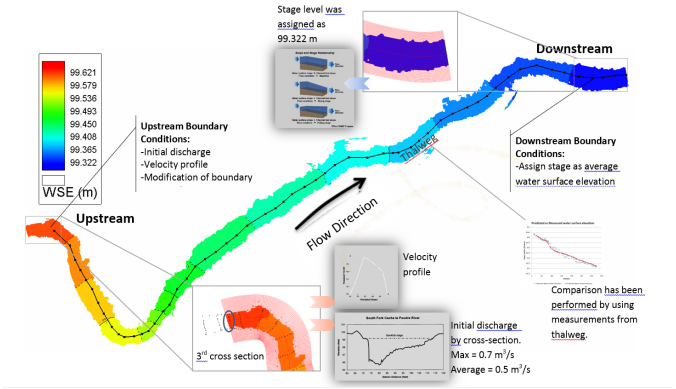


**Figure 4.2:** Summary of Free Surface-Flow model setup and validation over water surface elevation map within the model domain

where $\mathbf{u}$ is the Darcy velocity, $\mathbf{x}$ is the coordinate vector, $k$ is the hydraulic conductivity of the sediment in one dimension, and $h$ is the hydraulic head.

The mathematical model of the subsurface flow is based on the semi-analytical work of (Taylor, 1954) that gave a mathematical description of the basic processes that govern the transport of dissolved substance in flowing fluids. Those processes later analyzed for a sand-bedded river under the hypothesis of homogeneous and isotropic medium by Boano et al. (2007). Three-dimensional non stationary flow in homogeneous porous media with hydraulic conductivity tensor $K_H = (K_x, K_y, K_z)$ was solved.

$$K_x \frac{\partial^2 h}{\partial x^2} + K_y \frac{\partial^2 h}{\partial x^2} + K_z \frac{\partial^2 h}{\partial z^2} = S_s \frac{\partial h}{\partial t} \tag{4.2}$$

where the hydraulic head included as $h(x, y, z)$ as spatial form and $S_s$ is the storage coefficient which is the source term in equation 4.2. Storage coefficient represents the volume of water released from storage per unit drawdown of hydraulic head in the sediment, per unit area of the sediment bulk. The pressure variation responsible of water storage is smaller respect to its spatial variation. According with this considerations, we assume negligible the head variation in time.

$$S_s \frac{\partial h}{\partial t} \approx 0 \tag{4.3}$$

With the assumptions above the numerical solutions have been succeeded according to equation 4.4:

$$K_x \frac{\partial^2 h}{\partial x^2} + K_y \frac{\partial^2 h}{\partial x^2} + K_z \frac{\partial^2 h}{\partial z^2} = 0 \tag{4.4}$$

### Finite difference method and domain design

Finite difference methods are used to numerically approximate differential equations, which involves employing the derivation of bed-surface head values. The calculations were performed by using MODFLOW based on finite difference model (McDonald and Harbaugh, 1984) to solve equation 4.2 on steady-state conditions and calculate the head distribution throughout the subsurface based on the boundary head distribution along the stream channel boundary (stream bed).

The subsurface model domain is 248 m long, 110 m wide and 6 m depth (Figure 4.3). The depth is chosen in order to see the effect of groundwater and try to represent the transition zone from groundwater to hyporheic zone over the flat bottom boundary. Grid spacing across the model domain is $0.3 \times 0.3$ m and 0.5 m on vertical direction. Twelve layers were defined for the domain. For hydraulic conductivity an average value of 0.005 m/s was use for the all layers inside the domain, which is the highest value according to particle size analysis, at the same time the minimum hydraulic conductivity for unconsolidated sedimentary gravel media Domenico and Schwartz (1998).

The stream was represented by constant head nodes in the upper layer of streambed cells and upper five layers arranged according to streambed topography. Grid cells were activated or inactivated according to topography and the depth of the corresponding layer (Figure 4.3). The bottom layer was bounded on all sides by constant heads to permit local groundwater flow and to define heads for the reach. Values for the constant head boundaries were calculated by surface model and interpolated over the constant head boundaries. The bottom of layer 12 is a no-flow boundary and the side boundaries of layers 1-11 (which followed the catchment boundaries and groundwater flow lines) also were no-flow boundaries.

The model was run at steady state, and certain parameters as boundary discharge values, and groundwater levels were altered according to the amounts by which they are known to vary in the River Bure. The impact of the topography was analyzed on the exchange at a homogeneous, isotropic riverbed for different river discharges. Discharge values of $0.2, 0.5$ and $1\,\mathrm{m}^3/\mathrm{s}$ were chosen in order to see the effect of different discharge on residence time in hyporheic zone. The lower discharge condition represents just before the drying conditions of the reach and higher discharge value represents flooding condition according to surface water model runs. The average discharge was calculated from in-situ velocity readings of the reach. Discharge to the stream is defined as the volumetric flux of water removed from the model by all constant head cells that represents the stream.

The groundwater boundaries have been arranged according to water level measurements from wells that were set for the data logging. It was observed that the groundwater level from 2 m from the starting point of the bank

is between 99.455 m to 99.798 m minimum to maximum elevation from the datum (see Chapter 2). The effect of groundwater values were added as constant boundary conditions according to groundwater measurements from the field as 99.8 m for upstream and 99.64 m for downstream.

While the model was an attempt to reproduce a real system, some assumptions were made in order to simplification of the model. Only exchange flows induced by pool-riffle transition and morphological feature such as meander were considered. Boulders and large woody debris were not represented in the model.

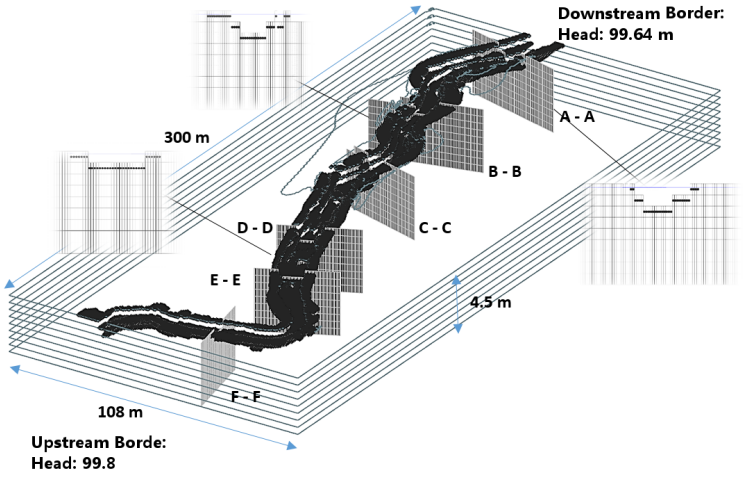


**Figure 4.3:** General demonstration of subsurface model domain and cross-sections over bathymetry as cascade grids, upper boundary condition is arranged as constant boundary condition which was represented by black points

### Particle tracking and residence time distribution

Hyporheic exchange flow paths and subsurface residence time distributions were determined with the particle tracking method implemented in MODPATH (1994). To evaluate exchange, approximately 3006 particles were distributed over the streamed surface at 11 equidistant locations selected from a probability distribution proportional to the boundary influx (see figure 4.5). Particle motion in the subsurface was deterministic, as it was calculated based solely on the calculated subsurface velocity field. It was considered as the advective non-reactive particle transport through the porous media and scale of topography included.

In each iteration the local seepage velocity was calculated from a linear

interpolation of the head distribution at each particle location, and each particle was then translated by the distance in the direction of the seepage velocity. The periodicity imposed on the model domain allowed us to track the fate of particles that reached the downstream boundary simply by reintroducing them into the domain at the corresponding location of the upstream boundary. The location of each particle was tracked relative to the streambed surface at every step in the particle-tracking routine. The subsurface residence time distribution was calculated simply by recording the amount of time that each tracked particle took to return to the surface water. Reach has been divided and analyzed into 3 basic zones those have been chosen according to morphologic and topographical reasons (see Figure 4.5(d)). The resulting residence time distribution of each zone was flux-weighted because the particles were introduced to the subsurface in proportion to the boundary flux.

### 4.2.3 Prediction of aerobic/anaerobic zones

N transforming processes (in this case nitrification) and respiration of the biomass (DOC reduction) consume oxygen within the hyporheic zone, such that aerobic processes are active from the downwelling area where initial concentration, $C_0 = C_{0,0}$, as spatial representation is also starting point of trajectories. As suggested by the work of Marzadri et al. (2012), the ratio between hyporheic median residence time, $\tau_{50}$, and the oxygen time limit, $\tau_{\text{lim}}$ can be used as an index prevailing aerobic or anaerobic conditions within HZ:

$$Da_{O_2} = \frac{\tau_{50}}{\tau_{\text{lim}}} \tag{4.5}$$

With this consideration, the dimensionless number, $Da_{50}$ , is a sufficient metric to provide immediate indication of the previling conditions within the HZ from the downwelling area to upwelling surface. The portion of the streamline whose travel time is larger than $\tau = \tau_{\text{lim}}$ the aerobic processes are assumed to switch off as the systems is anaerobic. Such that $\tau_{\text{lim}}$ is the time within the HZ for which dissolved oxygen concentrations, $DO$ , reach the threshold value, $DO_{\text{lim}}$ below which aerobic reactions stop. The following equation is suggested for $\tau_{\text{lim}}$

$$\tau_{\text{lim}} = \frac{1}{K_R + K_N} \ln(\frac{DO_0}{DO_{\text{lim}}}) \tag{4.6}$$

where $DO_0$ the dissolved oxygen concentration at the downwelling area and assumed as the stream DO concentration, and $K_R + K_N$ represents the reaction rate of the dissolved oxygen consumption by respiration and nitrification processes respectively (see Table 4.1 for the calculated and used coefficients).

Median residence time can be used as an indicator to define aerobic and anaerobic conditions for a particular location in hyporheic zone. Values of $Da > 1$ proves that anaerobic conditions and most likely denitrification prevails in the location, where can be considered as a sink of nitrates and a source of nitrogen gases. In contrast, once $Da < 1$, aerobic conditions prevail and the hyporheic zone may be considered as source of nitrate, which is a typical condition of Nitrification dominated locations.

**Table 4.1:** Biogeochemical parameters for the calculation of $Da$ numbers as a function of time and space

| **Coefficients** | **Units** | **Values** |
|---|---|---|
| $DO_0$ | $(\mathrm{mg\,l^{-1}})$ | 7.5 |
| $DO_{\mathrm{lim}}$ | $(\mathrm{mg\,l^{-1}})$ | 2 |
| $T_{\mathrm{pore}}, w$ | (°C) | 11.7 |
| $K_R$[a], 20°C | $(\mathrm{d^{-1}})$ | 0.1 |
| $K_N$[b], 20°C | $(\mathrm{d^{-1}})$ | 3.46 |
| $\varphi_R$[c], 20°C | $(-)$ | 1.047 |
| $\varphi_N$[d], 20°C | $(-)$ | 1.04 |
| $K_R$, 11.7°C | $(\mathrm{d^{-1}})$ | 0.086 |
| $K_N$, 11.7°C | $(\mathrm{d^{-1}})$ | 2.499 |

[a] Reported in Rutherford (1994)
[b] Reported in Sjodin et. al. (1997)
[c] Reported in Rutherford (1994)
[d] Reported in Sjodin et. al. (1997)

## 4.3 Results and discussion

### 4.3.1 Surface water elevations

Surface water elevations were calculated over the bed topography, which was created by interpolation of topographical data. The surface water profiles fluctuates according to slope changes at the measured cross-sections, changes on the gradient of water surface elevations are essential for further hyporheic modeling (Subsurface flow). For this purpose, water surface model was validated with measured water surface elevations. Final model gives good representation of water surface elevation with 30 cm grid size, $0.5\,\mathrm{m^3/s}$ boundary discharge. The calculated surface water elevations agree with the measurements on $0.5\,\mathrm{m^3/s}$ discharge conditions (see Figure 4.1). The Root Mean square Error for the simulated surface water elevations compared to the measured elevations at the transects is low, with 0.0169 m.

### 4.3.2 Subsurface head predictions

The effect of head gradients on the stream was analyzed for a model domain with homogeneous, isotropic sediment. The results show more exchange flow over the model domain than at the banks. The exchange patterns for the cascade grid represents the topography as small blocks instead of interpolated grid spaces (see Figure 4.3).

Results show that $1\,m^3/s$ is the maximum discharge value that the river can hold, because this value causes flooding condition according to properties arranged. Generally head values over the domain are between the range of 99.8 m to 99.3 m in all cases. Demonstration of the steady-state solution shows that head values are mostly in agreement with the measured water table on the bank and under the bed. The model predicts equipotential heads that are parallel with river channel, however, the effect of groundwater increasing with lower discharge conditions (see Figure 4.4(f)).

### 4.3.3 Trajectories and residence time distribution

Model simulations show that the output parameters, exchange flux, lateral and vertical flows, and hyporheic travel times, are determined by two factors: These factors are two conditions at the boundaries of the hyporheic zone: the head difference over the stream, and the flux of groundwater entering the sediment area from the sides and beneath. Figure 4.5 shows that down-welling and upwelling zones over the reach are not changing but infiltration rate of the water increases by the amount of stream discharge. Also, hyporhiec zone takes its deeper form in low discharge condition for about 4.5 m, however, longer and continuous trajectories can be observed in higher stream discharge conditions.

One particle injected into each cell in the upper four layer of the model domain which corresponds to cells that represent river bed and the same practice followed over the reach from upstream to downstream. Particles have been calculated over the specified three zones (see Figure 4.5). Figure 4.6 shows the cumulative frequency distributions of residence time of particles initiated from each location, according to simulations the highest residence time is mostly around meander part of the river, which is approximately 22 hours in average on low discharge condition and 336 hours for high discharge condition.

Particles are giving different responses to each discharge rate, any change in surface water elevation value leads noticeable differences on particle pathways.

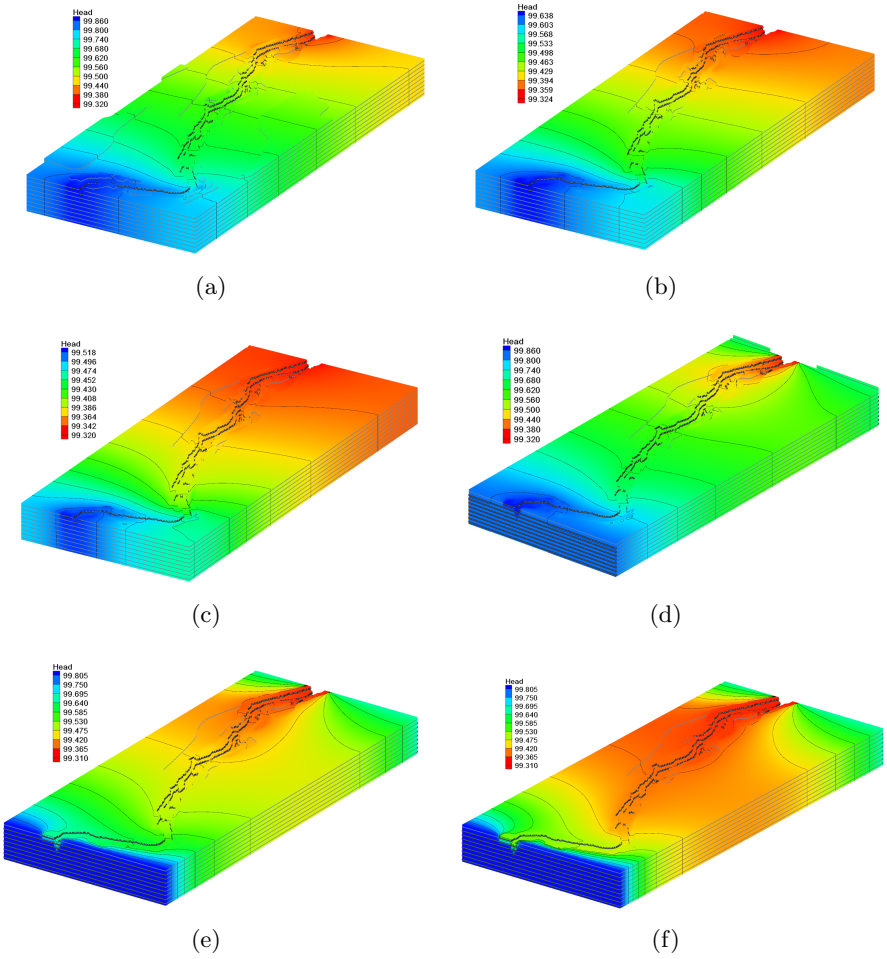


**Figure 4.4:** Subsurface steady-state head solutions (a) $1\,m^3/s$ ; (b) $0.5\,m^3/s$ ; (c) $0.2\,m^3/s$ discharge values without groundwater effect and (d) $1\,m^3/s$; (e) $0.5\,m^3/s$; (f) $0.2\,m^3/s$ with groundwater

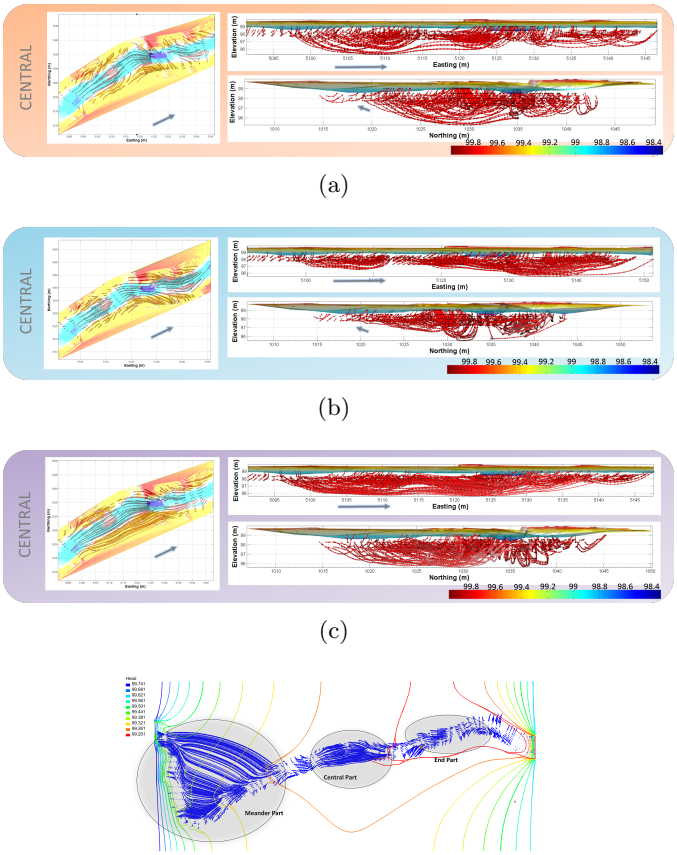


**Figure 4.5:** Particle trajectories for different discharge conditions for central part of the river; Grey arrows shows the direction of the flow, red trajectories occupies the area of residence of a particle until upwelling point, the particles demonstrated as x-y, x-z cross-sections and plan view. (a) is for $0.2\,\mathrm{m}^3/\mathrm{s}$; (b) is for $0.5\,\mathrm{m}^3/\mathrm{s}$ ; and (c) is for $0.8\,\mathrm{m}^3/\mathrm{s}$; (d) plan map of domain divided into zones according to morphological features.

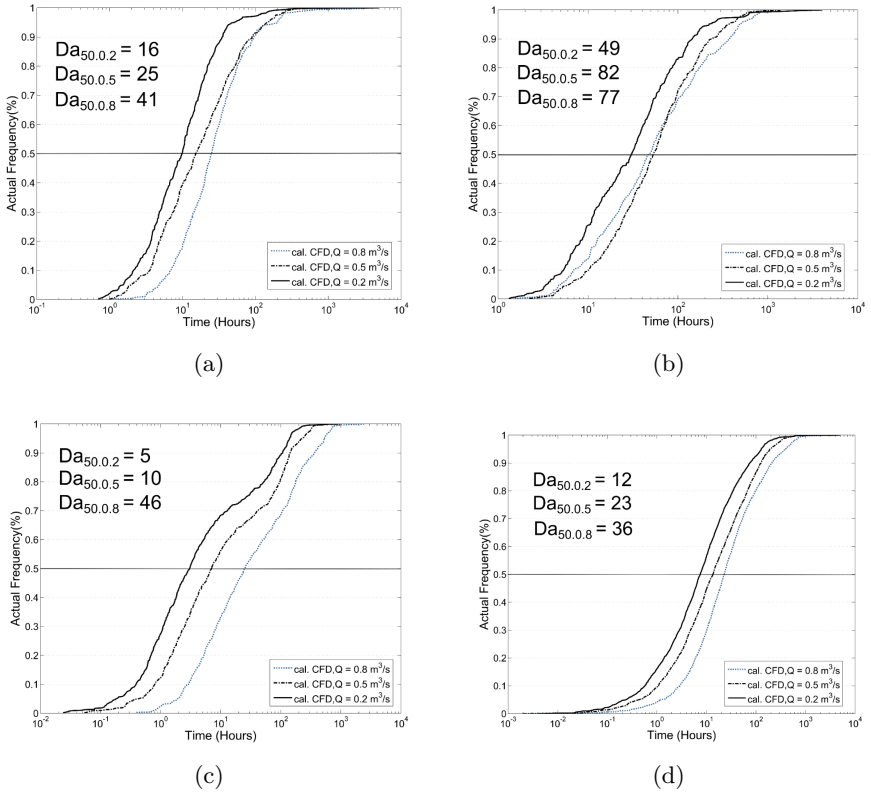


**Figure 4.6:** *Da* numbers and residence time distributions of three different zones as, (a) is for downstream part; (b) is for central riffle and pool part; (c) is for meander; (d) is to demonstrate distribution of whole reach.

### 4.3.4 Prevailing aerobic/anarobic zones using Damköhler number

Geochemical transformations occurring in the hyporheic zone depend on the residence time of solutes advective travel time. The time needed to reach the anoxic conditions as expressed by the ratio between the residence time, and the time needed to deplete oxygen concentration, $DO_0$.

According to the biogeochemical reaction rates which deplete the oxygen source, $Da_{50}$ values can be different, mostly high numbers ($Da >> 1$) shows that prevailing anaerobic conditions. Observations of cumulative frequency distribution of residence time shows high damköhler numbers, or instance in central part, the highest is 82 since the lowest is around 50. We can see high $Da_{O_2}$ values also for the other zones and also for whole reach, therefore, calculations indicate that more than 50 % of the streamlines are already in anaerobic conditions where they cross river bed which is at the same time upper boundary of the subsurface model.

**Figure 4.7:** Prevailing anaerobic/aerobic zones as distribution of Damköhler index. Only central part has been demonstrated with three discharges. On the figure the cross-section on the left demonstrates X-Y, the center, Z-Y, and the right one shows Z-X. (a) is for $0.2\,\mathrm{m}^3/\mathrm{s}$; (b) is for $0.5\,\mathrm{m}^3/\mathrm{s}$ ; and (c) is for $0.8\,\mathrm{m}^3/\mathrm{s}$

For given hydraulic and biogeochemical characteristics of the sediment, $Da$ increases passing from shallow groundwater fed zone to deeper riffle-pool

zone (Figure 4.6). The changes along the zones are not evident, even the residence time curve of central zone is distributed on slightly higher residence time values. However, the response of the zones to high and low discharge values varies, therefore, we can observe how the local oxygen depletion is related with discharge values. On the other hand, predictions show that the spatial distribution of prevailing aerobic/anaerobic zones shifts drastically depending on different stream discharge values. The spatial distribution of prevailing aerobic/anaerobic zones shifts drastically. The cross-sections of central part in Figure 4.7 shows that in low discharge condition with the chosen reaction rates, most of the anaerobic zone ($Da < 1$) is mostly around 2 m under the streambed. Conversely, in higher discharge conditions, variability of distributions of the zones are higher, such that we may see anaerobic portions on through the surface of the sediment (see Figure 4.7(c)).

## 4.4 Conclusion

Hyporheic exchange process at River Bure are mostly controlled by groundwater and even more on bed topography and morphological features. Subsurface model is capable of calculating the hyporheic exchange processes and the controlling parameters. Numerical subsurface model is constructed to approach realistic hydraulic conditions measured at River Bure. Water surface elevation that was calculated applied over the streambed domain of the subsurface model by interpolation through longitudinal profile of the river reach. The results show that exchange flows tend to be stronger but variable at the sides than at the center of the stream channel. Groundwater discharge prevents vertical and lateral exchange flows at the sides while vertical exchange still occurs beneath the center of the stream under the conditions of regular and lower surface water discharge. However, the morphological features as meanders or point bars and flooding conditions (high discharge) buffers the effect of groundwater and increases residence time adjacent zones. Therefore, as the flux of subsurface increased proportionally with stream slope, hyporheic flow paths became shallower and hyporheic residence time became shorter.

According to findings it can be concluded that higher water surface values increases the hyporheic flux and so the hyporheic residence time in regional scale. However, it can be seen from the residence time distribution curves that increase is not proportional in local scale of the river bed, such that in lower discharge condition of surface water shows higher hyporheic residence time on central part of the reach which has the lowest elevation of the reach.

$Da$ values lower than 1 results in prevailing aerobic conditions with low reactive nitrogen removal at the unit scale. Values of Da larger than 1 indicate prevailing anaerobic condition with large opportunity of Nr removal

and production of nitrogen gases. The observations and predictions of local hyporheic flow dynamics and related residence time distributions shows the response of the system to different discharge conditions with local morphological properties. It can be concluded that the denitrification dominates mostly riffle and pool, and point bar parts of the reach because of high $Da_{50}$ values, which leads us to anaerobic zones. Nevertheless, simulations show that aerobic zones are mostly more spread into the system than anaerobic ones in normal conditions.

# Chapter 5

# Composition of Sediment Heterogeneity: Effects on Hyporhec Flow

## 5.1 Introduction

Transport of reactive solutes such as dissolved inorganic reactive nitrogen (Galloway and Cowling, 2002) in the hyporheic zone is controlled by the combination of hyporheic exchange , sorption processes, and biogechemical dynamics (Kim et al., 1992; Runkel and Bencala, 1995; Wood and Baptista, 1993). In such combination hyporheic mechanisms hold importance in order to analyze the transport and fate of the reactive solutes by advection-dispersion mechanisms in stream flow (Bencala, 1983; Runkel and Bencala, 1995; Wörman et al., 2002). Residence time distribution holds key importance in order to quantify the concentration of the reactive solutes within the hyporheic zone (Bencala, 1983; Cardenas et al., 2004; Elliott and Brooks, 1997; Haggerty et al., 2002; Stonedahl et al., 2010). The residence time distribution encapsulates the net subsurface flow and transport characteristics. The residence time here may comprise the whole path lengths within the reach or specified system, however, travel time of particles and their distributions in hyporheic zone is attributed as the hyporheic residence time (Gooseff, 2010). Hyporheic residence time can also be considered as the key concept that connects the hyporheic flow mechanisms with biogeochemical processes. Biogeochemical activities occur in the streambed sediment depending on the time that a reactive particle spends within HZ. (Duff and Triska, 2000; Mulholland and DeAngelis, 2000; Naiman and Bilby, 1998; Thomas et al., 2003).

Numerical models of hyporheic flow and transport have been widely used in studies of hyporheic hydraulics and related exchange conditions (Saenger et al., 2005; Gooseff et al., 2003; Wondzell et al., 2009a; Ward et al., 2013).

Most of the basic models of hyporheic zone has been designed as coupling of stream-flow with groundwater in order to resolve simple hydraulic behavior on a single triangular bed form (Cardenas and Wilson, 2007b; Cardenas, 2008; Cardenas and Wilson, 2007a). Conversely, later on the models that includes the effect of system of bed forms (Tonina and Buffington, 2007) or the effect of macro formations as alternate bars (Marzadri et al., 2010), and meanders (Peterson and Sickbert, 2006; Revelli et al., 2008) were developed. Some models also enhanced the understanding of hyporheic zone by aiming to define deeper groundwater effect (Boano et al., 2009) or the effect of different discharge conditions (Boano et al., 2010b) including the alterations on the stream (e.g. rehabilitations, riffle-step restoration) (Kasahara and Hill, 2006). Besides those enhancements and novel works have been done, a number of field and modeling studies carried out to expose the relation between observed stream characteristics and hyporheic exchange (Bencala, 1983; Packman and Brooks, 2001; Kasahara and Wondzell, 2003; Cardenas et al., 2004).

There is now a considerable amount of knowledge about the influence of stream hydrology and morphology on the spatial patterns of exchange. On top of that, the implications of the temporal variations of stream discharge and effect of the depth of hyporheic zone have been included (Boano et al., 2010b). However, previous studies have basically demonstrated the existence of complex feedbacks between stream hydrology and hyporheic exchange on homogeneous domain in order to refine their models to explain one or few specific problem. The need to account for natural heterogeneity and spatial variability became more evident by the advancement of mathematical models and demand of representations of real time events especially on riparian systems (Bardini et al., 2013). The first implication to numerical model in search for the effect of streambed texture on hyporheic flux was demonstrating that the hyporheic change is being inhibited if the hydraulic conductivity ($K$) of streambed is below a certain threshold (Storey et al., 2003).

Initial field studies practiced by tracer tests indicate that depositional and diagenetic processes dominate the spatial structure of sedimentary aquifers (Freyberg, 1986; Sudicky, 1986; LeBlanc et al., 1991, e.g.). According to this, in particular, the large scale structure of hydraulic conductivity controls the paths of subsurface water while both large and small-scale variations in the domain control the rate of solute dispersion (Adams and Gelhar, 1992; Boggs and Adams, 1992; Rehfeldt et al., 1992; Boggs and Adams, 1992). Other studies have examined small and large scale spatial variability in fluvial and alluvial deposits and indicate that hydraulic conductivity can be predictably related to stratification type and depositional processes (Davis et al., 1993; Stalkup, 1986; Smith, 1981). Fluvial and micro-scale sediments show much more complex structure, and it was proved that this structure plays critical role in the biogeochemical dynamics, especially $NO_3^-$ reduction

in hyporheic zone (Boulton et al., 1998; Sophocleous, 2002; Cardinale et al., 2002).

The influence on hyporheic flow of permeability heterogeneity, arising from certain types of streambed stratification, has also been examined supported by numerical modeling works (Cardenas et al., 2004; Conant, 2004; Krause et al., 2013; Sawyer and Cardenas, 2009; Fleckenstein et al., 2006, e.g.). However, mostly the formations have been evaluated according to few sedimentary strata or dual-type formations, such as stratifications between high hydraulic conductivity zones and low hydraulic conductivity zones (Storey et al., 2003; Krause et al., 2013; Schornberg et al., 2010) or with a scale of hydraulic conductivity zones that represents relatively lesser difference between the highest to lowest values (magnitude of 20 ) (Cardenas et al., 2004). Conversely, it was observed that many different type of texture can form the sediments on the riverbed those have variations in hydraulic conductivity of higher magnitude difference (Anderson, 1989; Webb and Anderson, 1996) and also clogging is another effect which changes the magnitude of hydraulic conductivity values (Blaschke et al., 2003). Another focus on heterogeneity on sedimentary deposits in rivers is the scale from microforms as sediment surfaces to mesoforms as riffle - pool and/or step-pool formations on the riverbed to macroform scale as point-bar and meander (Ritzi et al., 2004). It was proved that hyporheic flow paths often encounter mesoforms such as cross beds that could influence the hyporheic exchange (Sawyer and Cardenas, 2009). Furthermore it was seen that grain size variations impact the ecological health and structure of hyporheic fauna at small scales of formations (Boulton, 2007; Wagner and Bretschko, 2002).Sometimes sediment heterogeneity affects by limiting groundwater flow-paths through upwelling zones (Krause et al., 2013). Therefore, resolving the impact of subsurface heterogeneity on hyporheic zone with the combinations of mesoforms and macroforms over the complex river bed formations.

This chapter focuses on the effect of subsurface heterogeneity arising from stratification under the stream. The streambed was depicted as low hydraulic conductivity texture with silty layers that have high organic content. The goal of this chapter is to investigate the effects of sediment subsurface heterogeneity over hyporheic flow by the residence time concept. The discrete features of the conductivity field as the formation of hydrofacies and the magnitude of the hydraulic conductivities were considered based on the field observations and data. Different hydraulic conductivity zones were depicted over 3D discretized representation of the reach. In order to simplify the heterogeneity over the subsurface domain, the complexity over bank sides were not represented, and the subsurface formation of the reach defined as four different bed form configurations based on the sediment size analysis (see Chapter 2, section 2.3.1). Hyporheic exchange through immobile bed forms was numerically simulated with created complex topography.

Fluxes of over 114 realizations of heterogeneous hydraulic conductivity fields were simulated by the stochastic approach, and residence time distributions observed.

## 5.2 Methods

The river bed formation was created by interpolation based on the topographical data that was collected from River Bure (for details see Chapter2). The head boundary for subsurface model was obtained by solving numerically the surface flow on the interpolated streambed (Sawyer and Cardenas, 2009; Jin et al., 2010; Bayani Cardenas and Wilson, 2006). Steady-state Reynolds-averaged Navier-Stokes (RANS) equations are applied to solve the surface water domain and provide a head distribution for the interface between the surface and subsurface regions (represents hyporhec zone and shallow aquifer domain). Spatially variable specified head values are then assigned as a Dirichlet boundary condition for groundwater flow equation along the interpolated bed surface. The model consider the combination of several riffle-pool and meander sequences along the 300m reach and apply spatially variable head values on their lateral subsurface boundary.

### 5.2.1 *Heterogeneous Subsurface Model Description*

Subsurface model is utilized to calculate 3-D flow in the porous medium induced by the streambed head gradients. Hyporheic flow was treated as groundwater flow through the heterogeneous porous media using Darcy's law. It was assumed that the laminar Darcy flow is the main mechanism through a heterogeneous and anisotropic sediment for modeling purposes and our analysis. Basically boundary conditions for the model consist of a no-flow boundary. Dirichlet conditions were set at the lateral boundaries which faces to north to south, and mixed boundary conditions were defined where variable head values and constant groundwater boundary intercepts on upstream and downstream faces.

For most practical hydraulic problems that involves heterogeneous porous media and the irregular shape of the local boundaries, it is not possible to solve the mathematical models analytically (Marzadri et al., 2010). In our case mathematical model was transformed into the numerical model that was explained in detail on Chapter 4.

#### *Domain design*

The design of the domain was re-done in order to facilitate the hydrofacies simulations via transition probabilities. In this domain smooth representation of river bed recreated instead of cascade type representation with the same scale and according to topographical measurements (see Figure 5.1).

By this it would better to capture the changes and continuum of the flow on the first few centimeters of the river bed.

Four hydrofacies; gravel, fine sand, high organic content silt, and clay were distinguished according to field observations for the models (see Chapter 2). Cell dimensions have been chosen according to river interpolations. Mesh sizes for surface flow model are arranged as $0.5 \times 0.5$ m on the surface (Cartesian X and Y coordinates), however, grid size in the vertical direction is varied in order to capture the effect of surface formations and heterogeneity in the upper layers of the sediment ( Figure 5.1 first 2 meters in the domain). Depositional strike-, dip- and vertical directions were adjusted as $0.3, 0.5$ and $0.1$m respectively for all clusters individually. A $300 \times 110$ m wide and 6 m thick sub-domain was used in order to compute initial stochastic realizations. Subsurface domain was discretized as $0.5 \times 0.5 \times$ cells horizontal and $0.05 - 0.5$ m vertical directions. K-values in Table 5.1 were assigned to the all hydrofacies based on the field data and the literature (Domenico and Schwartz, 1998).

### 5.2.2 *Geostatistical simulation of subsurface heterogeneity*

Three-dimensional geostatistical models of geologic heterogeneity were generated by sequential indicator simulations based on transition probabilities and Markov Chains using the software T-PROGS (Carle, 1999; Carle and Fogg, 1996, 1997). T-PROGS is based on the probabilities of transitions from one hydrofacies to another, and the modeling of statistical probabilities over the specified domain is called Transitional Probability Geostatistics (TPG) method (Carle and Fogg, 1996). The spatial variability of sediment on the domain is defined as hydrofacies units that is defined by several works (Engdahl et al., 2010; Fleckenstein et al., 2006; dell'Arciprete et al., 2012, e.g.). Indicator variables are used to describe the possibility of existence or absence of particular hydrofacies at a particular location. Indicator variable $I_n(x)$ can be represented as

$$I_n(x) = \left\{ \begin{array}{c} 1, \text{if n is present at x} \\ 0, \text{vice versa} \end{array} \right\} \tag{5.1}$$

where the category n, which is predefined according to sediment cores, represents a particular hydrofacies at location $x$ (Carle, 1999). Indicator hydrofacies were selected from $30 - 40$ cm sediment core logs for representation of spatial heterogeneity. Datasets were sampled at an approximate lag interval of $0.2 - 1$ m$(h)$ in order to calculate and to keep the continuity of transitional probability between adjacent hydrofacies at the location $x$. According to that transition probability $T_{jn}(h_x, h_y, hz)$ in three - dimension

can be defined as

$$T_{jn}(h_x, h_y, h_z) = Pr \left\{ \begin{array}{l} n\text{present at}x + h_x | j\text{present at}x \\ n\text{present at}y + h_y | j\text{present at}y \\ n\text{present at}z + hz | j\text{present at}z \end{array} \right\}, \qquad (5.2)$$

where $j$ and $k$ are two indicator hydrofacies (Carle, 1999). If hydrofacies $j$ is exist at location $x, y, z$, then $T_{jn}(h_x, h_y, h_z)$ is the likelihood of finding hydrofacies $n$ at three directional lag distances $h_x, h_y, h_z$ from positions of $x, y, z$ (for one dimension see Carle and Fogg (1996)).

Stratigraphy model description and heterogeneous model development relied on the core data collected from the field (see Chapter 2). Core samples analyzed from the site was approximately 50% of total depth that was cored, the rest was observed and similar textures were noted. Noticeably different layer samples were also recovered in order to analyze. The cumulative length of the core that was represented is approximately 7 m for the purposes of model construction. Four separate hydrofacies were identified from inspection of recovered core on the basis of sediment type (Table 5.1). Hydrofacies 1 is a moderately sorted, fine sand dominated unit. Hydrofacies 2 is a mud to silty sand dominated unit referred to herein as the mud. hydrofacies 3 is another thype of mud that poorly sorted, polymodal, clay dominated unit. And the fourth hydrofacies is formed from the material that is moderately to well sorted, coarser than sand gravel, which represents the scale classification of grain size larger than 2 mm

**Table 5.1:** Hydraulic conductivity values according to Hydrofacies type

| | Type of Material | Mean $D_{50}$ ( µm ) | Proportion (%) | Horizontal conductivity (m/min) | Vertical Conductivity (m/min) |
|---|---|---|---|---|---|
| F1 | Fine Sand | 225.6 | 56 | 2.54E-3 | 1.27E-6 |
| F2 | Silt | 17.9 | 17 | 4.23E-4 | 2.12E-4 |
| F3 | Clay | 0.95 | 19 | 6.4E-6 | 3.2E-6 |
| F4 | Gravel | $> 2000$ | 8 | 0.18 | 0.36 |

Porosity values were accepted as 30% and hydraulic conductivity values have been assumed from the book of Domenico and Schwarz (1998)

The same procedure followed as in the work of Engdahl et.al. (2010);

1. The interpreted core was translated into a categorized data of indicator hydrofacies (for an example see (Deutsch CV, 1998)).

2. Hard-weighted indicator variables were used in order to describe data set on the presence or absence of the variable at some location as described by equation 5.1.

3. The data format (as in the data file) was expended by the indicator method of soft weighting. The expansion of the format is that any number of indicator variables may be present at one location in space, therefore, the sum of hydrofacies proportions is one (Carle, 1999; Engdahl et al., 2010).

This process is useful if description of a location may not fit precisely into one of the selected categorical variable. Interpreted core data were input for the T-PROGS software package, and the simulations are implemented with the T-PROGS library of FORTRAN programs. Transition probability matrices are generated using GAMEAS Carle (1999) for estimating spatial statistics irregularly spaced data. Transition probabilities in the horizontal plane are assumed isotropic; separate transition probabilities are determined for the vertical direction and simulations are performed with TSIM Carle (1999).

***Realizations***

Modeling sediment heterogeneity with geostatistical methods only provides an approximation of the real stream sediment system. However, conditioned geostatistical models are able to incorporate geologic properties for locations where borehole data are available. Data gaps between these (often sparse) locations are filled by a statistical process based on the calculated correlations between hydrofacies. By this, it is possible to create an infinite number of heterogeneous models for the specified domain. However, incomplete knowledge and lack of validation of subsurface structure creates the uncertainty in the flow simulation. A common approach accounts for the uncertainty in the flow simulation is to generate results as statistical distributions (Frei et al., 2009; Walker et al., 2005; Trangenstein, 2002), rather than deterministic single values. For this reason sufficient number of heterogeneity realizations are created, and stochastic flow simulations are performed for all realizations to compare residence time distributions of each realization.

Distance between calculated hydrofacies are not constant, and structure of the sediment core data is clustered over a certain zones (see Chapter 2). Such that embedded transition probability matrices and mean hydrofacies lengths were calculated according to scarce data over discretized domain. Mean vertical hydrofacies lengths of whole data have been calculated with 20 cm interval in order to avoid the problems arise from the sparsity of core data. Average lengths of data were estimated towards the eastern and northern directions according to clusters (to see matrices on Table 5.2).

Firstly, three model domains have been used in order to compare the changes on residence time distributions; two of them are heterogeneous reference models and the third one is the homogeneous model. In the latter one, hydraulic conductivity was arranged according to average fine

sand component (background material for heterogeneous realizations, $k_h = 0.00254\,\mathrm{m/min}$). In simulations with heterogeneous permeability over a certain domain with the same dimensions, initially two different model created in order to compare the differences on structure. The main heterogeneous domain created according to field data (Withdata), and the second one was synthetically created with 40° anisotropy with assigned strike-, dip- and vertical directions as $20, 10$ and 1m respectively (Nodata). The second domain is discretized as $0.3 - 0.5\,\mathrm{m}$ vertically. Hypothetical discretization over discretized domain arranged as the half of the vertical height of the single unit. This procedure was followed in order to calculate heterogeneous hydraulic conductivity over the domain. As a next step 114 realizations were generated based on the T-PROGS hydrofacies scale heterogeneity model which was estimated from field data. Both, reference runs and the two different sets of simulations (with data and no-data), were then used for subsequent flow simulations.

### 5.2.3 *Stochastic Subsurface Flow Simulation*

The model is discretized as a 220 row, 845 column, and 27 layer model grid using all total grids as active. First 6 layers differ from the rest of the domain. Instead of constant upper layer elevations, they fit into a nodal function that fits to the attributed elevations of first layer that represents river bed topography. On the first layer thickness reduces until 0.1 m and increases max. 0.1 m on the edges in order to accommodate sediment transactions and detailed hydrofacies. On the upper layers, bottom elevation values were imposed as the minimum water level in order to avoid convergence problems caused by wetting and drying cells in MODFLOW. For each heterogeneous and homogeneous domain, the system was modeled under steady state conditions.

Numerical model for each unit cell head values was calculated according to equation 4.4 based on the same principle that was applied in Chapter 4. Simulation of subsurface flow at the study site was done with the three-dimensional finite difference model, MODFLOW-2005 (Harbaugh A. W. and G., 2005). The model boundary conditions were selected to most closely match to the physical system as specified in Chapter 4, and incorporating specific observed conditions for the stage values of surface water and head values for groundwater (see Chapter 2). No-flow conditions were used for the base of the model that corresponds to the bottom of the domain.

The resulting finite difference scheme was solved using the preconditioned conjugate gradient with improved nonlinear control (PCGN) (Naff R.L., 2008). Initial boundary values for the river bed were imposed over the computational nodes on the top layer of the domain. Calculated solutions of head values were compared with the groundwater level measurements from piezometers at the time of the field measurements in order to calibrate

groundwater boundaries.

The range for allowable hydraulic conductivities for each hydrofacies was chosen from the published intervals for the corresponding grain sizes (see Table 2.1, on Chapter 2) (Domenico and Schwartz, 1998). According to sediment analysis the selection of hydraulic conductivities that were assigned to hydrofacies is quite variable, therefore, the difference of magnitude of conductivity between hydrofacies might be very large. Such that, during the solution of head values, transition to higher K value to lower one may cause convergence problem in some heterogeneous hydraulic conductivity realizations. This problem was solved by preserving the hierarchical order of hydrofacies in order to maintain grain size definitions of the hydrofacies categories. K values for each hydrofacies were randomly selected from a uniform probability distribution according to calculated transition matrices for each set of simulations, and fine sand was chosen as the background material.

## 5.3 Results and Discussions

### 5.3.1 Sediment Heterogeneity

In this part of the study the main purpose is to combine geostatistical simulations to represent complex sediment structure at a hydrofacies and sub-hydrofacies. Sediment core data representations for each sample points have been calculated via parallel computing for steady-state, saturated subsurface flow to simulate the dynamics of hyporheic zone. This type of representation was also followed as two-dimensional system representation (Bruen and Osman, 2004), and used to estimate variability of vertical flow between water table and hyporheic zone (Fleckenstein et al., 2006). Different than this work, previous works that practiced same approach are mostly focused on regional scale (in kms) modeling. They treated river as a factor of in-charge/discharge into the regional vertical fluxes rather than an hyporheic system (Engdahl et al., 2010; Fleckenstein and Fogg, 2008). In another work small parcel of agricultural river side system ( A test volume as $11.4 \times 11.4 \times 2.85\,\mathrm{m}$, entire volume as $46 \times 74 \times 8.4\,\mathrm{m}$ ) was modeled for comparison purposes of different heterogeneous techniques (dell'Arciprete et al., 2012). Most of the prominent heterogeneous flow field models search for the problem of refined system dynamics, in which, effects of channel sinuosity, and complex topography are not included (Cardenas, 2008; Cardenas and Wilson, 2007b; Revelli et al., 2008). Similar to the approach in this work, Zhou et. al. (2014) includes channel morphology units as meanders, point bars, dunes, and ripples, however, the main application of domain is evaluated based on two-magnitude gravel sediment deposits (sandy-gravel and gravel).

Some of the preliminary realizations of hydrofacies that are created with-

**Table 5.2:** Embedded Transition Probability Matrices and mean hydrofacies Lengths according to core data calculations

| Vertical (z) Direction | | | | | Strike (x) Direction | | | | | Dip (y) Directions | | | | |
|---|---|---|---|---|---|---|---|---|---|---|---|---|---|---|
| | $fs$ | $c$ | $si$ | $g$ | | $fs$ | $c$ | $si$ | $g$ | | $fs$ | $c$ | $si$ | $g$ |
| $fs$ | 0.094 | $b$ | $b$ | $b$ | $fs$ | 20 | $b$ | $b$ | $b$ | $fs$ | 10 | $b$ | $b$ | $b$ |
| $c$ | $b$ | 0.067 | 0.3 | 0.40 | $c$ | $b$ | 12 | 0.3 | 0.25 | $c$ | $b$ | 6 | 0.3 | 0.25 |
| $si$ | $b$ | 0.35 | 0.065 | 0.25 | $si$ | $b$ | $s$ | 12 | 0.15 | $si$ | $b$ | $s$ | 6 | 0.25 |
| $g$ | $b$ | 0.15 | 0.15 | 0.1 | $g$ | $b$ | $s$ | $s$ | 20 | $g$ | $b$ | $s$ | $s$ | 10 |

fs = fine sand; c = Clay; si = Silt; g = gravel; s = symmetry; b = background category

out data resulted in non-convergence of hydraulic solution in subsurfrace model. The allowable K values were later restricted to avoid this problem. The optimum distances and embedded transitional probability matrices were calculated according to sparse data (Table 5.2), such that the problem of non-convergence has never been observed in realizations that were calculated based on the core data from the field.

Two selected realizations were compared according to preparations of the heterogeneous domains. The model created by using data shows patchy representations of the field and the model with anisotropy shows more local hydraulic conductivity fields over a layer (up to 20 - 30 m horizontally over a layer). Volumetric proportions of four hydrofacies (input proportions ) were preserved for the both realizations, however, the proportions in the simulated volumes (output proportions) are different from the proportions from the field data, because of the averaging effect between the conditions imposed by different parameters (anisotropy, difference in cell size, lag distances, etc.[see Table 5.3]).

In the realization based on the data, the proportion of simulated values of a specific category tends to increase on the points that are located vicinity of that specific category. This effect is related with the ranges of the indicator variograms, in which this effect becomes more significant the range increases (Soares, 1998).

**Table 5.3:** Input and output facies proportions in the entire volume, coarse grid.

| | Input Proportions (%) | Withdata (%) | Nodata (%) | All Realizations (%) |
|---|---|---|---|---|
| Fine Sand | 56 | 55.6 | 53.9 | $55.9 \pm 1.1$ |
| Silt | 17 | 17.3 | 18.8 | $17.1 \pm 0.6$ |
| Clay | 19 | 19.2 | 18.0 | $19 \pm 0.6$ |
| Gravel | 8 | 7.9 | 9.3 | $8 \pm 0.3$ |

The output proportions for all realizations are expressed as mean±standard deviation over the ensemble of 114 realizations those were created based on the data.

### 5.3.2 Effects of sediment heterogeneity

The results of calculated head and velocity fields in homogeneous and heterogeneous system are compared from the different aspects as head distributions over streambed and cumulative residence time distributions according to specified parts of the reach. Stochastic subsurface flow simulations on specified domain ran on $0.5\,\mathrm{m}^3/\mathrm{s}$ stream discharge which is also calibrated

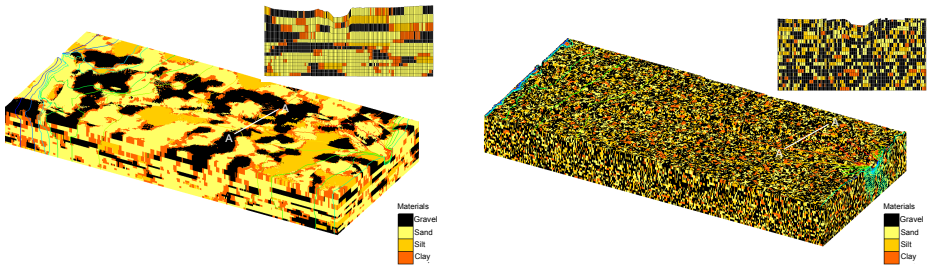


(a) (b)

**Figure 5.1:** Demonstrations of two realizations and cross-sections over river-bed area, models are ; (a) Nodata that based on synthetic data ; and (b) Withdata that based on core data.

initial discharge value of surface flow model. It should be noted that three different set of simulation results were evaluated in order to analyze their changes on heterogeneous condition. Homogeneous subsurface material was set to be fine sand that is also the background facies of heterogeneous realizations.

### Heterogeneous Subsurface head predictions

The connected gravel strata sets enable a great deal of water to move through the heterogeneous system relative to the homogeneous system. The steady-state total-volume inflow rate equals the total-volume outflow rate in both heterogeneous and homogeneous models. The flow passes through the system with higher- and lower conductivity pathways connected in parallel conduits (rather than in series), in such locations the hydraulic conductivity is expected to be above the geometric mean of hydraulic conductivity of all domain (Hunt and Ewing, 2009). Plus, the interior parts of the channel has varying positive and negative flux regions, conversely the change in parallelization of head contours related to heterogeneity of the field. The head simulations of homogeneous case (Figure 5.2(c), the heterogeneous realizations of Nodata (Figure 5.2(e) ) and, the other realizations (the rest of the Figure 5.2) show different patterns according to formation of hydrofacies. Results also demonstrates that the differences of head values according to following zones are higher in heterogeneous cases, in other words, which shows higher magnitude velocity field inside the subsurface domain.

### Trajectories and residence time distribution

The hyporheic residence times ,$\tau$, were calculated from the particle runs that are initiated on upper 4 m of the domain. Cumulative frequency distribution (CFDs) were determined from total tracking times for all particles regularly

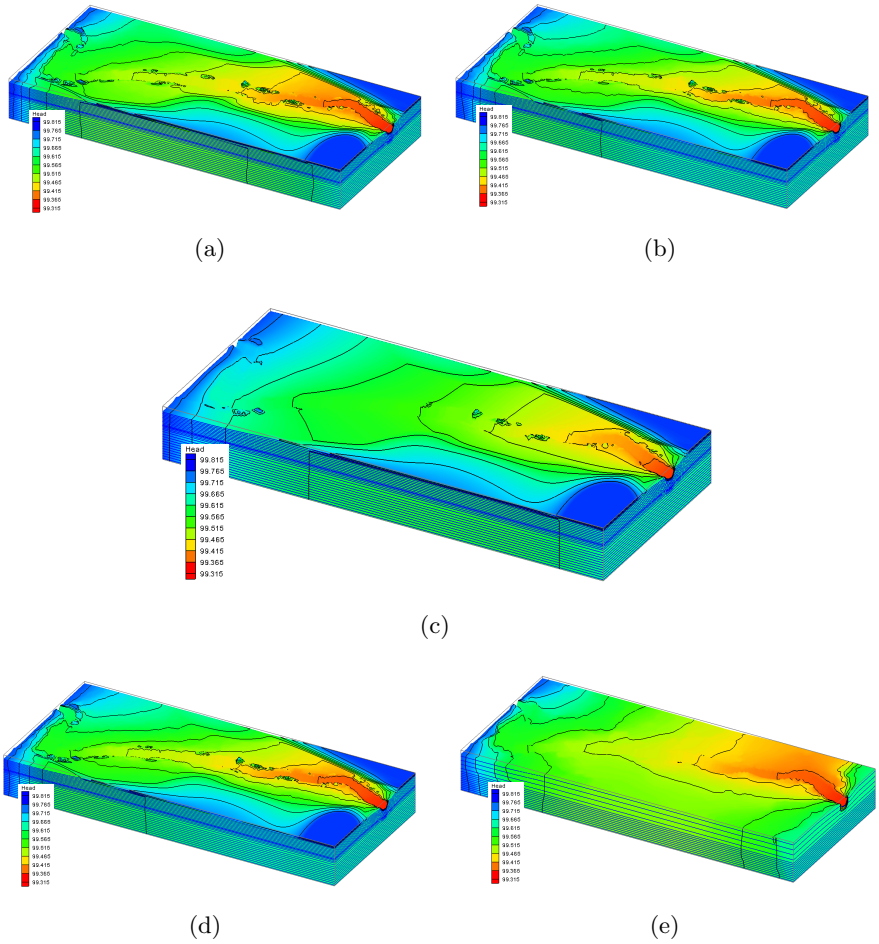


**Figure 5.2:** Subsurface steady-state head solutions for heterogeneous realizations with groundwater boundary values (a) random realization 1 according to data ; (b) random realization 2 ; (c) Homogeneous realization (d) random realization 3; (e) Nodata realization.

distributed over the river for meander, central and downstream parts of the reach. The CFDs for two chosen heterogeneous realizations are shown in Figure 5.3. Particles initiated from constant head cells were not included into calculations since their total tracking times are zero. From CFDs the fraction of the particles initiated on upper layers that remain in hyporheic zone can be seen, and the time zones of the most of the particles that leave the system from upwelling zones can be calculated. The residence time distributions are closely approximated by lognormal distributions (Cardenas et al., 2004), it has been shown that exchange models based on advection are best represented by log-normal residence times (Wörman et al., 2002, 2006).

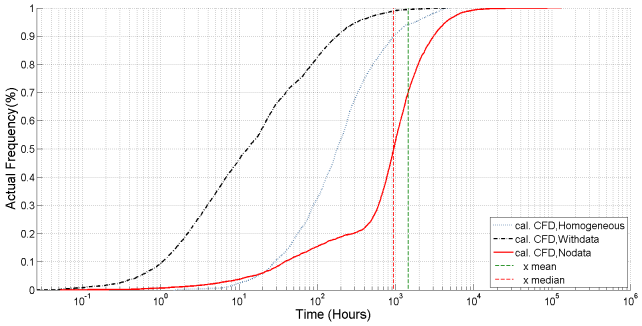


(a)

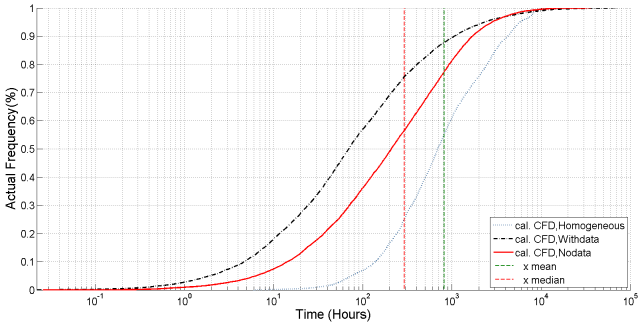


(b)

**Figure 5.3:** Comparison of cumulative frequency distributions (CFDs) of Nodata, Withdata and homogeneous cases; (a) comparison on meander part ; and (b) comparison on central part .

Along the particles, it is difficult to identify the path that the particles would have taken to return to the stream. These particles do not have any direct path to validate like in homogeneous case because these particles might remain in the hyporheic zone until they encounter low hydraulic con-

ductivity zone, which will force them to go back toward the stream or reduce the remaining residence time (Cardenas et al., 2004; Sawyer and Cardenas, 2009). This relationship can be observed via residence time distribution as shown in Figure 5.3(a) by focusing on first 500 hours interval of the CFD of Nodata model. According to demonstration only max 20% of the particles remain under subsurface within hyporhiec zone of the meander part. It most likely stems from the exact zone where transition from high head value (99.8 m from see level) to lower head value (99.6 m from see level) is more dominant for the flow movement (high flux condition)(see Figure 5.2(e) ). CFD of Nodata has median value as 948 hours that corresponds to the 50% of the particles and mean value as 1462 corresponds to the 70% of the particles remains in the subsurface. The discrepancy between the curves are getting lesser by the increase of time, however, on central part, the median time of homogeneous realization (812 Hours) excesses the one of Nodata realization unlike meander part (293 hours). According to this, residence times are changing drastically due to the pathways. The residence time distributions of more anisotropic and zonal formations (not patchy) with longer lag distances show more changeable dynamics depending on the volume of the hydrofacies type. Unlike the deeper hyporheic zone as a result of the effect of heterogeneous formations or longer flow paths (Woessner, 2000), heterogeneous formations may restrict the pathways or makes the trajectories longer but proportionally faster.

In our case, median residence times of heterogeneous flow are either lower or higher than the one in homogeneous model in comparison with each part of the reach. According to this, the hydrofacies that has been chosen for homogeneous representation plays bigger role on the subsurface flow than the formation of topography over the reach. General finding is that subsurface heterogeneity increases the complexity of hyporheic exchange paths but may increase or decrease the depth of mixing, depending on the subsurface structure.

Previous attempts to simulate local effects of hyporheic exchange considering sediment heterogeneity proves that heterogeneity on hydraulic conductivity impacts the distribution of residence time. Heterogeneity can increase or decrease the proportion of short or long residence times. Changes in residence times was proved in the work of Sawyer and Cardenas (2009) by comparison of two heterogeneous domains. In this work while heterogeneity of one domain increases thew longer residence times, the other one shortens them due to their different formations. In our case, including the changes on the residence time, different locations with identical formations (meander, bars, riffle-pool etc.) also shows different median residence times. Figure 5.3(a) proves that the high shift of particle trajectories and time can be possible in case of meander part, which may stem from the high possibility of the particle that coincides with more different hydrofacies because of the long path way (for trajectories see Figure 5.4).

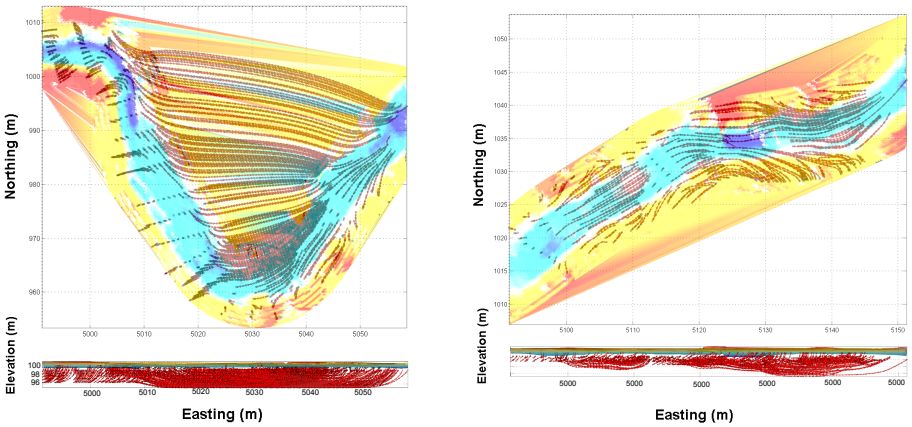


(a) (b)

**Figure 5.4:** Plan and side (Easting) view of predicted trajectories in homogeneous conditions. Demonstrations show ; (a) meander ; and (b) central part trajectories.

For the second part of the analysis; hydraulic head solutions and velocity fields were calculated for different heterogeneous realizations. Three different parts of the reach was analyzed besides whole domain. 114 heterogeneous models based on the field data were stochastically simulated. Each model shows different residence time scales, however, only slight shifts were observed along the time scale. Average simulation curve shows that residence time is lower than the homogeneous case for each location of the reach.

According to CFDs of the simulations, the median value for whole reach is 37.2 hours and $\tau_{50}$ values for all realizations are ranging between 20 - 50 hours. Different than meander part and downstream part that ranges between 35 - 57 and 41 - 71 hours respectively, central part has more diverse $\tau_{50}$ as it ranges between 20 - 100 hours. Stochastic simulations for the specific reach suggest that the differences on 50% of the particles that remains inside the hyproheic zone and groundwater affected by the subsurface and riverbed heterogeneity, which was stated as two major control on hyporheic exchange in the work of Wroblicky et al. (1998). This may elucidate the question of the effect of small-scale subsurface heterogeneity as pointed out by Fleckenstein et al. (2006) and also demonstrated for aquifer scale in Fleckenstein et al. (2008). It should be noted that models suggest less impact on hyporheic exchange by river-bed formation under low hydraulic conductivity conditions.

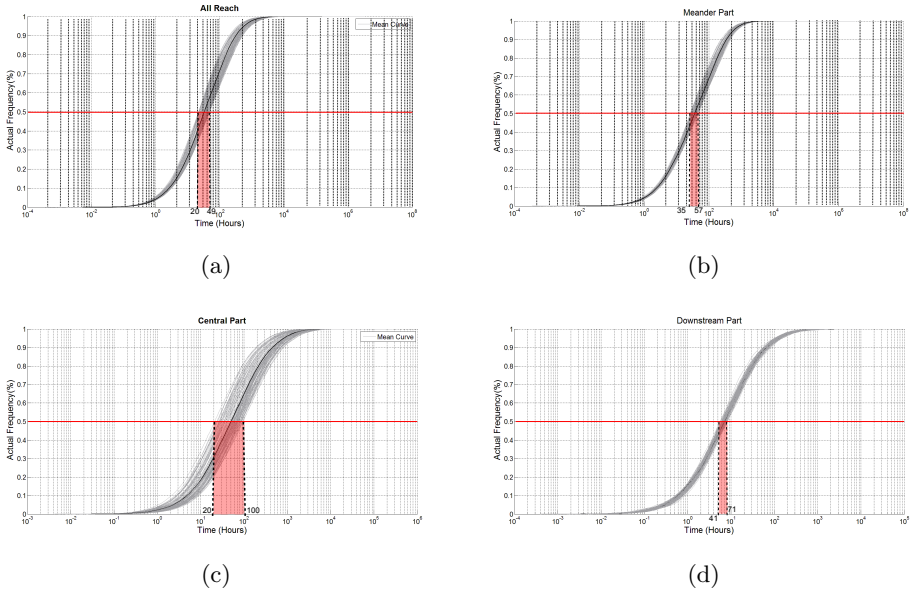


**Figure 5.5:** CDFs of 114 heterogeneous realizations for entire reach and different parts of the domain. Red line demonstrates the 50% of the particles remains inside the subsurface, and red area shows the variance of the time corresponds to 50%, $\tau_{50}$, in all realization curves. (a) is for cumulative frequency distributions of all reach ; (b) is for meander part ; (c) is for central part ; and (d) is for downstream part for all stochastic simulations

**Effect of Heterogeneity on aerobic/anarobic zones using Damköhler number**

In this part Damköhler number was used in order to see spatial distribution of potential aerobic and anaerobic zones over subsurface, and effect of sediment heterogeneity was observed. Brief description of central zone was prepared in order to observe the possible diversification of oxygenated and hypoxic/anoxic zones. The comparison is made between homogeneous case which has hydraulic conductivity of fine sand ($K_h$ = 2.54E-3 m/min) and heterogeneous domain based on the field data. The general picture of the domain was depicted on Figure 5.6 via volumetric comparison, and more detailed demonstration of cross-sections were shown in Figure C.1 in Appendix C. The comparison figures were created according to particle trajectories which are enters to the local system, and travels through hyporheic zone then goes back to surface water via upwelling zones. In other words, the volume that was shown also shows the spatial dimensions of the local HZ. Only the particles which are leaving the zone were used.

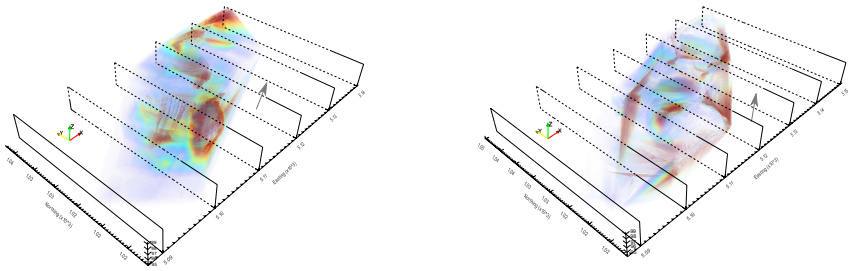

(a) (b)

**Figure 5.6:** Volumetric demonstration of distribution of Damköhler number (Da) on central part where riffle and pool conditions prevail. 3D demonstrations made on single (a) homogeneous ; and (b) heterogeneous cases.

Mostly anoxic and hypoxic conditions prevail upper and lower parts of the domain in homogeneous realization. It can be seen that the area on planar view of hyporheic zone shows slight difference between two cases, however, heterogeneous case predictions demonstrates deeper hyporheic zone on vertical direction ( $1 - 2$ m ). Therefore, the same particles are taking longer paths vertically in heterogeneous domain than the homogeneous one. This shows that if there is lower hydraulic conductivity materials as silt ($K_h$ = 4.23E-4 m/min) and same proportion of higher hydraulic conductivity hydrofacies as gravel ($K_h$ = 0.18 m/min) in the same domain, water particles have the tendency to follow the high conductivity path. This behavior increases the connectivity of hyporheic zone, such that, having equivalent hydraulic conductivity to represent any hyproheic zone can be misleading.

In this study, numerical experiments were done based on the high magnitude differences of hydraulic conductivity. However, it is difficult to achieve on which level of difference on magnitude leads field migration in this way, which was not seen in lower magnitude simulations on heterogeneity (Cardenas et al., 2004; Fleckenstein et al., 2006; Fleckenstein and Fogg, 2008; Bardini et al., 2013; Sawyer and Cardenas, 2009).

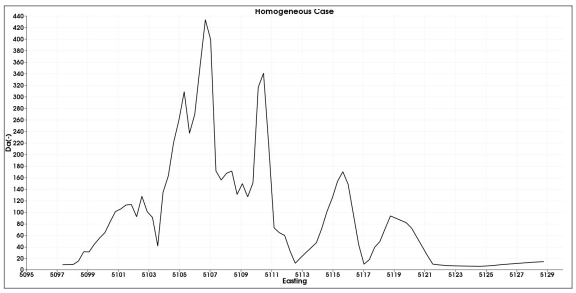


(a)

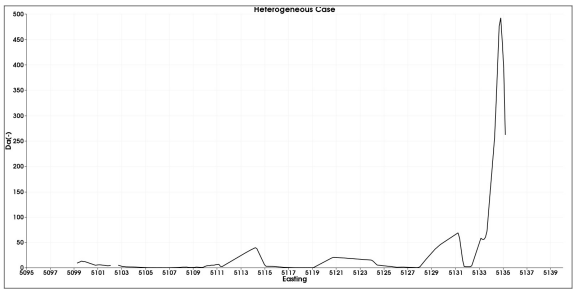


(b)

**Figure 5.7:** Da values of longitudinal cross-section for average values for central part of the reach. Plots show (a) homogeneous ; and (b) heterogeneous cases along the thalweg.

The importance of discrete features in the conductivity field were illustrated for the first time by Fogg (1986). In this, the effect of vertical flow in subsurface formations related with the type of hydraulic facies. It proves that geological structures begin to exert more control on the paths and rates of fluid migration as the contrast increases. This also shows us the clues of how chemical transformation may alter according to this dynamic on complex groundwater system. Then the problem of representation of hydrofacies in complex groundwater systems was solved by development of transition probability models (Carle and Fogg, 1996, 1997; Carle et al., 1998). According to cross-sectional Da analysis on Figure 5.7 and demonstrations of Da zones on Figure C.1, heterogeneous case with high conductivity patterns shows less alterations on aerobic and anaerobic zones. In

this particular case we can observe that the sediments have more textural complexity as a resemblance to the complex groundwater systems, however, it does not mean the same complexity will be reflected to spatial availability of dissolved oxygen. Such that, the difference on the average residence time is more than 100 times between homogeneous and heterogeneous domains in certain cases according to differences on Da values on the same locations ($Da_{hom} >> Da_{het}$).

## 5.4 Conclusion

In this chapter previously prepared subsurface model was modified and arranged in order to capture realistic heterogeneity conditions, which relies on the sediment core data of the river bed from River Bure. Heterogeneity of the model was created according to two basic models; one of them is a realization with anisotropy and longer lag distances, the second realization is based on the sediment core calculations. Second model was restricted with point data from the sediments. Three matrices were calculated for three directions of the model. Calculated matrices were used in order to simulate heterogeneous subsurface via Markov chains algorithm. The hydrofacies heterogeneity field simulated based on the small lag distances and embedded transitional probability matrices. Heterogeneous fields based on field data show patchy structure, conversely anisotropic and bigger lag distance model shows bigger hydrofacies zones. However, locally, simulated head values based on the heterogeneous field over the domain do not show big differences. On the other hand, the gradient on the head contour lines was shifting more frequently according to heterogeneity. Base on the model predictions it can be said that the heterogeneous field that has more transitional probability and less lag distance shows bigger head gradient over subsurface.

Comparison of heterogeneous models with low hydraulic conductivity homogeneous model demonstrates that median hyporheic residence times can exceed the median time of homogeneous model. They can also get lesser time average according to the part of the reach. However, it was also predicted that median time or $\tau_{50}$ values are changing drastically due to the different spatial probabilities and/or spatial formations of hydrofacies with the same proportions around the subsurface domain. On the other hand, stochastic simulations of 114 heterogeneous realizations prove that the range of the average times of the particles which remains inside the hyporheic zone are different. In this model central part that is mostly dominated with groundwater intrusion and riffle and pool sequences has the biggest range, conversely, mean CFD curves of each group do not show big differences and all remain between 20 - 100 hours band.

Da values lower than 1 results in prevailing aerobic conditions with low

reactive nitrogen removal at the unit scale. Values of Da larger than 1 indicate prevailing anaerobic condition with large opportunity of liable nitrogen removal and production of nitrogen gases. Calculated Da values also useful to show the boundaries of hyporheic zone according to discharge and sediment heterogeneity. Analysis shows that the hyporheic zone is vertically deeper in heterogeneous domain with respect to the homogeneous case. In heterogeneous case prevailing aerobic zone potential is higher than the homogeneous case. Even high hydraulic conductivity hydrofacies (gravel) is proportionally smallest ($8 \pm 0.3\%$), its impact on hyporheic flow is functionally higher by facilitating the connectivity of the subsurface flow. Such that even flow paths are longer than homogeneous case, distribution of median residence time predicted as lower. In theory, the subsurface flow that has tendency to move through high hydraulic conductivity facies creates a corridor of pathways which continues until coinciding with lower hydraulic conductivity facies. which was called tunneling effect in this work. Therefore, such area is potentially more aerobic than the homogeneous case, also aerobic zones are more spread than anaerobic zones along the domain. In this chapter, magnitudes of hydraulic conductivity of hydrofacies depicted as relatively higher, however, it was not proven that what is the limiting magnitude of this flow behavior and in which ratio of the hydraulic conductivities does not show any tunneling behavior.

# Chapter 6

# Conclusion

## 6.1 Summary and Conclusions

This thesis uses hydraulic numerical modeling, and a suite of other methodological techniques as bed surface interpolation and field work practices to investigate hyporheic exchange dynamics, prevailing redox conditions and the effect of heterogeneity. The research identifies several open ended features of hyporheic zone in three distinct direction. First can be considered as hydraulic aspects as effect of mixed topography on hyporheic flow paths and different discharge conditions with groundwater boundary conditions; second feature is to define heterogeneity and creating link to application of sediment analysis in order to create heterogeneous realizations, and the third approach elucidates the potential denitrification/nitrification zones via spatial redox conditions in order to create a link between hydraulic conditions and hyporheic biogeochemistry.

## 6.2 Discoveries of the research

The primary contribution of this research is the development of mixed topography reach scale model with heterogeneous subsurface domain. The model allows to calculate hyporheic paths and exchange rates. The changes on the stream discharges and the effect of topography can be observed by cumulative frequency distributions (CFDs) of residence time. This approach was developed to investigate the effects of multiple scales of topography on rates and patterns of hyporheic exchange based on a field investigation, and changes on the hydraulic dynamics based on the subsurface heterogeneity. The system was formed by two distinct models as surface flow and subsurface flow models. Model includes input as upstream and downstream stage functions and system topography as a river bed boundary condition for stream flow. The ones for subsurface model includes system topography as upper boundary, mean surface water velocity, mean hydraulic conduc-

tivity, mean porosity, and groundwater level for homogeneous case. For analysis hyporheic flux distributions, hyporheic flow paths, and residence time distributions can be investigated via subsurface flow model.

The model was presented after wide review of field practices (Chapter 2) and comparison of topographical techniques (Chapter 3). The models can be summarized as one surface flow model set as an input to subsurface model, and three distinctive subsurface models those can be defined by homogeneous gravel, homogeneous fine sand, and heterogeneous sets. From the structural point of view subsurface models can be divided into two as cascade type bed surface for high conductivity model (Chapter 4), and smooth topography surface for low conductivity and heterogeneous sediment models (Chapter 5).

In addition, two main model designs were introduced; the one is high conductivity homogeneous model assumed as gravel bed to predict the effect of topographical changes in 6 meters depth and 15 equivalent layers, and the second is homogeneous with equivalent hydraulic conductivity model with different grid structure but same depth. In the least model upper boundary designed as smooth bed topography that was interpolated on the first layer, and thickness of the layers are not uniform, where the domain was divided into 27 layers. Groundwater discharge was included all model sets and applied to a sparse topography dataset. They were applied to base flow river which is flowing among agricultural area (small agricultural stream) with micro and macro stream morphologies. Findings from each of these applications improve our understanding of complex hyporheic processes.

In chapter 2 wide description of a reach that is a part of River Bure, UK in an agricultural lowland setting was made. The emphasis for this reach is its buffering capacity of biogeochemical parameters in relation with hydraulic dynamics. In order to reach that goal, the characteristics of the chosen reach were described from three aspects, which are set to be; 1)Sedimentological, 2)hydrological, and 3)Biogeochemical. The main focus in this chapter is especially important for the sediment profile that was trying to be created. Analysis indicate that a 30 cm core sample has wide range of sediment types, however, it was observed that sediments are poorly sorted and it is hard to define the exact location of a certain sediment type in such reaches. For this purpose the characteristics of sediments were statistically refined. These treatment was done in order to facilitate the creation of heterogeneous field for subsurface model. From the Hydrological perspective, the most distinctive characteristic of the gradient of water surface level (and river bed elevation) is lower than the gradient of subsurface water level. However, it is not clear to understand the detailed groundwater flow conditions from the bank. Nevertheless, the models indicates that the reach has the groundwater flow either perpendicular or parallel with the river channel with initial boundary conditions. Subsurface flow underneath streambed moves mostly upwards and 90% of subsurface water again turns back to the

river, which is a strong characteristic of a gaining reach. Biogeochemical observations represent 15 cm depth for porewater samples. However, the reach has high concentration of nutrient, and reduction of nutrient inside the hyporheic zone is not observed. As a final comment along the reach, hyporhiec zone is not a media to move away the excess nutrient loading.

Another important contribution centers around the effect of surface water discharge on hyporheic exchange. Three different discharge levels (low, average, high) were incorporated into the modeling framework in chapter 4. It was found that the changes in discharge significantly influence hyporheic exchange. More specifically, groundwater discharge inhibited exchange near the stream banks, thus restricting exchange to the middle of the stream. On the other hand, it was also observed that the higher river discharge had a disproportionately large effect on the interfacial flux. However, in some point higher stream discharge condition does not lead to higher residence time. Especially in riffle and pool part average stream discharge fluxes may exceed higher stream discharge fluxes on gravel bed case as shown in Figure 4.6(b). The findings also depicts an interaction with groundwater discharges, therefore, findings emphasizes that it is essential to include groundwater discharge and calibrate stream discharge on accordance with them. It should be noted that the work presented here was restricted in steady-state condition, which is a representation of the time when the data was collected in situ from the field. The work strongly suggests that careful measurements of groundwater and modeling are needed in systems where the groundwater level is close to the stream water level.

Natural media are heterogeneous at different scales and heterogeneity brings complexity in the flow problem. Spatial variability of flow parameters complicate a precise description of the media, if not impossible, to obtain. Even if it would be possible to have a detailed description of the media, the amount of information would be practically impossible to handle and the large scale behavior of the flow would be difficult to interpret. Because of these reasons we choose a stochastic approach. Stochastic approach provides a systematic way to quantify the effect of heterogeneity into large scale models. Chapter 5 is centered on the integration of the effects of heterogeneity on Darcy flow into reach scale models which are linked with a description of natural media. Homogeneous model was created with the background material of heterogeneous realizations in order to compare hydraulic differences. Initial results demonstrate that median hyporheic residence times can exceed the median time of homogeneous model or can get into lesser time average according to the part of the reach.

The average residence time is on the scale of 20 - 100 hours, and fine sand homogeneous case is reaching to 100 - 1000 hours average time on central part according to stochastic hydraulic simulations. On the other hand, the gravel bed model in Chapter 4 also ranges between 10 - 100 hours in average discharge condition. Therefore, the comparisons indicate

that hyporheic fluxes are changing in case of gravel and heterogeneous flow, however, the residence times of particles that remains in the hyporheic zone is not changing, and also higher discharge conditions show longer average residence times along the reach.

Prevailing aerobic and anaerobic conditions predicted by using certain microbiological kinetics in the models that are defined in Chapter 4 and 5. Da values lower than 1 indicate prevailing aerobic condition which means low reactive nitrogen removal at unit scale. Values of Da larger than 1 indicate prevailing anaerobic condition which means opportunity of liable nitrogen removal and production of nitrogen gases. Results indicate that low hydraulic conductivity model shows higher Da values, thus mostly more anaerobic redox conditions. On the other hand, prevailing aerobic conditions can be seen especially upper part of the domain in the gravel bed model, however, it is possible to observe anaerobic redox conditions on the upper layers ($0.1 - 1\,\mathrm{m}$) especially in meander and riffle parts of the reach. Same intensity of aerobic zone also observed on heterogeneous case, conversely, distribution of anaerobic zones are more sparse and it changes due to the distribution of low hydraulic conductivity facies of the domain. The most significant evidence of this method is that the impact of high hydraulic conductivity zones is higher on the connectivity inside the hyporheic zone, in other words, subsurface flow has tendency to flow through the facies with high conductance, therefore, high hydraulic conductivity facies as gravel are determining the flow inside the sediment and low conductivity facies have respectively minor role on hyporheic flow.

# Appendix A

# Statistical Analysis

## A.1 Statistical Comparison between Thalweg and Bank samples

Descriptives

| | | N | Mean | Std. Deviation | Std. Error | 95% Confidence Interval for Mean | |
|---|---|---|---|---|---|---|---|
| | | | | | | Lower Bound | Upper Bound |
| NH3_N | Bank | 21 | .0685 | .14232 | .03106 | .0037 | .1333 |
| | Thalweg | 14 | .0516 | .10177 | .02720 | -.0072 | .1103 |
| | Total | 35 | .0617 | .12628 | .02134 | .0183 | .1051 |
| NO3_N | Bank | 21 | 7.7550 | 4.44540 | .97006 | 5.7315 | 9.7785 |
| | Thalweg | 14 | 8.1855 | 5.15644 | 1.37812 | 5.2083 | 11.1627 |
| | Total | 35 | 7.9272 | 4.67296 | .78987 | 6.3220 | 9.5324 |
| DO | Bank | 21 | .9608 | .76770 | .16753 | .6113 | 1.3102 |
| | Thalweg | 14 | .9233 | .58241 | .15566 | .5870 | 1.2596 |
| | Total | 35 | .9458 | .69046 | .11671 | .7086 | 1.1830 |
| DOC | Bank | 20 | 7.4190 | 10.97989 | 2.45518 | 2.2803 | 12.5577 |
| | Thalweg | 14 | 4.6271 | 4.25784 | 1.13796 | 2.1687 | 7.0855 |
| | Total | 34 | 6.2694 | 8.85997 | 1.51947 | 3.1780 | 9.3608 |
| FDE | Bank | 7 | .005949 | .00282395 | .001067 | .0033373 | .0085607 |
| | Thalweg | 5 | .008887 | .00410328 | .001835 | .0037922 | .0139820 |
| | Total | 12 | .007173 | .00357227 | .001031 | .0049035 | .0094429 |
| Sulphate | Bank | 21 | 17.0045 | 13.65517 | 2.97980 | 10.7888 | 23.2203 |
| | Thalweg | 14 | 16.8054 | 9.88963 | 2.64312 | 11.0953 | 22.5155 |
| | Total | 35 | 16.9249 | 12.12808 | 2.05002 | 12.7587 | 21.0910 |
| Chloride | Bank | 21 | 10.5053 | 7.33060 | 1.59967 | 7.1684 | 13.8421 |
| | Thalweg | 14 | 11.3013 | 6.82738 | 1.82469 | 7.3593 | 15.2434 |
| | Total | 35 | 10.8237 | 7.04199 | 1.19031 | 8.4047 | 13.2427 |

**Figure A.1:** Descriptive statistics of the groups.

## *A.1. Statistical Comparison between Thalweg and Bank samples*

ANOVA

| | | | | Sum of Squares | df | Mean Square | F | Sig. |
|---|---|---|---|---|---|---|---|---|
| NH3_N | Between Groups | (Combined) | | .002 | 1 | .002 | .147 | .704 |
| | | Linear Term | Unweighted | .002 | 1 | .002 | .147 | .704 |
| | | | Weighted | .002 | 1 | .002 | .147 | .704 |
| | Within Groups | | | .540 | 33 | .016 | | |
| | Total | | | .542 | 34 | | | |
| NO3_N | Between Groups | (Combined) | | 1.557 | 1 | 1.557 | .069 | .794 |
| | | Linear Term | Unweighted | 1.557 | 1 | 1.557 | .069 | .794 |
| | | | Weighted | 1.557 | 1 | 1.557 | .069 | .794 |
| | Within Groups | | | 740.886 | 33 | 22.451 | | |
| | Total | | | 742.443 | 34 | | | |
| DO | Between Groups | (Combined) | | .012 | 1 | .012 | .024 | .878 |
| | | Linear Term | Unweighted | .012 | 1 | .012 | .024 | .878 |
| | | | Weighted | .012 | 1 | .012 | .024 | .878 |
| | Within Groups | | | 16.197 | 33 | .491 | | |
| | Total | | | 16.209 | 34 | | | |
| DOC | Between Groups | (Combined) | | 64.190 | 1 | 64.190 | .813 | .374 |
| | | Linear Term | Unweighted | 64.190 | 1 | 64.190 | .813 | .374 |
| | | | Weighted | 64.190 | 1 | 64.190 | .813 | .374 |
| | Within Groups | | | 2526.280 | 32 | 78.946 | | |
| | Total | | | 2590.470 | 33 | | | |
| FDE | Between Groups | (Combined) | | .000 | 1 | .000 | 2.186 | .170 |
| | | Linear Term | Unweighted | .000 | 1 | .000 | 2.186 | .170 |
| | | | Weighted | .000 | 1 | .000 | 2.186 | .170 |
| | Within Groups | | | .000 | 10 | .000 | | |
| | Total | | | .000 | 11 | | | |
| Sulphate | Between Groups | (Combined) | | .333 | 1 | .333 | .002 | .963 |
| | | Linear Term | Unweighted | .333 | 1 | .333 | .002 | .963 |
| | | | Weighted | .333 | 1 | .333 | .002 | .963 |
| | Within Groups | | | 5000.735 | 33 | 151.537 | | |
| | Total | | | 5001.068 | 34 | | | |
| Chloride | Between Groups | (Combined) | | 5.324 | 1 | 5.324 | .105 | .749 |
| | | Linear Term | Unweighted | 5.324 | 1 | 5.324 | .105 | .749 |
| | | | Weighted | 5.324 | 1 | 5.324 | .105 | .749 |
| | Within Groups | | | 1680.724 | 33 | 50.931 | | |
| | Total | | | 1686.048 | 34 | | | |

Page 1

**Figure A.2:** ANOVA analysis between and within groups. The mean difference is significant at the 0.05 level

Test of Homogeneity of Variances

| | Levene Statistic | df1 | df2 | Sig. |
|---|---|---|---|---|
| NH3_N | .434 | 1 | 33 | .515 |
| NO3_N | 1.343 | 1 | 33 | .255 |
| DO | 1.829 | 1 | 33 | .185 |
| DOC | 3.851 | 1 | 32 | .058 |
| FDE | .403 | 1 | 10 | .540 |
| Sulphate | .741 | 1 | 33 | .396 |
| Chloride | .225 | 1 | 33 | .638 |

**Figure A.3:** Levene's test of homogeneity of variances per parameter. Variances of cases are homogeneous in case of mean variance is more than 0.05

## A.2 Comparison of parameters in between clusters

Multiple Comparisons

Tukey HSD

| Dependent Variable | (I) Clusters | (J) Clusters | Mean Difference (I-J) | Std. Error | Sig. |
|---|---|---|---|---|---|
| NH3_N | C1 | C2 | .22000* | .05419 | .004 |
| | | C3 | .22000* | .05134 | .002 |
| | | C4 | .22000* | .04753 | .001 |
| | | C5 | .17000* | .04753 | .016 |
| | | SW | .22000* | .05821 | .009 |
| | | GW | -.24780* | .05419 | .001 |
| | C2 | C1 | -.22000* | .05419 | .004 |
| | | C3 | .00000 | .05756 | 1.000 |
| | | C4 | .00000 | .05419 | 1.000 |
| | | C5 | -.05000 | .05419 | .966 |
| | | SW | .00000 | .06377 | 1.000 |
| | | GW | -.46780* | .06012 | .000 |
| | C3 | C1 | -.22000* | .05134 | .002 |
| | | C2 | .00000 | .05756 | 1.000 |
| | | C4 | .00000 | .05134 | 1.000 |
| | | C5 | -.05000 | .05134 | .957 |
| | | SW | .00000 | .06136 | 1.000 |
| | | GW | -.46780* | .05756 | .000 |
| | C4 | C1 | -.22000* | .04753 | .001 |
| | | C2 | .00000 | .05419 | 1.000 |
| | | C3 | .00000 | .05134 | 1.000 |
| | | C5 | -.05000 | .04753 | .938 |
| | | SW | .00000 | .05821 | 1.000 |
| | | GW | -.46780* | .05419 | .000 |
| | C5 | C1 | -.17000* | .04753 | .016 |
| | | C2 | .05000 | .05419 | .966 |
| | | C3 | .05000 | .05134 | .957 |
| | | C4 | .05000 | .04753 | .938 |
| | | SW | .05000 | .05821 | .976 |
| | | GW | -.41780* | .05419 | .000 |
| | SW | C1 | -.22000* | .05821 | .009 |
| | | C2 | .00000 | .06377 | 1.000 |
| | | C3 | .00000 | .06136 | 1.000 |

**Figure A.4:** Multiple comparison of all dependent parameters acoording to cluster groups on the reach

Multiple Comparisons

Tukey HSD

| Dependent Variable | (I) Clusters | (J) Clusters | Mean Difference (I-J) | Std. Error | Sig. |
|---|---|---|---|---|---|
| | | C4 | .00000 | .05821 | 1.000 |
| | | C5 | -.05000 | .05821 | .976 |
| | | GW | -.46780* | .06377 | .000 |
| | GW | C1 | .24780* | .05419 | .001 |
| | | C2 | .46780* | .06012 | .000 |
| | | C3 | .46780* | .05756 | .000 |
| | | C4 | .46780* | .05419 | .000 |
| | | C5 | .41780* | .05419 | .000 |
| | | SW | .46780* | .06377 | .000 |
| NO3_N | C1 | C2 | -4.22343 | 2.44104 | .601 |
| | | C3 | -1.78246 | 2.31247 | .986 |
| | | C4 | -2.31025 | 2.14093 | .930 |
| | | C5 | .14062 | 2.14093 | 1.000 |
| | | SW | 1.47563 | 2.62209 | .997 |
| | | GW | 4.28117 | 2.44104 | .586 |
| | C2 | C1 | 4.22343 | 2.44104 | .601 |
| | | C3 | 2.44097 | 2.59280 | .963 |
| | | C4 | 1.91317 | 2.44104 | .985 |
| | | C5 | 4.36405 | 2.44104 | .564 |
| | | SW | 5.69905 | 2.87236 | .441 |
| | | GW | 8.50460* | 2.70809 | .047 |
| | C3 | C1 | 1.78246 | 2.31247 | .986 |
| | | C2 | -2.44097 | 2.59280 | .963 |
| | | C4 | -.52779 | 2.31247 | 1.000 |
| | | C5 | 1.92308 | 2.31247 | .980 |
| | | SW | 3.25808 | 2.76393 | .898 |
| | | GW | 6.06363 | 2.59280 | .254 |
| | C4 | C1 | 2.31025 | 2.14093 | .930 |
| | | C2 | -1.91317 | 2.44104 | .985 |
| | | C3 | .52779 | 2.31247 | 1.000 |
| | | C5 | 2.45088 | 2.14093 | .910 |
| | | SW | 3.78588 | 2.62209 | .775 |
| | | GW | 6.59143 | 2.44104 | .127 |

**Figure A.4** (cont.)**:** First figure continued

Multiple Comparisons

Tukey HSD

| Dependent Variable | (I) Clusters | (J) Clusters | Mean Difference (I-J) | Std. Error | Sig. |
|---|---|---|---|---|---|
| | C5 | C1 | -.14062 | 2.14093 | 1.000 |
| | | C2 | -4.36405 | 2.44104 | .564 |
| | | C3 | -1.92308 | 2.31247 | .980 |
| | | C4 | -2.45088 | 2.14093 | .910 |
| | | SW | 1.33500 | 2.62209 | .999 |
| | | GW | 4.14055 | 2.44104 | .623 |
| | SW | C1 | -1.47563 | 2.62209 | .997 |
| | | C2 | -5.69905 | 2.87236 | .441 |
| | | C3 | -3.25808 | 2.76393 | .898 |
| | | C4 | -3.78588 | 2.62209 | .775 |
| | | C5 | -1.33500 | 2.62209 | .999 |
| | | GW | 2.80555 | 2.87236 | .956 |
| | GW | C1 | -4.28117 | 2.44104 | .586 |
| | | C2 | -8.50460* | 2.70809 | .047 |
| | | C3 | -6.06363 | 2.59280 | .254 |
| | | C4 | -6.59143 | 2.44104 | .127 |
| | | C5 | -4.14055 | 2.44104 | .623 |
| | | SW | -2.80555 | 2.87236 | .956 |
| Sulphate | C1 | C2 | -9.03545 | 6.57118 | .811 |
| | | C3 | 2.93063 | 6.22508 | .999 |
| | | C4 | -.41395 | 5.76331 | 1.000 |
| | | C5 | 1.69075 | 5.76331 | 1.000 |
| | | SW | -10.93019 | 7.05858 | .714 |
| | | GW | -8.42809 | 7.05858 | .892 |
| | C2 | C1 | 9.03545 | 6.57118 | .811 |
| | | C3 | 11.96608 | 6.97971 | .611 |
| | | C4 | 8.62150 | 6.57118 | .842 |
| | | C5 | 10.72620 | 6.57118 | .663 |
| | | SW | -1.89474 | 7.73229 | 1.000 |
| | | GW | .60736 | 7.73229 | 1.000 |
| | C3 | C1 | -2.93063 | 6.22508 | .999 |
| | | C2 | -11.96608 | 6.97971 | .611 |
| | | C4 | -3.34458 | 6.22508 | .998 |

**Figure A.4** (cont.)**:** Previous figure continued

Multiple Comparisons

Tukey HSD

| Dependent Variable | (I) Clusters | (J) Clusters | Mean Difference (I-J) | Std. Error | Sig. |
|---|---|---|---|---|---|
| | | C5 | -1.23988 | 6.22508 | 1.000 |
| | | SW | -13.86082 | 7.44040 | .517 |
| | | GW | -11.35872 | 7.44040 | .727 |
| | C4 | C1 | .41395 | 5.76331 | 1.000 |
| | | C2 | -8.62150 | 6.57118 | .842 |
| | | C3 | 3.34458 | 6.22508 | .998 |
| | | C5 | 2.10470 | 5.76331 | 1.000 |
| | | SW | -10.51624 | 7.05858 | .749 |
| | | GW | -8.01414 | 7.05858 | .913 |
| | C5 | C1 | -1.69075 | 5.76331 | 1.000 |
| | | C2 | -10.72620 | 6.57118 | .663 |
| | | C3 | 1.23988 | 6.22508 | 1.000 |
| | | C4 | -2.10470 | 5.76331 | 1.000 |
| | | SW | -12.62094 | 7.05858 | .564 |
| | | GW | -10.11884 | 7.05858 | .780 |
| | SW | C1 | 10.93019 | 7.05858 | .714 |
| | | C2 | 1.89474 | 7.73229 | 1.000 |
| | | C3 | 13.86082 | 7.44040 | .517 |
| | | C4 | 10.51624 | 7.05858 | .749 |
| | | C5 | 12.62094 | 7.05858 | .564 |
| | | GW | 2.50210 | 8.15055 | 1.000 |
| | GW | C1 | 8.42809 | 7.05858 | .892 |
| | | C2 | -.60736 | 7.73229 | 1.000 |
| | | C3 | 11.35872 | 7.44040 | .727 |
| | | C4 | 8.01414 | 7.05858 | .913 |
| | | C5 | 10.11884 | 7.05858 | .780 |
| | | SW | -2.50210 | 8.15055 | 1.000 |
| Chloride | C1 | C2 | -3.07602 | 4.38130 | .992 |
| | | C3 | 3.40937 | 4.15054 | .981 |
| | | C4 | .95796 | 3.84266 | 1.000 |
| | | C5 | 1.38421 | 3.84266 | 1.000 |
| | | SW | -6.80432 | 4.70627 | .774 |
| | | GW | -4.51186 | 4.38130 | .944 |

**Figure A.4** (cont.)**:** Previous figure continued

Multiple Comparisons

Tukey HSD

| Dependent Variable | (I) Clusters | (J) Clusters | Mean Difference (I-J) | Std. Error | Sig. |
|---|---|---|---|---|---|
| | C2 | C1 | 3.07602 | 4.38130 | .992 |
| | | C3 | 6.48540 | 4.65369 | .802 |
| | | C4 | 4.03399 | 4.38130 | .967 |
| | | C5 | 4.46024 | 4.38130 | .947 |
| | | SW | -3.72830 | 5.15547 | .990 |
| | | GW | -1.43584 | 4.86062 | 1.000 |
| | C3 | C1 | -3.40937 | 4.15054 | .981 |
| | | C2 | -6.48540 | 4.65369 | .802 |
| | | C4 | -2.45141 | 4.15054 | .997 |
| | | C5 | -2.02516 | 4.15054 | .999 |
| | | SW | -10.21370 | 4.96085 | .397 |
| | | GW | -7.92124 | 4.65369 | .619 |
| | C4 | C1 | -.95796 | 3.84266 | 1.000 |
| | | C2 | -4.03399 | 4.38130 | .967 |
| | | C3 | 2.45141 | 4.15054 | .997 |
| | | C5 | .42625 | 3.84266 | 1.000 |
| | | SW | -7.76229 | 4.70627 | .652 |
| | | GW | -5.46983 | 4.38130 | .870 |
| | C5 | C1 | -1.38421 | 3.84266 | 1.000 |
| | | C2 | -4.46024 | 4.38130 | .947 |
| | | C3 | 2.02516 | 4.15054 | .999 |
| | | C4 | -.42625 | 3.84266 | 1.000 |
| | | SW | -8.18854 | 4.70627 | .595 |
| | | GW | -5.89608 | 4.38130 | .826 |
| | SW | C1 | 6.80432 | 4.70627 | .774 |
| | | C2 | 3.72830 | 5.15547 | .990 |
| | | C3 | 10.21370 | 4.96085 | .397 |
| | | C4 | 7.76229 | 4.70627 | .652 |
| | | C5 | 8.18854 | 4.70627 | .595 |
| | | GW | 2.29246 | 5.15547 | .999 |
| | GW | C1 | 4.51186 | 4.38130 | .944 |
| | | C2 | 1.43584 | 4.86062 | 1.000 |
| | | C3 | 7.92124 | 4.65369 | .619 |

**Figure A.4** (cont.)**:** Previous figure continued

Multiple Comparisons

Tukey HSD

| Dependent Variable | (I) Clusters | (J) Clusters | Mean Difference (I-J) | Std. Error | Sig. |
|---|---|---|---|---|---|
| | | C4 | 5.46983 | 4.38130 | .870 |
| | | C5 | 5.89608 | 4.38130 | .826 |
| | | SW | -2.29246 | 5.15547 | .999 |

*. The mean difference is significant at the 0.05 level.

**Figure A.4** (cont.)**:** Previous figure continued

# A.3 Statistical comparison of surface water, groundwater and pore water chemistry

Descriptives

| | | N | Mean | Std. Deviation | Std. Error | 95% Confidence ... Lower Bound |
|---|---|---|---|---|---|---|
| NH3_N | Porewater | 35 | .0617 | .12628 | .02134 | .0183 |
| | Surfacewater | 4 | .0000 | .00000 | .00000 | .0000 |
| | Groundwater | 5 | .4678 | .12851 | .05747 | .3082 |
| | Total | 44 | .1023 | .17887 | .02696 | .0479 |
| NO3_N | Porewater | 35 | 7.9272 | 4.67296 | .78987 | 6.3220 |
| | Surfacewater | 4 | 5.0467 | 1.34582 | .67291 | 2.9053 |
| | Groundwater | 5 | 2.2412 | 1.76966 | .79141 | .0439 |
| | Total | 44 | 7.0192 | 4.62292 | .69693 | 5.6137 |
| DO | Porewater | 35 | .9458 | .69046 | .11671 | .7086 |
| | Surfacewater | 2 | 6.6069 | .11773 | .08325 | 5.5491 |
| | Groundwater | 0 | . | . | . | . |
| | Total | 37 | 1.2518 | 1.46110 | .24020 | .7646 |
| DOC | Porewater | 34 | 6.2694 | 8.85997 | 1.51947 | 3.1780 |
| | Surfacewater | 0 | . | . | . | . |
| | Groundwater | 5 | 9.2820 | 6.23884 | 2.79009 | 1.5355 |
| | Total | 39 | 6.6556 | 8.56204 | 1.37102 | 3.8801 |
| Sulphate | Porewater | 35 | 16.9249 | 12.12808 | 2.05002 | 12.7587 |
| | Surfacewater | 4 | 27.3585 | 7.33059 | 3.66530 | 15.6939 |
| | Groundwater | 4 | 24.8564 | 5.66041 | 2.83020 | 15.8494 |
| | Total | 43 | 18.6332 | 11.77162 | 1.79516 | 15.0105 |
| Chloride | Porewater | 35 | 10.8237 | 7.04199 | 1.19031 | 8.4047 |
| | Surfacewater | 4 | 18.3084 | 5.49593 | 2.74797 | 9.5631 |
| | Groundwater | 5 | 16.0159 | 11.53501 | 5.15861 | 1.6933 |
| | Total | 44 | 12.0941 | 7.77107 | 1.17153 | 9.7315 |
| NO2_N | Porewater | 35 | .3700 | 1.04545 | .17671 | .0109 |
| | Surfacewater | 4 | .0305 | .00947 | .00473 | .0154 |
| | Groundwater | 5 | .2424 | .07547 | .03375 | .1487 |
| | Total | 44 | .3247 | .93555 | .14104 | .0402 |

**Figure A.5:** Descriptive statistics of the chemical parameters according to different water types

ANOVA

| | | | | Sum of Squares | df | Mean Square | F | Sig. |
|---|---|---|---|---|---|---|---|---|
| NH3_N | Between Groups | (Combined) | | .767 | 2 | .384 | 25.867 | .000 |
| | | Linear Term | Unweighted | .721 | 1 | .721 | 48.633 | .000 |
| | | | Weighted | .539 | 1 | .539 | 36.350 | .000 |
| | | | Deviation | .228 | 1 | .228 | 15.384 | .000 |
| | Within Groups | | | .608 | 41 | .015 | | |
| | Total | | | 1.376 | 43 | | | |
| NO3_N | Between Groups | (Combined) | | 158.565 | 2 | 79.282 | 4.275 | .021 |
| | | Linear Term | Unweighted | 141.446 | 1 | 141.446 | 7.627 | .009 |
| | | | Weighted | 158.560 | 1 | 158.560 | 8.549 | .006 |
| | | | Deviation | .005 | 1 | .005 | .000 | .988 |
| | Within Groups | | | 760.403 | 41 | 18.546 | | |
| | Total | | | 918.968 | 43 | | | |
| DO | Between Groups | (Combined) | | 60.631 | 1 | 60.631 | 130.809 | .000 |
| | | Linear Term | Unweighted | 60.631 | 1 | 60.631 | 130.809 | .000 |
| | | | Weighted | 60.631 | 1 | 60.631 | 130.809 | .000 |
| | Within Groups | | | 16.223 | 35 | .464 | | |
| | Total | | | 76.854 | 36 | | | |
| DOC | Between Groups | (Combined) | | 39.561 | 1 | 39.561 | .533 | .470 |
| | | Linear Term | Unweighted | . | 1 | . | . | . |
| | | | Weighted | 39.561 | 1 | 39.561 | .533 | .470 |
| | Within Groups | | | 2746.162 | 37 | 74.221 | | |
| | Total | | | 2785.723 | 38 | | | |
| Sulphate | Between Groups | (Combined) | | 561.582 | 2 | 280.791 | 2.136 | .131 |
| | | Linear Term | Unweighted | 225.829 | 1 | 225.829 | 1.718 | .197 |
| | | | Weighted | 430.706 | 1 | 430.706 | 3.276 | .078 |
| | | | Deviation | 130.875 | 1 | 130.875 | .996 | .324 |
| | Within Groups | | | 5258.401 | 40 | 131.460 | | |
| | Total | | | 5819.983 | 42 | | | |
| Chloride | Between Groups | (Combined) | | 287.862 | 2 | 143.931 | 2.556 | .090 |
| | | Linear Term | Unweighted | 117.948 | 1 | 117.948 | 2.094 | .155 |
| | | | Weighted | 210.054 | 1 | 210.054 | 3.730 | .060 |
| | | | Deviation | 77.808 | 1 | 77.808 | 1.382 | .247 |
| | Within Groups | | | 2308.890 | 41 | 56.314 | | |
| | Total | | | 2596.752 | 43 | | | |
| NO2_N | Between Groups | (Combined) | | .452 | 2 | .226 | .249 | .781 |

**Figure A.6:** ANOVA analysis between and within groups. The mean difference is significant at the 0.05 level

Test of Homogeneity of Variances

| | Levene Statistic | df1 | df2 | Sig. |
|---|---|---|---|---|
| NH3_N | 2.343 | 2 | 41 | .109 |
| NO3_N | 5.464 | 2 | 41 | .008 |
| DO | 2.257 | 1 | 35 | .142 |
| DOC | .145 | 1 | 37 | .706 |
| Sulphate | .710 | 2 | 40 | .498 |
| Chloride | 1.166 | 2 | 41 | .322 |
| NO2_N | 1.107 | 2 | 41 | .340 |

**Figure A.7:** Levene's test of homogeneity of variances per parameter. Variances of cases are homogeneous in case of mean variance is more than 0.05

ANOVA

| | | | Sum of Squares | df | Mean Square |
|---|---|---|---|---|---|
| | Linear Term | Unweighted | .071 | 1 | .071 |
| | | Weighted | .204 | 1 | .204 |
| | | Deviation | .248 | 1 | .248 |
| | Within Groups | | 37.184 | 41 | .907 |
| | Total | | 37.636 | 43 | |

ANOVA

| | | | F | Sig. |
|---|---|---|---|---|
| | Linear Term | Unweighted | .079 | .781 |
| | | Weighted | .225 | .637 |
| | | Deviation | .273 | .604 |
| | Within Groups | | | |
| | Total | | | |

**Figure A.8:** Summary of the ANOVA analysis within groups

# Appendix B

# Final Topography

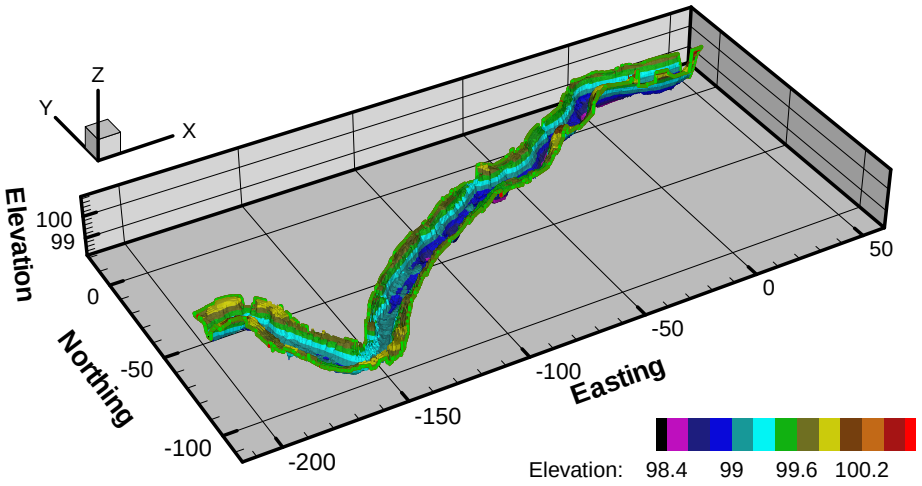


**Figure B.1:** Demonstration of final map of the reach created by using w/template method in order to use top layers of subsurface model

# Appendix C

# Upwelling/downwelling and spatial redox conditions

**Table C.1:** Clusters and the flux characters of the points

| Sample ID | Flux | Zone | $\tau$(hours) | Da(-) |
|---|---|---|---|---|
| S1 | 3.1E-5 | Upwelling | 27.0 | 2.10 |
| S2 | 3.8E-5 | Upwelling | 26.4 | 2.04 |
| S3 | 2.9E-5 | Upwelling | 28.3 | 2.20 |
| S4 | 2.8E-5 | Upwelling | 29 | 2.24 |
| S5 | 2.7E-5 | Upwelling | 30.3 | 2.34 |
| S6 | 2.4E-5 | Upwelling | 32.3 | 2.49 |
| S7 | 2.9E-5 | Upwelling | 31.6 | 2.44 |
| S8 | 2.5E-5 | Upwelling | 34 | 2.62 |
| S9 | 4.2E-5 | Upwelling | 17.5 | 1.35 |
| S10 | 4.0E-5 | Upwelling | 22 | 1.70 |
| S11 | 3.3E-5 | Upwelling | 24.1 | 1.86 |
| S12 | 2.7E-5 | Upwelling | 36.5 | 2.82 |
| S13 | 3.0E-5 | Upwelling | 28.1 | 2.17 |
| S14 | 2.7E-5 | Upwelling | 31 | 2.39 |
| S15 | 2.5E-5 | Upwelling | 35.8 | 2.76 |
| S16 | 4.7E-5 | Upwelling | 35.2 | 2.72 |
| S17 | −8.7E-7 | Downwelling | 77.4 | 5.97 |
| S18 | −1.2E-6 | Downwelling | 84.8 | 6.54 |
| S19 | −1.7E-6 | Downwelling | 84.3 | 6.50 |
| S20 | −2.4E-6 | Downwelling | 75.8 | 5.84 |
| S21 | 1.5E-5 | Upwelling | 56.1 | 4.34 |
| S22 | 1.6E-5 | Upwelling | 53.4 | 4.12 |

| | | | | |
|---|---|---|---|---|
| S23 | 1.4E-5 | Upwelling | 56.4 | 4.35 |
| S24 | 1.8E-5 | Upwelling | 53.6 | 4.14 |
| S25 | 1.5E-5 | Upwelling | 76.3 | 5.89 |
| S26 | 9.6E-6 | Upwelling | 94.2 | 7.27 |
| S27 | 1.1E-5 | Upwelling | 76.4 | 5.89 |
| S28 | 1.4E-5 | Upwelling | 78.3 | 6.04 |
| S29 | 8.9E-6 | Upwelling | 232.5 | 17.94 |
| S30 | 6.8E-6 | Upwelling | 123.6 | 9.54 |
| S31 | 5.8E-6 | Upwelling | 208 | 16.05 |
| S32 | 1.0E-5 | Upwelling | 198 | 15.28 |
| S33 | 1.4E-5 | Upwelling | 38.5 | 2.97 |
| S34 | 2.4E-5 | Upwelling | 40.5 | 3.15 |
| S35 | 2.5E-5 | Upwelling | 43.0 | 3.32 |
| S36 | 2.5E-5 | Upwelling | 35.3 | 2.72 |
| S37 | 2.4E-5 | Upwelling | 50.5 | 3.90 |
| S38 | 1.8E-5 | Upwelling | 83.6 | 6.45 |
| S39 | 2.9E-5 | Upwelling | 39.0 | 3.01 |
| S40 | 2.8E-5 | Upwelling | 35.4 | 2.73 |

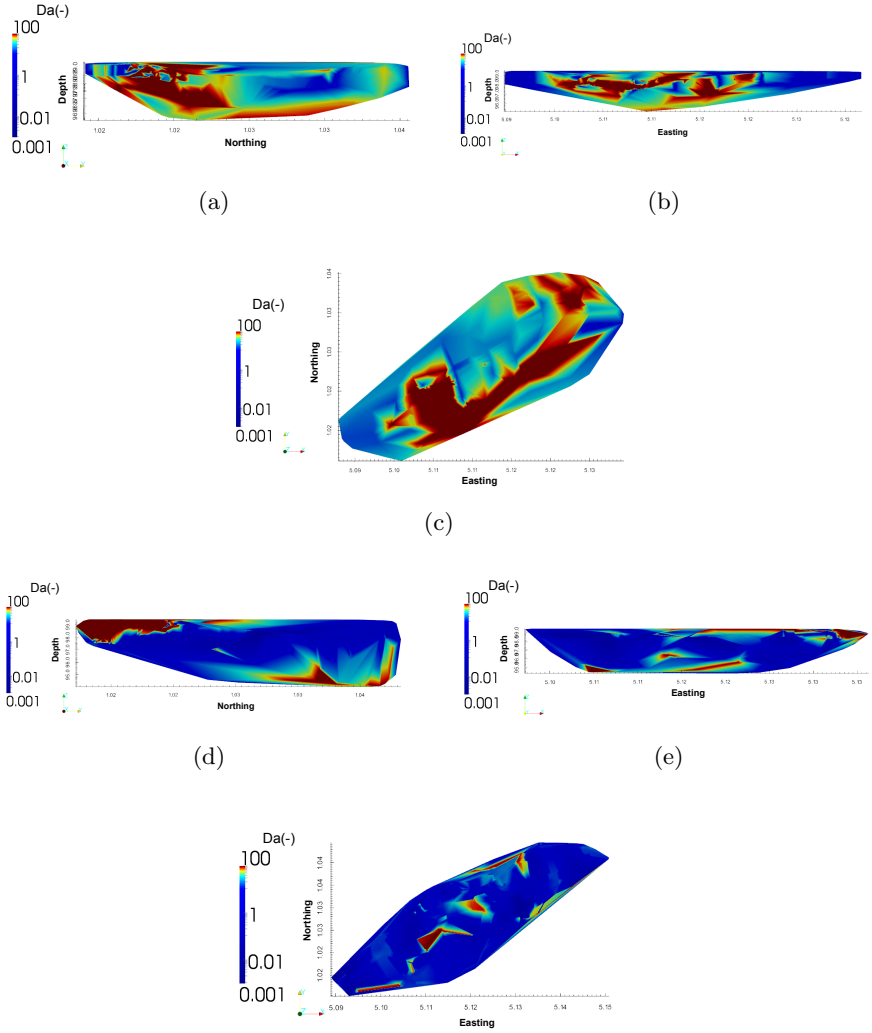


**Figure C.1:** Prevailing anaerobic/aerobic zones as distribution of Damköhler index. Only central part has been demonstrated in order to compare homogeneous and heterogeneous case. The figures shows the cross-sections of (a) Y-Z section ; (b) X-Z section ; and (c) plan view of homogeneous realization ; (d) Y-Z section; (e) X-Z section; and (f) plan view of heterogeneous realization.

# Bibliography

E Eric Adams and Lynn W Gelhar. Field study of dispersion in a heterogeneous aquifer: 2. spatial moments analysis. *Water Resources Research*, 28(12):3293–3307, 1992.

Richard B Alexander, Richard A Smith, and Gregory E Schwarz. Effect of stream channel size on the delivery of nitrogen to the gulf of mexico. *Nature*, 403(6771):758–761, 2000.

Mary P Anderson. Hydrogeologic facies models to delineate large-scale spatial trends in glacial and glaciofluvial sediments. *Geological Society of America Bulletin*, 101(4):501–511, 1989.

Sarit Ashckenazi-Polivoda, Carmi Rak, Ahuva Almogi-Labin, Berner Zsolt, Ofer Ovadia, and Sigal Abramovich. Paleoecology of the K-Pg mass extinction survivor Guembelitria (Cushman): isotopic evidence from pristine foraminifera from Brazos River, Texas (Maastrichtian). *Paleobiology*, 40(1):24–33, WIN 2014. ISSN 0094-8373. doi: {10.1666/13317}.

Jean-Stéphane Bailly, Yann Le Coarer, Pascal Languille, Carl-Johann Stigermark, and Tristan Allouis. Geostatistical estimations of bathymetric lidar errors on rivers. *Earth Surface Processes and Landforms*, 35(10): 1199–1210, 2010.

Laura Bardini, Fulvio Boano, MB Cardenas, AH Sawyer, Roberto Revelli, and Luca Ridolfi. Small-scale permeability heterogeneity has negligible effects on nutrient cycling in streambeds. *Geophysical Research Letters*, 40(6):1118–1122, 2013.

Colden Baxter, F Richard Hauer, and William W Woessner. Measuring groundwater–stream water exchange: new techniques for installing minipiezometers and estimating hydraulic conductivity. *Transactions of the American Fisheries Society*, 132(3):493–502, 2003.

M Bayani Cardenas and JL Wilson. The influence of ambient groundwater discharge on exchange zones induced by current–bedform interactions. *Journal of Hydrology*, 331(1):103–109, 2006.

Jeffrey S Beis and David G Lowe. Shape indexing using approximate nearest-neighbour search in high-dimensional spaces. In *Computer Vision and Pattern Recognition, 1997. Proceedings., 1997 IEEE Computer Society Conference on*, pages 1000–1006. IEEE, 1997.

Kenneth E Bencala. Simulation of solute transport in a mountain pool-and-riffle stream with a kinetic mass transfer model for sorption. *Water Resources Research*, 19(3):732–738, 1983.

Jöran Bergh and Jörgen Löfström. Interpolation spaces. an introduction. 1976.

Alfred Paul Blaschke, Karl-Heinz Steiner, Roland Schmalfuss, Dieter Gutknecht, and Dieter Sengschmitt. Clogging processes in hyporheic interstices of an impounded river, the danube at vienna, austria. *International Review of Hydrobiology*, 88(3-4):397–413, 2003.

Simon J Blott and Kenneth Pye. Gradistat: a grain size distribution and statistics package for the analysis of unconsolidated sediments. *Earth surface processes and Landforms*, 26(11):1237–1248, 2001.

Fulvio Boano, AI Packman, A Cortis, R Revelli, and L Ridolfi. A continuous time random walk approach to the stream transport of solutes. *Water resources research*, 43(10), 2007.

Fulvio Boano, Roberto Revelli, and Luca Ridolfi. Quantifying the impact of groundwater discharge on the surface–subsurface exchange. *Hydrological Processes*, 23(15):2108–2116, 2009.

Fulvio Boano, Andrea Demaria, Roberto Revelli, and Luca Ridolfi. Biogeochemical zonation due to intrameander hyporheic flow. *Water resources research*, 46(2), 2010a.

Fulvio Boano, Roberto Revelli, and Luca Ridolfi. Effect of streamflow stochasticity on bedform-driven hyporheic exchange. *Advances in Water Resources*, 33(11):1367–1374, 2010b.

J Mark Boggs and E Eric Adams. Field study of dispersion in a heterogeneous aquifer: 4. investigation of adsorption and sampling bias. *Water Resources Research*, 28(12):3325–3336, 1992.

John Karl Böhlke, Ronald C Antweiler, Judson W Harvey, Andrew E Laursen, Lesley K Smith, Richard L Smith, and Mary A Voytek. Multi-scale measurements and modeling of denitrification in streams with varying flow and nitrate concentration in the upper mississippi river basin, usa. *Biogeochemistry*, 93(1-2):117–141, 2009.

Galina Borisova, Nadezhda Chukina, Maria Maleva, and M. N. V. Prasad. Ceratophyllum Demersum L. and Potamogeton Alpinus Balb. from Iset' River, Ural region, Russia differe in adaptive strategies to heavy metals exposure - A comparative Study. *International Journal of Phytoremediation*, 16(6):621–633, JUN 3 2014. ISSN 1522-6514. doi: {10.1080/15226514.2013.803022}.

Andrew J Boulton. Hyporheic rehabilitation in rivers: restoring vertical connectivity. *Freshwater Biology*, 52(4):632–650, 2007.

Andrew J Boulton, Stuart Findlay, Pierre Marmonier, Emily H Stanley, and H Maurice Valett. The functional significance of the hyporheic zone in streams and rivers. *Annual Review of Ecology and Systematics*, 29(1): 59–81, 1998.

Andrew J Boulton, Thibault Datry, Tamao Kasahara, Michael Mutz, and Jack A Stanford. Ecology and management of the hyporheic zone: stream-groundwater interactions of running waters and their floodplains. *Journal of the North American Benthological Society*, 29(1):26–40, 2010.

Jay A Brandes and Allan H Devol. Simultaneous nitrate and oxygen respiration in coastal sediments: Evidence for discrete diagenesis. *Journal of Marine Research*, 53(5):771–797, 1995.

Michael P Bruen and Yassin Z Osman. Sensitivity of stream–aquifer seepage to spatial variability of the saturated hydraulic conductivity of the aquifer. *Journal of Hydrology*, 293(1):289–302, 2004.

M Brunke and T Gonser. The ecological significance of exchange processes between rivers and groundwater. *Freshwater Biology*, 37(1):1–33, Feb 1997. ISSN 0046-5070. doi: {10.1046/j.1365-2427.1997.00143.x}.

Matthias Brunke and TOM Gonser. The ecological significance of exchange processes between rivers and groundwater. *Freshwater biology*, 37(1):1–33, 1997.

John M Buffington and Daniele Tonina. Hyporheic exchange in mountain rivers ii: Effects of channel morphology on mechanics, scales, and rates of exchange. *Geography Compass*, 3(3):1038–1062, 2009.

M Bayani Cardenas. Surface water-groundwater interface geomorphology leads to scaling of residence times. *Geophysical Research Letters*, 35(8), 2008.

M Bayani Cardenas and JL Wilson. Hydrodynamics of coupled flow above and below a sediment–water interface with triangular bedforms. *Advances in water resources*, 30(3):301–313, 2007a.

M Bayani Cardenas and John L Wilson. Dunes, turbulent eddies, and interfacial exchange with permeable sediments. *Water resources research*, 43(8), 2007b.

M Bayani Cardenas, JL Wilson, and Vitaly A Zlotnik. Impact of heterogeneity, bed forms, and stream curvature on subchannel hyporheic exchange. *Water Resources Research*, 40(8), 2004.

M Bayani Cardenas, Perran LM Cook, Houshuo Jiang, and Peter Traykovski. Constraining denitrification in permeable wave-influenced marine sediment using linked hydrodynamic and biogeochemical modeling. *Earth and Planetary Science Letters*, 275(1):127–137, 2008.

Bradley J Cardinale, Margaret A Palmer, Christopher M Swan, Shane Brooks, and N LeRoy Poff. The influence of substrate heterogeneity on biofilm metabolism in a stream ecosystem. *Ecology*, 83(2):412–422, 2002.

Steven F Carle. T-progs: Transition probability geostatistical software. *University of California, Davis, CA*, 1999.

Steven F Carle and Graham E Fogg. Transition probability-based indicator geostatistics. *Mathematical Geology*, 28(4):453–476, 1996.

Steven F Carle and Graham E Fogg. Modeling spatial variability with one and multidimensional continuous-lag markov chains. *Mathematical Geology*, 29(7):891–918, 1997.

Steven F Carle, Eric M Labolle, Gary S Weissmann, David Van Brocklin, and Graham E Fogg. Conditional simulation of hydrofacies architecture: a transition probability/markov approach. *Hydrogeologic models of sedimentary aquifers, concepts in hydrogeology and environmental geology*, 1: 147–170, 1998.

Glenn S Carter and Ude Shankar. Creating rectangular bathymetry grids for environmental numerical modelling of gravel-bed rivers. *Applied Mathematical Modelling*, 21(11):699–708, 1997.

Jungyill Choi, Judson W Harvey, and Martha H Conklin. Characterizing multiple timescales of stream and storage zone interaction that affect solute fate and transport in streams. *Water Resources Research*, 36(6): 1511–1518, 2000.

Fred C Collins. *A comparison of spatial interpolation techniques in temperature estimation*. PhD thesis, 1995.

Brewster Conant. Delineating and quantifying ground water discharge zones using streambed temperatures. *Groundwater*, 42(2):243–257, 2004.

Perran LM Cook, Frank Wenzhöfer, Søren Rysgaard, Oleksiy S Galaktionov, Filip JR Meysman, Bradley D Eyre, Jeffrey Cornwell, Markus Huettel, and Ronnie N Glud. Quantification of denitrification in permeable sediments: Insights from a two-dimensional simulation analysis and experimental data. *Limnology and Oceanography: Methods*, 4(OCT):294–307, 2006.

Richard M Cooper and Jonathan D Istok. Geostatistics applied to groundwater contamination. i: Methodology. *Journal of Environmental Engineering*, 114(2):270–286, 1988.

Noel Cressie. Statistics for spatial data. *Terra Nova*, 4(5):613–617, 1992.

BT Croll and CR Hayes. Nitrate and water supplies in the united kingdom. *Environmental pollution*, 50(1):163–187, 1988.

DW Crowder and P Diplas. Using two-dimensional hydrodynamic models at scales of ecological importance. *Journal of hydrology*, 230(3):172–191, 2000.

Henry Philibert Gaspard Darcy. *Dètermination des lois d'ècoulement de l'eau à travers le sable*. 1856.

Eric A Davidson and Sybil Seitzinger. The enigma of progress in denitrification research. *Ecological Applications*, 16(6):2057–2063, 2006.

J Matthew Davis, Ruth C Lohmann, Fred M Phillips, John L Wilson, and David W Love. Architecture of the sierra ladrones formation, central new mexico: Depositional controls on the permeability correlation structure. *Geological Society of America Bulletin*, 105(8):998–1007, 1993.

Pierre Delfiner. Linear estimation of non stationary spatial phenomena. In *Advanced geostatistics in the mining industry*, pages 49–68. Springer, 1976.

Diana dell'Arciprete, Riccardo Bersezio, Fabrizio Felletti, Mauro Giudici, Alessandro Comunian, and Philippe Renard. Comparison of three geostatistical methods for hydrofacies simulation: a test on alluvial sediments. *Hydrogeology journal*, 20(2):299–311, 2012.

CV Deutsch and AG Journel. Gslib: Geostatistical software library and user's guide: Oxford univ. *Press, New York*, 340, 1992.

Journel AG Deutsch CV. *GSLIB: Geostatistical Software Library—and user's guide*. Oxford University Press, New York, 1998.

Robert J Diaz and Rutger Rosenberg. Spreading dead zones and consequences for marine ecosystems. *science*, 321(5891):926–929, 2008.

Council Directive et al. Council directive 91/676/eec of 12 december 1991 concerning the protection of waters against pollution caused by nitrates from agricultural sources. *Official Journal L*, 375(31):12, 1991.

EC Directive. Relating to the quality of water intended for human consumption (80/778/eec). *Off J Eur Communities L*, 229, 1980.

Patrick A Domenico and Franklin W Schwartz. *Physical and chemical hydrogeology*, volume 44. Wiley New York, 1998.

RA Downing, FJ Pearson, and DB Smith. The flow mechanism in the chalk based on radio-isotope analyses of groundwater in the london basin. *Journal of Hydrology*, 40(1):67–83, 1979.

D Dudley Williams and HBN Hynes. The occurrence of benthos deep in the substratum of a stream. *Freshwater biology*, 4(3):233–256, 1974.

JH Duff and FJ Triska. Nitrogen biogeochemistry and surface-subsurface exchange in streams. *Streams and ground waters*, pages 197–220, 2000.

WM Edmunds and NRG Walton. The lincolnshire limestone—hydrogeochemical evolution over a ten-year period. *Journal of Hydrology*, 61(1):201–211, 1983.

Kenneth J Edwardson, William B Bowden, Cliff Dahm, and John Morrice. The hydraulic characteristics and geochemistry of hyporheic and parafluvial zones in arctic tundra streams, north slope, alaska. *Advances in Water Resources*, 26(9):907–923, 2003.

Alexander H Elliott and Norman H Brooks. Transfer of nonsorbing solutes to a streambed with bed forms: Theory. *Water Resources Research*, 33 (1):123–136, 1997.

Nicholas B Engdahl, Eric T Vogler, and Gary S Weissmann. Evaluation of aquifer heterogeneity effects on river flow loss using a transition probability framework. *Water resources research*, 46(1), 2010.

NA Feast, KM Hiscock, PF Dennis, and SH Bottrell. Controls on stable isotope profiles in the chalk aquifer of north-east norfolk, uk, with special reference to dissolved sulphate. *Applied geochemistry*, 12(6):803–812, 1997.

NA Feast, KM Hiscock, PF Dennis, and JN Andrews. Nitrogen isotope hydrochemistry and denitrification within the chalk aquifer system of north norfolk, uk. *Journal of Hydrology*, 211(1):233–252, 1998.

Charles Willard Fetter and CW Fetter. *Applied hydrogeology*, volume 3. Prentice Hall Upper Saddle River, NJ, 2001.

Alan H Fielding and John F Bell. A review of methods for the assessment of prediction errors in conservation presence/absence models. *Environmental conservation*, 24(01):38–49, 1997.

Stuart Findlay. Importance of surface-subsurface exchange in stream ecosystems: the hyporheic zone. *Limnology and oceanography*, 40(1):159–164, 1995.

Helmut Fischer, Frank Kloep, Sabine Wilzcek, and Martin T Pusch. A river's liver–microbial processes within the hyporheic zone of a large lowland river. *Biogeochemistry*, 76(2):349–371, 2005.

Jan H Fleckenstein and Graham E Fogg. Efficient upscaling of hydraulic conductivity in heterogeneous alluvial aquifers. *Hydrogeology journal*, 16 (7):1239–1250, 2008.

Jan H Fleckenstein, Richard G Niswonger, and Graham E Fogg. River-aquifer interactions, geologic heterogeneity, and low-flow management. *Groundwater*, 44(6):837–852, 2006.

Graham E Fogg. Groundwater flow and sand body interconnectedness in a thick, multiple-aquifer system. *Water Resources Research*, 22(5):679–694, 1986.

Robert L Folk and William C Ward. Brazos river bar: a study in the significance of grain size parameters. *Journal of Sedimentary Research*, 27(1), 1957.

Richard Franke and Gregory M Nielson. Scattered data interpolation and applications: A tutorial and survey. In *Geometric Modeling*, pages 131–160. Springer, 1991.

S Frei, JH Fleckenstein, SJ Kollet, and RM Maxwell. Patterns and dynamics of river–aquifer exchange with variably-saturated flow using a fully-coupled model. *Journal of Hydrology*, 375(3):383–393, 2009.

JR French and NJ Clifford. Hydrodynamic modelling as a basis for explaining estuarine environmental dynamics: some computational and methodological issues. *Hydrological Processes*, 14(11-12):2089–2108, 2000.

David L Freyberg. A natural gradient experiment on solute transport in a sand aquifer: 2. spatial moments and the advection and dispersion of nonreactive tracers. *Water Resources Research*, 22(13):2031–2046, 1986.

Gerald M Friedman. Differences in size distributions of populations of particles among sands of various origins: addendum to ias presidential address. *Sedimentology*, 26(6):859–862, 1979.

James N Galloway and Ellis B Cowling. Reactive nitrogen and the world: 200 years of change. *AMBIO: A Journal of the Human Environment*, 31 (2):64–71, 2002.

John A Goff and Sylvia Nordfjord. Interpolation of fluvial morphology using channel-oriented coordinate transformation: a case study from the new jersey shelf. *Mathematical Geology*, 36(6):643–658, 2004.

Jesus D Gomez, John L Wilson, and M Bayani Cardenas. Residence time distributions in sinuosity-driven hyporheic zones and their biogeochemical effects. *Water Resources Research*, 48(9), 2012.

Michael N Gooseff. Defining hyporheic zones–advancing our conceptual and operational definitions of where stream water and groundwater meet. *Geography Compass*, 4(8):945–955, 2010.

Michael N Gooseff, Steve M Wondzell, Roy Haggerty, and Justin Anderson. Comparing transient storage modeling and residence time distribution (rtd) analysis in geomorphically varied reaches in the lookout creek basin, oregon, usa. *Advances in Water Resources*, 26(9):925–937, 2003.

Pierre Goovaerts. *Geostatistics for natural resources evaluation*. Oxford university press, 1997.

Ryan P Gordon, Laura K Lautz, and Timothy L Daniluk. Spatial patterns of hyporheic exchange and biogeochemical cycling around cross-vane restoration structures: Implications for stream restoration design. *Water Resources Research*, 49(4):2040–2055, 2013.

Mark B Green, Wilfred M Wollheim, Nandita B Basu, Gretchen Gettel, P Suresh Rao, Nathaniel Morse, and Robert Stewart. Effective denitrification scales predictably with water residence time across diverse systems. 2009.

Nicolas Gruber and James N Galloway. An earth-system perspective of the global nitrogen cycle. *Nature*, 451(7176):293–296, 2008.

Massimo Guarascio, Michel David, and CJ Huybrechts. *Advanced geostatistics in the mining industry*, volume 24. Springer, 1976.

Roy Haggerty, Steven M Wondzell, and Matthew A Johnson. Power-law residence time distribution in the hyporheic zone of a 2nd-order mountain stream. *Geophysical Research Letters*, 29(13):1640, 2002.

Donald A Hammer and RK Bastian. Wetland ecosystems: natural water purifiers. *Constructed wetlands for wastewater treatment: municipal, industrial and agricultural*, 5, 1989.

Peter J Hancock, Andrew J Boulton, and William F Humphreys. Aquifers and hyporheic zones: towards an ecological understanding of groundwater. *Hydrogeology Journal*, 13(1):98–111, 2005.

Hill M.C. Harbaugh A. W., Banta E. R. and McDonald M. G. Modflow-2005, the u. s. geological survey modular ground-water model—user guide to modularization concepts and the ground-water flow process. *U.S. Geol. Surv. Open File Rep.*, (00-92):107 pp, 2005.

Judson W Harvey and Kenneth E Bencala. The effect of streambed topography on surface-subsurface water exchange in mountain catchments. *Water Resources Research*, 29(1):89–98, 1993.

Judson W Harvey and BJ Wagner. Quantifying hydrologic interactions between streams and their subsurface hyporheic zones. *Streams and ground waters*, 344, 2000.

Judson W Harvey, JK Böhlke, Mary A Voytek, Durelle Scott, and Craig R Tobias. Hyporheic zone denitrification: Controls on effective reaction depth and contribution to whole-stream mass balance. *Water Resources Research*, 49(10):6298–6316, 2013.

S Majid Hassanizadeh and William G Gray. High velocity flow in porous media. *Transport in Porous Media*, 2(6):521–531, 1987.

HG Headworth. Hydrogeological characteristics of artesian boreholes in the chalk of hampshire. *Quarterly Journal of Engineering Geology and Hydrogeology*, 11(2):139–144, 1978.

JI Hedges and JH Stern. Carbon and nitrogen determinations of carbonate-containing solids. *Limnology and Oceanography*, 29(3):657–663, 1984. ISSN 0024-3590.

Susan P Hendricks and David S White. Physicochemical patterns within a hyporheic zone of a northern michigan river, with comments on surface water patterns. *Canadian Journal of Fisheries and Aquatic Sciences*, 48 (9):1645–1654, 1991.

Tomislav Hengl, Budiman Minasny, and Michael Gould. A geostatistical analysis of geostatistics. *Scientometrics*, 80(2):491–514, 2009.

M Herrera-Pantoja, KM Hiscock, and RR Boar. The potential impact of climate change on groundwater-fed wetlands in eastern england. *Ecohydrology*, 5(4):401–413, 2012.

Erich T Hester and Michael N Gooseff. Moving beyond the banks: Hyporheic restoration is fundamental to restoring ecological services and functions of streams. *Environmental science & technology*, 44(5):1521–1525, 2010.

Erich T Hester, Katie I Young, and Mark A Widdowson. Mixing of surface and groundwater induced by riverbed dunes: Implications for hyporheic zone definitions and pollutant reactions. *Water Resources Research*, 49 (9):5221–5237, 2013.

Alan R Hill, Carl F Labadia, and K Sanmugadas. Hyporheic zone hydrology and nitrogen dynamics in relation to the streambed topography of a n-rich stream. *Biogeochemistry*, 42(3):285–310, 1998.

John Hilton, Matthew O'Hare, Michael J Bowes, and J Iwan Jones. How green is my river? a new paradigm of eutrophication in rivers. *Science of the Total Environment*, 365(1):66–83, 2006.

KM Hiscock. The influence of pre-devensian glacial deposits on the hydrogeochemistry of the chalk aquifer system of north norfolk, uk. *Journal of Hydrology*, 144(1):335–369, 1993.

KM Hiscock, DH Lister, RR Boar, and FML Green. An integrated assessment of long-term changes in the hydrology of three lowland rivers in eastern england. *Journal of environmental management*, 61(3):195–214, 2001.

A Hodskinson and RI Ferguson. Numerical modelling of separated flow in river bends: Model testing and experimental investigation of geometric controls on the extent of flow separation at the concave bank. *Hydrological Processes*, 12(8):1323–1338, 1998.

Robert M Holmes, Jeremy B Jones Jr, Stuart G Fisher, and Nancy B Grimm. Denitrification in a nitrogen-limited stream ecosystem. *Biogeochemistry*, 33(2):125–146, 1996.

KWF Howard. Denitrification in a major limestone aquifer. *Journal of Hydrology*, 76(3):265–280, 1985.

KA Hubbard, LK Lautz, MJ Mitchell, B Mayer, and ER Hotchkiss. Evaluating nitrate uptake in a rocky mountain stream using labelled 15n and ambient nitrate chemistry. *Hydrological processes*, 24(23):3322–3336, 2010.

Allen Hunt and Robert Ewing. *Percolation theory for flow in porous media*, volume 771. Springer, 2009.

Edward H Isaaks and R Mohan Srivastava. An introduction to applied geostatistics. 1989.

Felix Janssen, M Bayani Cardenas, Audrey H Sawyer, Thea Dammrich, Jana Krietsch, and Dirk Beer. A comparative experimental and multiphysics computational fluid dynamics study of coupled surface–subsurface flow in bed forms. *Water Resources Research*, 48(8), 2012.

Guangqiu Jin, Hongwu Tang, Badin Gibbes, Ling Li, and David Andrew Barry. Transport of nonsorbing solutes in a streambed with periodic bedforms. *Advances in Water Resources*, 33(11):1402–1416, 2010.

Jeremy B Jones and Patrick J Mulholland. *Streams and ground waters*. Access Online via Elsevier, 1999.

Jeremy B Jones Jr, Stuart G Fisher, and Nancy B Grimm. Nitrification in the hyporheic zone of a desert stream ecosystem. *Journal of the North American Benthological Society*, pages 249–258, 1995.

Andre G Journel and Ch J Huijbregts. *Mining geostatistics*. Academic press, 1978.

Tamao Kasahara and Alan R Hill. Effects of riffle step restoration on hyporheic zone chemistry in n-rich lowland streams. *Canadian Journal of Fisheries and Aquatic Sciences*, 63(1):120–133, 2006.

Tamao Kasahara and Steven M Wondzell. Geomorphic controls on hyporheic exchange flow in mountain streams. *Water Resources Research*, 39(1): SBH–3, 2003.

Daniel H Käser, Andrew Binley, A Louise Heathwaite, and Stefan Krause. Spatio-temporal variations of hyporheic flow in a riffle-step-pool sequence. *Hydrological Processes*, 23(15):2138–2149, 2009.

DH Käser, Andrew Binley, and AL Heathwaite. On the importance of considering channel microforms in groundwater models of hyporheic exchange. *River Research and Applications*, 29(4):528–535, 2013.

Barry F Kavanagh. *Surveying: with construction applications*. Prentice Hall, 2010.

Adam J Kessler, Ronnie N Glud, M Bayani Cardenas, Morten Larsen, Michael F Bourke, and Perran LM Cook. Quantifying denitrification in rippled permeable sands through combined flume experiments and modeling. *Limnology and Oceanography*, 57(4):1217, 2012.

Brian KA Kim, Alan P Jackman, and Frank J Triska. Modeling biotic uptake by periphyton and transient hyporrheic storage of nitrate in a natural stream. *Water Resources Research*, 28(10):2743–2752, 1992.

K-H Knorr. Doc-dynamics in a small headwater catchment as driven by redox fluctuations and hydrological flow paths–are doc exports mediated by iron reduction/oxidation cycles? *Biogeosciences*, 10(2):891–904, 2013.

Harvey P Knudsen and Young C Kim. *Application of Geostatistics to Roll Front Type Uranium Deposits*. Society of Mining Engineers of AIME, 1978.

Donald E Knuth. *Fundamental Algorithms: The art of computer programming*. 1973.

Joshua C Koch, Diane M McKnight, and Jenny L Baeseman. Effect of unsteady flow on nitrate loss in an oligotrophic, glacial meltwater stream. *Journal of Geophysical Research: Biogeosciences (2005–2012)*, 115(G1), 2010.

Stefan Krause, Louise Heathwaite, Andrew Binley, and Patrick Keenan. Nitrate concentration changes at the groundwater-surface water interface of a small cumbrian river. *Hydrological Processes*, 23(15):2195–2211, 2009.

Stefan Krause, Christina Tecklenburg, Matthias Munz, and Emma Naden. Streambed nitrogen cycling beyond the hyporheic zone: Flow controls on horizontal patterns and depth distribution of nitrate and dissolved oxygen in the upwelling groundwater of a lowland river. *Journal of Geophysical Research: Biogeosciences*, 118(1):54–67, 2013.

SN Lane, KF Bradbrook, KS Richards, PA Biron, and AG Roy. The application of computational fluid dynamics to natural river channels: three-dimensional versus two-dimensional approaches. *Geomorphology*, 29(1): 1–20, 1999.

SN Lane, RJ Hardy, L Elliott, and DB Ingham. Numerical modeling of flow processes over gravelly surfaces using structured grids and a numerical porosity treatment. *Water Resources Research*, 40(1), 2004.

Stuart N Lane. Hydraulic modelling in hydrology and geomorphology: a review of high resolution approaches. *Hydrological Processes*, 12(8):1131–1150, 1998.

K Lansdown, Mark Trimmer, CM Heppell, F Sgouridis, Sami Ullah, AL Heathwaite, Andrew Binley, and Hao Zhang. Characterization of the key pathways of dissimilatory nitrate reduction and their response to complex organic substrates in hyporheic sediments. *Limnol. Oceanogr*, 57 (2):387–400, 2012.

Laura K Lautz and Donald I Siegel. Modeling surface and ground water mixing in the hyporheic zone using modflow and mt3d. *Advances in Water Resources*, 29(11):1618–1633, 2006.

LK Lautz and RM Fanelli. Seasonal biogeochemical hotspots in the streambed around restoration structures. *Biogeochemistry*, 91(1):85–104, 2008.

Denis R LeBlanc, Stephen P Garabedian, Kathryn M Hess, Lynn W Gelhar, Richard D Quadri, Kenneth G Stollenwerk, and Warren W Wood.

Large-scale natural gradient tracer test in sand and gravel, cape cod, massachusetts: 1. experimental design and observed tracer movement. *Water Resources Research*, 27(5):895–910, 1991.

Carl J Legleiter and Phaedon C Kyriakidis. Spatial prediction of river channel topography by kriging. *Earth Surface Processes and Landforms*, 33 (6):841–867, 2008.

Song Lin-Hua and TC Atkinson. Dissolved iron in chalk groundwaters from norfolk, england. *Quarterly Journal of Engineering Geology and Hydrogeology*, 18(3):261–274, 1985.

Florian Malard, Klement Tockner, MARIE-JOSÉ DOLE-OLIVIER, and JV Ward. A landscape perspective of surface–subsurface hydrological exchanges in river corridors. *Freshwater Biology*, 47(4):621–640, 2002.

Andrea Marion, Matteo Bellinello, Ian Guymer, and Aaron Packman. Effect of bed form geometry on the penetration of nonreactive solutes into a streambed. *Water Resources Research*, 38(10):1209, 2002.

A Marzadri, D Tonina, A Bellin, G Vignoli, and M Tubino. Semianalytical analysis of hyporheic flow induced by alternate bars. *Water Resources Research*, 46(7), 2010.

A Marzadri, D Tonina, and A Bellin. Morphodynamic controls on redox conditions and on nitrogen dynamics within the hyporheic zone: Application to gravel bed rivers with alternate-bar morphology. *Journal of Geophysical Research: Biogeosciences (2005–2012)*, 117(G3), 2012.

Michael E McClain, Elizabeth W Boyer, C Lisa Dent, Sarah E Gergel, Nancy B Grimm, Peter M Groffman, Stephen C Hart, Judson W Harvey, Carol A Johnston, Emilio Mayorga, et al. Biogeochemical hot spots and hot moments at the interface of terrestrial and aquatic ecosystems. *Ecosystems*, 6(4):301–312, 2003.

Michael G McDonald and Arlen W Harbaugh. *A modular three-dimensional finite-difference ground-water flow model*. Scientific Publications Company, 1984.

RR McDonald, JP Bennett, and JM Nelson. The us geological survey multidimensional surface water modeling system. In *AGU Spring Meeting Abstracts*, volume 1, 2001.

RR McDonald, JP Bennett, and JM Nelson. Multi-dimensional surface-water modeling system user's guide. *US Geological Survey Technical Methods*, 6, 2005.

Diane M McKnight, Robert L Runkel, Cathy M Tate, John H Duff, and Daryl L Moorhead. Inorganic n and p dynamics of antarctic glacial meltwater streams as controlled by hyporheic exchange and benthic autotrophic communities. *Journal of the North American Benthological Society*, 23(2):171–188, 2004.

Venkatesh Merwade and David R Maidment. *River Channel Morphology Model: A Tool for Analyzing and Extrapolating River Channel Bathymetry*. University of Texas at Austin, Center for Research in Water Resources, JJ Pickle Research Campus, 2005.

Venkatesh Merwade, Aaron Cook, and Julie Coonrod. Gis techniques for creating river terrain models for hydrodynamic modeling and flood inundation mapping. *Environmental Modelling & Software*, 23(10):1300–1311, 2008.

HoAoCo Montgomery, NS Thom, and A Cockburn. Determination of dissolved oxygen by the winkler method and the solubility of oxygen in pure water and sea water. *Journal of Applied Chemistry*, 14(7):280–296, 1964.

Rory N Mortimore, Christopher J Wood, and Ramus William Gallois. *British upper cretaceous stratigraphy*, volume 23. Joint Nature Conservation Committee (JNCC), 2001.

Gleyci A. O. Moser, Robson Alves Takanohashi, Mariana de Chagas Braz, Domenica Teixeira de Lima, Fabiana Vasconcelos Kirsten, Josefa Varela Guerra, Alexandre M. Fernandes, and Ricardo Cesar Goncalves Pollery. Phytoplankton spatial distribution on the Continental Shelf off Rio de Janeiro, from Paraiba do Sul River to Cabo Frio. *Hydrobiologia*, 728(1): 1–21, May 2014. ISSN 0018-8158. doi: {10.1007/s10750-013-1791-3}.

Patrick J Mulholland and Donald L DeAngelis. Surface-subsurface exchange and nutrient spiraling. *Streams and ground waters*, pages 149–166, 2000.

Patrick J Mulholland, Ashley M Helton, Geoffrey C Poole, Robert O Hall, Stephen K Hamilton, Bruce J Peterson, Jennifer L Tank, Linda R Ashkenas, Lee W Cooper, Clifford N Dahm, et al. Stream denitrification across biomes and its response to anthropogenic nitrate loading. *Nature*, 452 (7184):202–205, 2008.

Banta E.R. Naff R.L. The u.s. geological survey modular ground-water model—pcgn: A preconditioned conjugate gradient solver with improved nonlinear control: U.s. geological survey. *U.S. Geol. Surv. Open File Rep.*, (1331):35 p, 2008.

Robert Joseph Naiman and Robert E Bilby. *River ecology and management: lessons from the Pacific coastal ecoregion*. Springer, 1998.

Iehisa Nezu, Akihiro Tominaga, and Hiroji Nakagawa. Field measurements of secondary currents in straight rivers. *Journal of Hydraulic Engineering*, 119(5):598–614, 1993.

Scott E Nielsen, Mark S Boyce, Gordon B Stenhouse, and Robin HM Munro. Modeling grizzly bear habitats in the yellowhead ecosystem of alberta: taking autocorrelation seriously. *Ursus*, pages 45–56, 2002.

Ben L O'Connor and Miki Hondzo. Enhancement and inhibition of denitrification by fluid-flow and dissolved oxygen flux to stream sediments. *Environmental science & technology*, 42(1):119–125, 2007.

Margaret A Oliver and R Webster. Kriging: a method of interpolation for geographical information systems. *International Journal of Geographical Information System*, 4(3):313–332, 1990.

Aaron I Packman and Kenneth E Bencala. Modeling surface-subsurface hydrological interactions. *Streams and ground waters*, pages 45–81, 2000.

Aaron I Packman and Norman H Brooks. Hyporheic exchange of solutes and colloids with moving bed forms. *Water Resources Research*, 37(10): 2591–2605, 2001.

Eric W Peterson and Timothy B Sickbert. Stream water bypass through a meander neck, laterally extending the hyporheic zone. *Hydrogeology Journal*, 14(8):1443–1451, 2006.

Gilles Pinay, Thomas C O'Keefe, Richard T Edwards, and Robert J Naiman. Nitrate removal in the hyporheic zone of a salmon river in alaska. *River research and applications*, 25(4):367–375, 2009.

PETER J PIZOR. Principles of geographical information systems for land resources assessment.. *Soil Science*, 144(4):306, 1987.

David W Pollock. *User's Guide for MODPATH/MODPATH-PLOT, Version 3: A Particle Tracking Post-processing Package for MODFLOW, the US: Geological Survey Finite-difference Ground-water Flow Model.* US Department of Interior, 1994.

JL Pretty, AG Hildrew, and M Trimmer. Nutrient dynamics in relation to surface–subsurface hydrological exchange in a groundwater fed chalk stream. *Journal of Hydrology*, 330(1):84–100, 2006.

Christel Prudhomme and Duncan W Reed. Mapping extreme rainfall in a mountainous region using geostatistical techniques: a case study in scotland. *International Journal of Climatology*, 19(12):1337–1356, 1999.

Kenneth R Rehfeldt, J Mark Boggs, and Lynn W Gelhar. Field study of dispersion in a heterogeneous aquifer: 3. geostatistical analysis of hydraulic conductivity. *Water Resources Research*, 28(12):3309–3324, 1992.

Roberto Revelli, Fulvio Boano, Carlo Camporeale, and Luca Ridolfi. Intra-meander hyporheic flow in alluvial rivers. *Water Resources Research*, 44 (12), 2008.

Robert W Ritzi, Zhenxue Dai, David F Dominic, and Yoram N Rubin. Spatial correlation of permeability in cross-stratified sediment with hierarchical architecture. *Water resources research*, 40(3), 2004.

Robert L Runkel and Kenneth E Bencala. Transport of reacting solutes in rivers and streams. In *Environmental hydrology*, pages 137–164. Springer, 1995.

JC Rutherford. *River mixing*. Wiley Chichester, 1994.

Nicole Saenger, Peter K Kitanidis, and Robert L Street. A numerical study of surface-subsurface exchange processes at a riffle-pool pair in the lahn river, germany. *Water Resources Research*, 41(12):W12424, 2005.

Mashfiqus Salehin, Aaron I Packman, and Matthew Paradis. Hyporheic exchange with heterogeneous streambeds: Laboratory experiments and modeling. *Water Resources Research*, 40(11), 2004.

S Anne Savant, Danny D Reible, and Louis J Thibodeaux. Convective transport within stable river sediments. *Water Resources Research*, 23 (9):1763–1768, 1987.

Audrey Hucks Sawyer and M Bayani Cardenas. Hyporheic flow and residence time distributions in heterogeneous cross-bedded sediment. *Water resources research*, 45(8), 2009.

Marc Schallenberg and Jacob Kalff. The ecology of sediment bacteria in lakes and comparisons with other aquatic ecosystems. *Ecology*, pages 919–934, 1993.

Christina Schornberg, Christian Schmidt, Edda Kalbus, and Jan H Fleckenstein. Simulating the effects of geologic heterogeneity and transient boundary conditions on streambed temperatures—implications for temperature-based water flux calculations. *Advances in Water Resources*, 33(11):1309–1319, 2010.

Donald Shepard. A two-dimensional interpolation function for irregularly-spaced data. In *Proceedings of the 1968 23rd ACM national conference*, pages 517–524. ACM, 1968.

MF Sheridan, KH Wohletz, and J Dehn. Discrimination of grain-size subpopulations in pyroclastic deposits. *Geology*, 15(4):367–370, 1987.

Arne L Sjodin, William M Lewis Jr, and James F Saunders III. Denitrification as a component of the nitrogen budget for a large plains river. *Biogeochemistry*, 39(3):327–342, 1997.

VBD Skerman and IC MacRae. The influence of oxygen availability on the degree of nitrate reduction by seudomonas denitrificans. *Canadian Journal of Microbiology*, 3(3):505–530, 1957.

JWN Smith, M Bonell, Janine Gibert, WH McDowell, EA Sudicky, JV Turner, and RC Harris. Groundwater–surface water interactions, nutrient fluxes and ecological response in river corridors: translating science into effective environmental management. *Hydrological Processes*, 22(1): 151–157, 2008.

Leslie Smith. Spatial variability of flow parameters in a stratified sand. *Journal of the International Association for Mathematical Geology*, 13 (1):1–21, 1981.

Amilcar Soares. Sequential indicator simulation with correction for local probabilities. *Mathematical geology*, 30(6):761–765, 1998.

Marios Sophocleous. Interactions between groundwater and surface water: the state of the science. *Hydrogeology journal*, 10(1):52–67, 2002.

FI Stalkup. Permeability variations observed at the faces of crossbedded sandstone outcrops. *Reservoir characterization. LW Lake and HB Carroll Jr.(eds.). Academic Press, London*, pages 141–179, 1986.

Theodore L Steck, Arun Sharma, and Peter Bartelmus. Human population explosion. 2008.

Robert S Stelzer, Lynn A Bartsch, William B Richardson, and Eric A Strauss. The dark side of the hyporheic zone: Depth profiles of nitrogen and its processing in stream sediments. *Freshwater Biology*, 56(10): 2021–2033, 2011.

Susa H Stonedahl, Judson W Harvey, Anders Wörman, Mashfiqus Salehin, and Aaron I Packman. A multiscale model for integrating hyporheic exchange from ripples to meanders. *Water resources research*, 46(12), 2010.

Richard G Storey, Kenneth WF Howard, and D Dudley Williams. Factors controlling riffle-scale hyporheic exchange flows and their seasonal changes in a gaining stream: A three-dimensional groundwater flow model. *Water Resources Research*, 39(2):1034, 2003.

Richard G Storey, D Dudley Williams, and Roberta R Fulthorpe. Nitrogen processing in the hyporheic zone of a pastoral stream. *Biogeochemistry*, 69(3):285–313, 2004.

DT Strong and IRP Fillery. Denitrification response to nitrate concentrations in sandy soils. *Soil Biology and Biochemistry*, 34(7):945–954, 2002.

Edward A Sudicky. A natural gradient experiment on solute transport in a sand aquifer: Spatial variability of hydraulic conductivity and its role in the dispersion process. *Water Resources Research*, 22(13):2069–2082, 1986.

Geoffrey Taylor. The dispersion of matter in turbulent flow through a pipe. *Proceedings of the Royal Society of London. Series A. Mathematical and Physical Sciences*, 223(1155):446–468, 1954.

Louis J Thibodeaux and John D Boyle. Bedform-generated convective transport in bottom sediment. 1987.

Steven A Thomas, H Maurice Valett, Jackson R Webster, and Patrick J Mulholland. A regression approach to estimating reactive solute uptake in advective and transient storage zones of stream ecosystems. *Advances in Water Resources*, 26(9):965–976, 2003.

Klement Tockner, Doris Pennetzdorfer, Niko Reiner, Fritz Schiemer, and JV Ward. Hydrological connectivity, and the exchange of organic matter and nutrients in a dynamic river–floodplain system (danube, austria). *Freshwater Biology*, 41(3):521–535, 1999.

Maciej Tomczak. Spatial interpolation and its uncertainty using automated anisotropic inverse distance weighting (idw)-cross-validation/jackknife approach. *Journal of Geographic Information and Decision Analysis*, 2(2): 18–30, 1998.

Daniele Tonina and John M Buffington. Hyporheic exchange in gravel bed rivers with pool-riffle morphology: Laboratory experiments and three-dimensional modeling. *Water Resources Research*, 43(1):W01421, 2007.

Daniele Tonina and John M Buffington. Hyporheic exchange in mountain rivers i: Mechanics and environmental effects. *Geography Compass*, 3(3): 1063–1086, 2009.

Jozsef Toth. A theoretical analysis of groundwater flow in small drainage basins. *Journal of Geophysical Research*, 68(16):4795–4812, 1963.

John A Trangenstein. Multi-scale iterative techniques and adaptive mesh refinement for flow in porous media. *Advances in Water Resources*, 25(8): 1175–1213, 2002.

Nico Trauth, Christian Schmidt, Uli Maier, Michael Vieweg, and Jan H Fleckenstein. Coupled 3-d stream flow and hyporheic flow model under varying stream and ambient groundwater flow conditions in a pool-riffle system. *Water Resources Research*, 49(9):5834–5850, 2013.

Mark Trimmer and Ian A Sanders. In-situ application of the 15 no 3-isotope pairing technique to measure denitrification in sediments at the surface water-groundwater interface. *Limnol. Oceanogr. Methods*, 4:142–152, 2006.

Frank J Triska, Vance C Kennedy, Ronald J Avanzino, Gary W Zellweger, and Kenneth E Bencala. Retention and transport of nutrients in a third-order stream in northwestern california: hyporheic processes. *Ecology*, pages 1893–1905, 1989.

Frank J Triska, John H Duff, and Ronald J Avanzino. Influence of exchange flow between the channel and hyporheic zone on nitrate production in a small mountain stream. *Canadian Journal of Fisheries and Aquatic Sciences*, 47(11):2099–2111, 1990.

Frank J Triska, John H Duff, and Ronald J Avanzino. The role of water exchange between a stream channel and its hyporheic zone in nitrogen cycling at the terrestrial?aquatic interface. pages 167–184, 1993.

DM Tubbing and W Admiraal. Inhibition of bacterial and phytoplanktonic metabolic activity in the lower river rhine by ditallowdimethylammonium chloride. *Applied and environmental microbiology*, 57(12):3616–3622, 1991.

Walter Gregson Vaux et al. *Interchange of stream and intragravel water in a salmon spawning riffle*. US Fish and Wildlife Service, 1962.

WG Vaux. Intragravel flow and interchange of water in a streambed. *United States Fish And Wildlife Service Fishery Bulletin*, 66(3):479, 1968.

Phillipe Vervier and Robert J Naiman. Spatial and temporal fluctuations of dissolved organic carbon in subsurface flow of the stillaguamish river (washington, ysa). *Archiv für Hydrobiologie*, 123(4):401–412, 1992.

Franz Helmut Wagner and Gernot Bretschko. Interstitial flow through preferential flow paths in the hyporheic zone of the oberer seebach, austria. *Aquatic sciences*, 64(3):307–316, 2002.

Douglas D Walker, Björn Gylling, and Jan-Olof Selroos. Upscaling of hydraulic conductivity and telescopic mesh refinement. *Groundwater*, 43(1): 40–51, 2005.

Adam S Ward, Michael N Gooseff, and Kamini Singha. How does subsurface characterization affect simulations of hyporheic exchange? *Ground Water*, 51(1):14–28, 2013.

David F Watson et al. *Contouring: a guide to the analysis and display of spatial data (with programs on diskette)*. Pergamon Press, 1992.

DF Watson and GM Philip. Neighborhood-based interpolation. *Geobyte*, 2 (2):12–16, 1987.

Erik K Webb and Mary P Anderson. Simulation of preferential flow in three-dimensional, heterogeneous conductivity fields with realistic internal architecture. *Water Resources Research*, 32(3):533–545, 1996.

Jackson R Webster, Patrick J Mulholland, Jennifer L Tank, H Maurice Valett, Walter K Dodds, Bruce J Peterson, William B Bowden, Clifford N Dahm, Stuart Findlay, Stanley V Gregory, et al. Factors affecting ammonium uptake in streams–an inter-biome perspective. *Freshwater Biology*, 48(8):1329–1352, 2003.

RL Westerman and TC Tucker. Effect of salts and salts plus nitrogen-15-labeled ammonium chloride on mineralization of soil nitrogen, nitrification, and immobilization. *Soil Science Society of America Journal*, 38(4): 602–605, 1974.

Sarah K Wexler, Kevin M Hiscock, and Paul F Dennis. Microbial and hydrological influences on nitrate isotopic composition in an agricultural lowland catchment. *Journal of Hydrology*, 468:85–93, 2012.

David S White, Charles H Elzinga, and Susan P Hendricks. Temperature patterns within the hyporheic zone of a northern michigan river. *Journal of the North American Benthological Society*, pages 85–91, 1987.

Thomas C Winter. *Ground water and surface water: a single resource*, volume 1139. DIANE Publishing, 1999.

William W Woessner. Stream and fluvial plain ground water interactions: rescaling hydrogeologic thought. *Ground Water*, 38(3):423–429, 2000.

Steven M Wondzell. Effect of morphology and discharge on hyporheic exchange flows in two small streams in the cascade mountains of oregon, usa. *Hydrological Processes*, 20(2):267–287, 2006.

Steven M Wondzell and Frederick J Swanson. Seasonal and storm dynamics of the hyporheic zone of a 4th-order mountain stream. i: Hydrologic processes. *Journal of the North American Benthological Society*, pages 3–19, 1996.

Steven M Wondzell, Justin LaNier, and Roy Haggerty. Evaluation of alternative groundwater flow models for simulating hyporheic exchange in a small mountain stream. *Journal of hydrology*, 364(1):142–151, 2009a.

Steven M Wondzell, Justin LaNier, Roy Haggerty, Richard D Woodsmith, and Richard T Edwards. Changes in hyporheic exchange flow following experimental wood removal in a small, low-gradient stream. *Water Resources Research*, 45(5), 2009b.

Tamara M Wood and António M Baptista. A model for diagnostic analysis of estuarine geochemistry. *Water Resources Research*, 29(1):51–71, 1993.

Anders Wörman, Aaron I Packman, Håkan Johansson, and Karin Jonsson. Effect of flow-induced exchange in hyporheic zones on longitudinal transport of solutes in streams and rivers. *Water Resources Research*, 38(1): 1001, 2002.

Anders Wörman, Aaron I Packman, Lars Marklund, Judson W Harvey, and Susa H Stone. Exact three-dimensional spectral solution to surface-groundwater interactions with arbitrary surface topography. *Geophysical research letters*, 33(7), 2006.

Gregory J Wroblicky, Michael E Campana, H Maurice Valett, and Clifford N Dahm. Seasonal variation in surface-subsurface water exchange and lateral hyporheic area of two stream-aquifer systems. *Water Resources Research*, 34(3):317–328, 1998.

Yongqiang Yang, Ling Zhang, Fanrong Chen, Mingliang Kang, Shijun Wu, and Jinsong Liu. Seasonal Variation of Acid Volatile Sulfide and Simultaneously Extracted Metals in Sediment Cores from the Pearl River Estuary. *Soil & Sediment Contamination*, 23(4):480–496, May 19 2014. ISSN 1532-0383. doi: {10.1080/15320383.2014.838207}.

Peter N Yianilos. Data structures and algorithms for nearest neighbor search in general metric spaces. In *Proceedings of the fourth annual ACM-SIAM Symposium on Discrete algorithms*, pages 311–321. Society for Industrial and Applied Mathematics, 1993.

H Murat Yilmaz. The effect of interpolation methods in surface definition: an experimental study. *Earth Surface Processes and Landforms*, 32(9): 1346–1361, 2007.

CP Young, DB Oakes, and WB Wilkinson. Prediction of future nitrate concentrations in ground watera. *Groundwater*, 14(6):426–438, 1976.

Jay P Zarnetske, Roy Haggerty, Steven M Wondzell, Vrushali A Bokil, and Ricardo González-Pinzón. Coupled transport and reaction kinetics con-

trol the nitrate source-sink function of hyporheic zones. *Water Resources Research*, 48(11), 2012.

R Zhang, DE Myers, and AW Warrick. Estimation of the spatial distribution of soil chemicals using pseudo-cross-variograms. *Soil Science Society of America Journal*, 56(5):1444–1452, 1992.

YaoQuan Zhou, Robert W Ritzi, Mohamad Reza Soltanian, and David F Dominic. The influence of streambed heterogeneity on hyporheic flow in gravelly rivers. *Groundwater*, 52(2):206–216, 2014.